The Heat Index: An Apparent Temperature that Maps Climate to Human Physiology

by

Yi-Chuan Lu

A dissertation submitted in partial satisfaction of the

requirements for the degree of

Doctor of Philosophy

in

Physics

in the

Graduate Division

of the

University of California, Berkeley

Committee in charge:

Professor David M. Romps, Co-chair
Professor Holger Müller, Co-chair
Professor Martin White
Associate Professor William R. Boos

Spring 2023

The Heat Index: An Apparent Temperature that Maps Climate to Human Physiology

Abstract

The Heat Index: An Apparent Temperature that Maps Climate to Human Physiology

by

Yi-Chuan Lu

Doctor of Philosophy in Physics

University of California, Berkeley

Professor David M. Romps, Co-chair

Professor Holger Müller, Co-chair

The heat index is an apparent temperature that measures how hot it feels when humidity is factored in with the actual air temperature. Defined in 1979 by Robert Steadman, the heat index is based on a model of human thermoregulation, and each value maps to a unique physiological and behavioral state of the human. The heat index thus defined is widely used by weather agencies to communicate the health risk associated with high heat and humidity. However, Steadman's model gives unphysical results at sufficiently high temperature and humidity, leading to an undefined heat index. In the 1970s, instances of an undefined heat index were uncommon, but global warming is increasing the frequency of conditions that leads to an undefined heat index. In this dissertation, the problem with the model is identified and fixed, allowing the heat index to be defined for all temperature and humidity. Similar to the existing heat index, the extended part also maps to physiological states of a human under extreme heat stress, such as hyperthermia or heat death, providing a tool to assess the regional health outcomes at different levels of global warming.

Before the problem with the model is fixed, weather agencies relied on a widespread polynomial extrapolation designed by the National Weather Service to estimate the heat index at high temperature and humidity. Now, with the extended heat index, we have an opportunity to reassess past heat waves in the United States. In this dissertation, three-hourly temperature and humidity are used to evaluate the extended heat index over the contiguous United States during the years 1984 to 2020. It is found that the 99.9th percentile of the daily maximum heat index is highest over the Midwest. Identifying and ranking heat waves by the spatially integrated exceedance of that percentile, the Midwest once again stands out as home to the most extreme heat waves, including the top-ranked July 2011 and July 1995 heat waves. The extended heat index can also be used to evaluate the physiological stress induced by heat and humidity. It is found that the most extreme Midwest heat waves tax

the cardiovascular system with a skin blood flow that is elevated severalfold, approaching the physiological limit. These effects are not captured by the National Weather Service's polynomial extrapolation, which underestimates the heat index by as much as 10 K during severe heat waves.

Another long-lasting problem of the heat index is that it has never been validated against laboratory data. In this dissertation, we use the laboratory data obtained by physiologists at Penn State, showing that the model underlying the heat index can correctly predict the combinations of temperature and humidity that cause hyperthermia. This is the first time the heat-index model has been validated against physiological data from laboratory experiments. For light and moderate exertion in an indoor setting, the heat-index model predicts hyperthermia would occur at the heat-index value of 345 K, consistent with the experimental results. For the same setting and exertion, the heat-index model predicts the core body temperature would equilibrate at the fatal value of 315 K at the heat-index value of 366 K, establishing a heat-index threshold for the survivability of humans.

Global warming poses a direct threat to human health. Many previous studies of future impacts have relied on the wet-bulb temperature, defined as the equilibrium temperature of a wet thermometer under an infinite wind, to predict human survivability. However, the wet-bulb temperature is not an accurate metric for human heat stress because it does not account for human exertion, finite wind speed and radiation heat exchange. With the laboratory-validated heat index, we find that a commonly used survivability threshold of 35 °C for wet-bulb temperature would overestimate the occurrence of heat death, but would underestimate the occurrence of hyperthermia. For example, in a world warmer than pre-industrial by 10 K, the best estimate is that 30% of the world's population would be exposed once or more per year to a wet-bulb temperature above 35 °C, but less than 2% would be exposed to fatal conditions and over 60% would be exposed to conditions that would cause hyperthermia.

To Plago Chen.

Contents

List of Figures

List of Tables

Acknowledgments

I would like to express my sincere gratitude to my adviser, David Romps, for his guidance throughout this academic journey. David has high expectations for his students, but he pushes them firmly and with patience. He cares about the well-being of the students and works diligently to help them achieve their goals while attributing most of the credit to his students. I am very honored to have had the opportunity to work with him. If luck exists, I probably have had spent a lot of it by meeting him in graduate school.

Additionally, I extend my gratitude to Holger Müller, the co-chair in the Physics Department, as well as Martin White and Bill Boos, for serving on my dissertation committee. Their valuable feedback has significantly contributed to improving my dissertation. I would also like to thank the dedicated staff members—Anne Takizawa and Joelle Miles—in the Physics Department for their assistance in resolving various administrative challenges throughout my Ph.D. study. Their unwavering and prompt support has ensured a smooth academic experience.

I am also lucky to have wonderful colleagues in David's group: Rusen Öktem, Jake Seeley, Nathaniel Tarshish, Suqin Duan, Harsha Hampapura, Katie Latimer, and Zhenyu He. Their willingness to share knowledge and discuss research topics has been instrumental in my professional growth. They also make the office not just productive but also enjoyable.

I am grateful for the friendships I have made during graduate school. They have made life here particularly entertaining. I would like to thank Benjamin Ponedel, Chien-I Chiang, Ethan Chang, Grace Liu, Jeff Chiu, and Raymond Co. Special thanks go to my housemates, Yi-Lun Wang, Li-Chiang Lin, Yen-Ta Huang, and Jiang Du–the folks who have made the apartment a joyful place to live.

I owe a significant debt of gratitude to my parents and my sister, who have always been understanding and supportive of my pursuit of physics overseas. Despite the distance between us, their love and belief in me have kept me motivated and focused.

Finally, I am deeply indebted to Plago (Chu-Yun) Chen, who gave me constant encouragement during my darkest time in graduate school before I joined David's group. I consider myself exceptionally fortunate to have had her patience and uplifting support: tirelessly exploring various avenues to motivate me and consistently reminding me to dream big. Without her company and encouragement, I would not have been able to complete the journey.

Chapter 1

Introduction

1.1 Definition of the heat index

The heat index, also known as the "feels like" temperature, is a measure of how hot it feels when humidity is factored in with the actual air temperature. In other words, it is an index that combines air temperature and humidity to provide a metric of how warm the air actually feels to the human body. Defined in 1979 by Robert G. Steadman [97], the heat index is based on a model of human thermoregulation, and each value maps to a unique physiological and behavioral state of the human, including the amount of clothes the human wears and the rate of skin blood flow between the core and the skin of the human. Precisely, the heat index is the temperature, with the "normal" water-vapor pressure of 1.6 kPa, that would induce the same behavioral/physiological state as that induced by the actual air temperature and humidity.

For example, to compute the heat index for a given combination of air temperature T_a and water-vapor pressure p_v, we first use Steadman's human model to calculate the physiological state it induces. Then, we move this human model to a "normal" environment where the water-vapor pressure is fixed at $p_{v0} = 1.6$ kPa, and we search for an air temperature T in this environment that would induce the same physiological state. The temperature T is called the heat index for T_a and p_v. Because the human model is in the same physiological state in both scenarios, (T_a, p_v) and (T, p_{v0}), it should feel the same in either case. That is why the heat index is also known as the "feels like" temperature.

Here is an example with some actual numbers: at air temperature of 300 K and water-vapor pressure of 3.0 kPa (relative humidity of 85%), the human model will run a skin blood flow of 0.7 liter per minute between its core and skin. In the normal scenario where the water-vapor pressure is fixed at 1.6 kPa, the air temperature has to be as high as 303 K to induce the same amount of skin blood flow (0.7 liter per minute). So the heat index is 303 K for the air temperature of 300 K and the water-vapor pressure of 3.0 kPa. In this case, the heat index is higher than the actual air temperature. This is because when the air is humid, the body's ability to cool itself through sweat evaporation is reduced, making the air

temperature feel warmer than it actually is. Notice that if the actual environment happens to have a water-vapor pressure of 1.6 kPa, the heat index will be identical to the actual air temperature.

1.2 Existing problems of the heat index

For decades, weather agencies (including United States National Weather Service) have relied on the heat index to communicate the health risk due to high heat and humidity. However, the heat index has had two major deficiencies: the heat index was not defined at high temperature and humidity, and it has not been validated against laboratory data.

Undefined at high temperature and humidity

The heat index was never defined at high temperature and humidity because the underlying human model would give unphysical results. At high temperature and humidity, the sweating rate would exceed the evaporating rate, but Steadman's model does not allow the excess sweat to drip off, causing the algorithm to generate a supersaturated water-vapor pressure near the skin. In chapter 2, we identify this problem and present a simple yet physical fix to the model: allowing sweat to drip off the skin while keeping the water-vapor pressure at the saturated level. That's it. The fix is simple and is probably the most natural way to fix the problem. However, in 1970s, an undefined heat index was a rare event, and this fix might not have been as urgent as it is now. In the present day, global warming is increasing the frequency of occurrence of an undefined heat index, making an extension of the heat index necessary. By applying the aforementioned fix to Steadman's model, we can define the heat index for all higher temperature and humidity. Similar to the existing heat index, the extended part also maps to several physiological states of the human, but this time they are debilitating states under extreme heat stress, such as hyperthermia or even heat death. The mapping between the extended heat index and the health outcomes of the human provides a tool to assess the health risk at different levels of global warming. In chapter 2, we also extend the heat index to cover conditions with low temperature and humidity for mathematical completeness. When the air temperature is sufficiently low, the heat index, which is the air temperature in the normal environment having a fixed water-vapor pressure of 1.6 kPa, would drop below the dew-point temperature. This is, of course, unphysical. A natural fix is to re-define the reference water-vapor pressure p_{v0} in the normal state to be the saturation vapor pressure at the temperature equal to the heat index. Defined this way, the heat index will be both continuous and physically sound.

Figure 1.1 shows the timeline for the history of the heat index. In 1979, Steadman introduced the heat index for the first time, albeit with undefined values at high temperature and humidity. Recently, in 2022, the heat index has been extended to encompass all conditions, as elaborated in chapter 2. However, discussions about the heat index frequently involve references to the Rothfusz polynomial. This polynomial was developed by Lans P. Rothfusz,

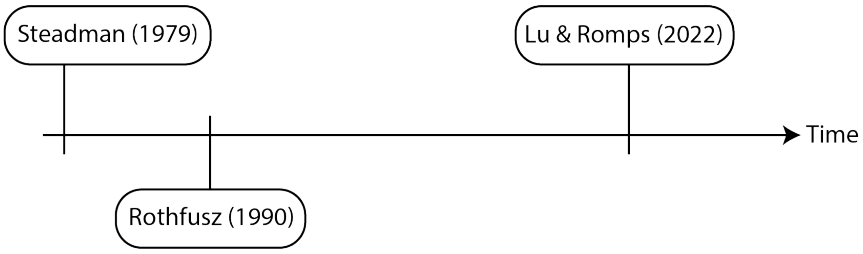

Figure 1.1: The timeline showing the history of the heat index. In 1979, Steadman introduced the heat index for the first time, albeit with undefined values at high temperature and humidity. In 1990, Rothfusz used Steadman's heat index to make a polynomial approximation. In 2022, Lu and Romps extended the heat index to cover all temperature and humidity.

who published a technical report on it in 1990 [83], which was motivated by a high demand for a simpler way to calculate the heat index. According to the report, during the summertime, the National Weather Service (NWS) received numerous phone calls about how to compute the heat index. The standard responses provided by the NWS - "it is derived from a collection of equations that comprise Steadman's model," "it is extremely complicated," or "go look up Steadman's heat-index table" - were not satisfactory to some people. As a result of frequent demands for a simple equation to compute the heat index, Rothfusz devised a solution: he used the heat-index values from Steadman's table, performed multiple regression analysis, and obtained the following polynomial:

$$\begin{aligned}\mathrm{HI} = &-42.379 + 2.04901523T + 10.14333127R - 0.22475541TR \\ &- 6.83783 \times 10^{-3}T^2 - 5.481717 \times 10^{-2}R^2 + 1.22874 \times 10^{-3}T^2R \\ &+ 8.5282 \times 10^{-4}TR^2 - 1.99 \times 10^{-6}T^2R^2,\end{aligned}$$

where T is the air temperature in Fahrenheit, R is the relative humidity in percentage, and HI is the heat index in Fahrenheit. In his technical report, Rothfusz emphasized that there is no true equation for the heat index, and that the polynomial he derived was intended for those who were dissatisfied with the existing methods. By construction, the polynomial only provides an approximation for the heat index values defined in Steadman's work, and it cannot predict the values that were not defined. Nevertheless, the polynomial has become widely adopted to *extrapolate* the heat index values that Steadman had not defined (those at high temperature and humidity), even by the National Weather Service itself[1].

The consequence of using the polynomial extrapolation is: it underestimates the heat index.

[1]Recently, NWS added some correction terms to reduce the error between Steadman's heat index and the polynomial fit [63]. However, despite the inclusion of these correction terms, the extrapolated values still deviate significantly from the actual heat index values. See chapter 2 for discussion.

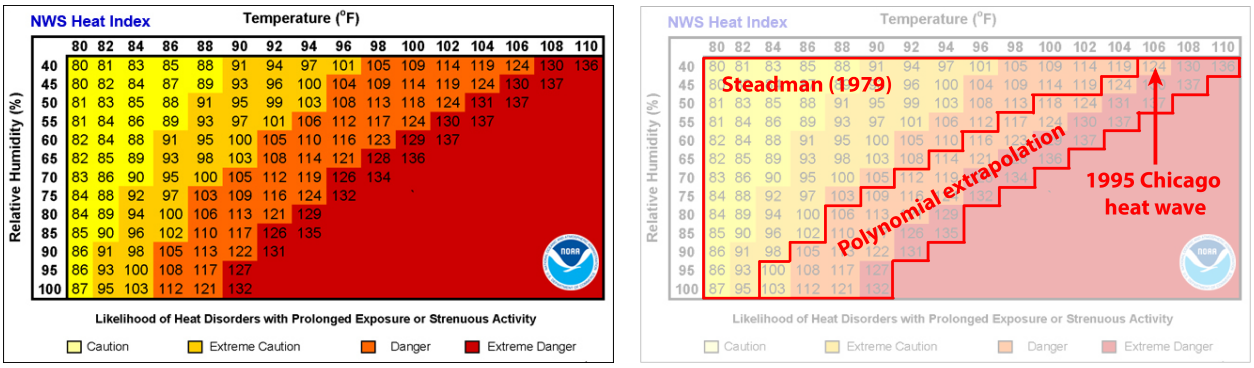

Figure 1.2: (left) Heat index chart from National Weather Service. (right) Same, but with annotations: the upper left portion labeled by "Steadman (1979)" are heat indices defined in Steadman's original work, the middle section labeled by "Polynomial extrapolation" are heat indices calculated using NWS polynomial, and the arrow with label "1995 Chicago heat wave" points to the extrapolated heat index reported during the heat wave.

The reader may ask: "Why does it matter if the heat index is underestimated?" "After all, the heat index is just the temperature it feels like. Is there a difference between hot and very hot?" It is true that the heat index is a perceived temperature, but in addition to that, the heat index also has a one-to-one mapping between the climate and the physiology of the human. In the extrapolated heat index, this mapping is simply lost. As shown in chapter 3, during the fatal 1995 Chicago heat wave, the highest heat index recorded according to NWS polynomial was 324 K [62], while the actual heat index was 334 K. Using the mapping between the heat index and physiology, we find that 324 K maps to a skin blood flow that is 90% higher than normal, while 334 K maps to an 170%-higher-than-normal skin blood flow. Reanalysis (a climate model that computes the meteorological variables between physical weather stations) shows that the discrepancy of the implied skin blood flow was even larger elsewhere in Illinois during the 1995 heat wave, with the required skin blood flow elevated by 120% according to the NWS polynomial, but elevated by 820% according to the actual heat index. Such high skin blood flows put a high demand on cardiac outputs, and are difficult to endure for elderly individuals or those with cardiovascular disease. In 1995, the Chicago heat wave killed more than 500 people, many of whom were elderly [14]. Had the actual heat index been forecasted with a warning about its health risk, the outcome could have been different.

As of today, the National Weather Service continues to employ the polynomial in their heat index calculations, as seen in the left panel of Figure 1.2, which displays the heat index chart from their website [60]. This chart uses the air temperature in Fahrenheit as the abscissa, relative humidity in percentage as the ordinate, and the color-coded numbers are the heat indices in Fahrenheit. While the chart appears to have undefined values at high temperatures and humidity levels, it does not adhere to Steadman's original work. The

right panel of Figure 1.2 displays the same chart but with some annotations. The upper left portion labeled "Steadman (1979)" shows the heat indices defined in Steadman's work. The middle section, labeled "Polynomial extrapolation," displays extrapolated heat indices using the NWS polynomial. The NWS uses the polynomial to some extent to extrapolate the heat index at high temperature and humidity, but for unknown reasons, it stops at even higher levels. The right panel also shows an arrow labeled "1995 Chicago heat wave," which points to the extrapolated heat index of 124 °F (or 324 K) reported during the heat wave, along with the air temperature (106 °F) and relative humidity (40%) at that time.

The readers may have noticed that NWS heat index chart also has four color-coded ranges, each labeled with a corresponding legend, such as "danger" and "extreme danger." These will be explained in the next section.

Not validated against laboratory data

Another long-lasting problem of the heat index is that it has never been validated by laboratory data. For this reason, in 2020 an administrative judge in the United States overturned fines that the Occupational Safety and Health Administration (OSHA) had imposed on the United States Postal Service (USPS).

In 2016 and 2017, OSHA issued five citations to the USPS, alleging that their employees had been exposed to hazardous levels of heat [87]. During the trial, OSHA presented the NWS heat index chart (the left panel of Figure 1.2) as evidence. In this chart, the heat index is color-coded into four ranges, with a corresponding legend titled "Likelihood of Heat Disorders With Prolonged Exposure or Strenuous Activity," asserting that those ranges correspond to conditions warranting "caution," "extreme caution," "danger," and "extreme danger." OSHA accused USPS of failing to maintain a safe workplace for its employees by allowing them to be exposed to a heat index at or above the "danger" range.

During the course of the defense, USPS's lawyers discovered that although the numbers in the NWS heat index chart were based on the work of Steadman and Rothfusz, there was no scientific source for the color-coded ranges and the corresponding warrants, and the NWS had not publicly disclosed the source for them either. Later, an expert witness for OSHA claimed that the source of the ranges was an article in a popular magazine on weather and climatology by Quayle and Doehring [74], titled "Heat Stress: A Comparison of Indices." While the article did mention the ranges and warrants, they were not supported by any source, and the article itself had not been peer-reviewed. USPS then argued that the four ranges of the NWS's heat index chart lacked a scientific basis and should be disregarded.

On July 15, 2020, Judge Sharon Calhoun agreed with USPS and held that "no evidence was presented to establish the scientific basis for the risk categories depicted on the NWS heat index chart." As a result of this finding, Judge Calhoun vacated all five citations [11].

Clearly, the heat index needs empirical testing and validations.

In chapter 4, we will use the experimental data collected recently by physiology experts at Penn State [111] to validate the heat index.

In that experiment, participants were put in a hot climate chamber where the temperature or humidity was slowly increased, and the combination of temperature and humidity that caused the onset of hyperthermia was recorded. The standard heat index is not suitable for this scenario because it assumes a wind speed of 1.5 m s^{-1}, while the indoor wind speed is only about 0.2 m s^{-1}. Additionally, the standard heat index assumes a metabolic rate of 180 W m^{-2}, whereas the participants in the experiment exerted at two lower metabolic rates of 82.9 and 133 W m^{-2}, respectively. However, by slightly modifying the heat-index model to account for the indoor wind speed and the measured metabolic rates of the participants, we are able to use the heat-index model to accurately predict the combinations of temperature and humidity that cause hyperthermia. This is the first time the heat index has been validated against physiological data from laboratory experiments. As shown in chapter 4, for light and moderate exertion in an indoor setting, the heat-index model predicts that hyperthermia would occur at the (extended) heat-index of 345 K, consistent with the experimental results. Using these experiments, the heat index has received its empirical validation.

1.3 Survivability thresholds

In the field of climate science, various metrics are used to establish thresholds for human livability or survivability, and the most popular one is probably the wet-bulb temperature. Proposed by Sherwood and Huber [93], a wet-bulb temperature of 35 °C is thought to be the threshold for human survivability, despite the fact that the argument lacks many considerations of human physiology. According to its definition, the wet-bulb temperature is the equilibrium temperature of a wet thermometer under infinite wind speed. Therefore, if a human is a dead body covered by sweat in a hurricane wind, the wet-bulb temperature is a good description of it. However, for living humans exposed to finite wind speeds, we need to consider metabolism that would heat up the body, and there is also an infrared radiation heat exchange between the skin and the environment. As proved mathematically in chapter 4, with the consideration of these factors, there does not exist any single wet-bulb temperature that predicts the survivability of the human.

On the other hand, the heat index takes into accounts metabolism of the human, finite wind speed and the infrared radiation. The heat-index model and the threshold corresponding to hyperthermia have also been validated against data from physiological experiments. In chapter 5, we will show that the wet-bulb temperature of 35 °C overestimates the occurrence of heat death, but underestimates the occurrence of hyperthermia. For example, in a world warmer than pre-industrial by 10 K, the best estimate is that 30% of the world's population would be exposed once or more per year to a wet-bulb temperature above 35 °C, but less than 2% would be exposed to fatal conditions and over 60% would be exposed to conditions that would cause hyperthermia.

1.4 Outline

This dissertation is structured around the development and validation of the heat index as a tool for assessing human heat stress.

In chapter 2, we review and extend the existing heat index developed by Steadman to cover all combinations of temperature and humidity. Chapter 3 investigates the consequences of using the NWS extrapolated heat index, with a focus on historical heat waves in the United States, including the 1995 Chicago heat wave. In chapter 4, we use physiological empirical data to validate the heat-index model and its thresholds, establishing a scientific basis for the first time. Finally, in chapter 5 we complete the dissertation by reviewing the traditional threshold of human survivability in climate science - the wet-bulb temperature of 35 °C - and demonstrate how the extended heat index offers a more sophisticated approach that accounts for human physiology.

Regarding the content of the thesis, chapter 2 has been published in the *Journal of Applied Meteorology and Climatology* [49], chapter 3 is published in the *Environmental Research Letters* [82], and chapter 4 is published in the *Journal of Applied Physiology* [50]. Chapter 5 is currently in review at a journal, and would be published in a form similar to its current state.

Chapter 2

Extending the Heat Index

2.1 Introduction

For a given combination of air temperature and humidity, the Heat Index is the air temperature at a reference water-vapor pressure of 1.6 kPa that would be experienced in the same way by a human. The Heat Index is calculated from a model of human thermoregulation assuming optimal physiology (with regards to the core-to-skin blood flow and sweat rate), optimal behavior (with regards to the choice of clothing), and optimal circumstances (in the shade with unlimited water). The Heat Index thus defined is widely used in the United States to communicate the health risk associated with high heat and humidity.

Despite its utility, the Heat Index is defined only within certain bounds of temperature and humidity due to some unphysical conditions occurring in the underlying human model when pushed outside those bounds [97]. For example, at a relative humidity of 80%, the Heat Index is not defined for temperatures above 304 K (31 °C, 88 °F) or below 288 K (15 °C, 59 °F) because the vapor pressure at the skin or in the air becomes supersaturated. These unphysical conditions will be discussed in detail later. To circumvent these problems, polynomial fits are often used to extrapolate the Heat Index to higher temperatures [5, 83], including by the National Weather Service [63], but those extrapolations have no basis in science.

In the current climate, the Heat Index is undefined over large swaths of the Earth at any given moment on average, mainly due to cold conditions, but also on occasion due to hot and humid conditions. As an example, Figure 2.1 shows the occurrence frequency for each near-surface temperature-humidity combination at the Department of Energy's Atmospheric Radiation Measurement (ARM) Southern Great Plains (SGP) site [53] measured every minute during June, July, and August (JJA) from 2012 to 2021, inclusive. The hatched areas are where the existing Heat Index is undefined. In the current climate, 5% of these nine hundred and twenty SGP summer days have an undefined Heat Index due to sufficiently cold and dry conditions, but only 0.9% of the summer days have an undefined Heat Index due to sufficiently hot and humid conditions. To estimate how often an undefined Heat Index would

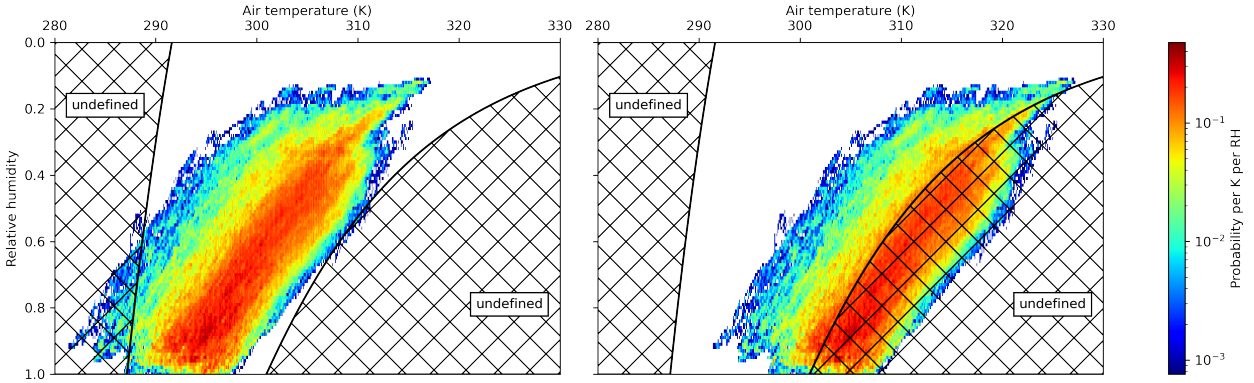

Figure 2.1: (left) Joint probability density of near-surface one-minute air temperature and relative humidity at the ARM SGP site during June, July, and August from 2012 to 2021. The hatched regions show where the Heat Index is undefined. (right) Same, but translating the density to warmer temperatures by 10 K, representing conditions that could be achieved in the 22nd century with business-as-usual fossil-fuel burning.

occur at a substantially different temperature anomaly (e.g., in a business-as-usual scenario in the 22nd century), we add 10 K to the JJA temperature while keeping the humidities unchanged. The peak of the distribution shifts out of the defined region, causing 91% of the SGP summer days to have an undefined Heat Index. Even a more modest +5 K warming (not shown) would cause the Heat Index to be undefined at some point during 39% of the SGP summer days.

To quantify future conditions using the Heat Index, it is necessary to extend the existing definition. Previous studies have used the Heat Index to explore warming scenarios [e.g., 4, 19, 21, 25, 26, 56, 69, 75, 77], but those studies used the aforementioned polynomial extrapolation and, therefore, they have relied on extrapolated values that have no grounding in physiology and no basis for interpretation with regards to health impacts. In this thesis, we aim to extend the Heat Index by correcting the underlying model of thermoregulation.

While several different "apparent" or "equivalent" temperatures have been proposed, we focus on the Heat Index, as defined by Steadman [97], because it is widely used and, unlike other apparent temperatures, Steadman's underlying model of human thermoregulation does not depend on uncertain physiological relations. Instead, Steadman's model assumes an ideal human and requires only easily measured physical parameters such as body mass, skin area, metabolic rate, and tissue conductance. Because the Heat Index is so widely used, one of the goals here is to ensure backwards compatibility; that is, we wish to extend the Heat Index to cover all conditions without affecting the Heat Index values already in use. In so doing, we adopt Steadman's original approach of assuming optimal behavior, physiology, and circumstances. This assumes a best-case scenario with regards to a human's physical conditioning and access to water and shade: no limits are placed on the human's capacity to

sweat or pump blood to the skin, it is assumed that the human's behavior with regards to choice of clothing is optimal, and the human is assumed to be in the shade with unlimited drinking water. For consistency, we use these same ideal assumptions when extending the Heat Index. Therefore, the thermoregulation model presented here, as with the original, represents an upper limit on the capacity of humans to endure high heat and humidity.

2.2 Derivation of the Heat Index

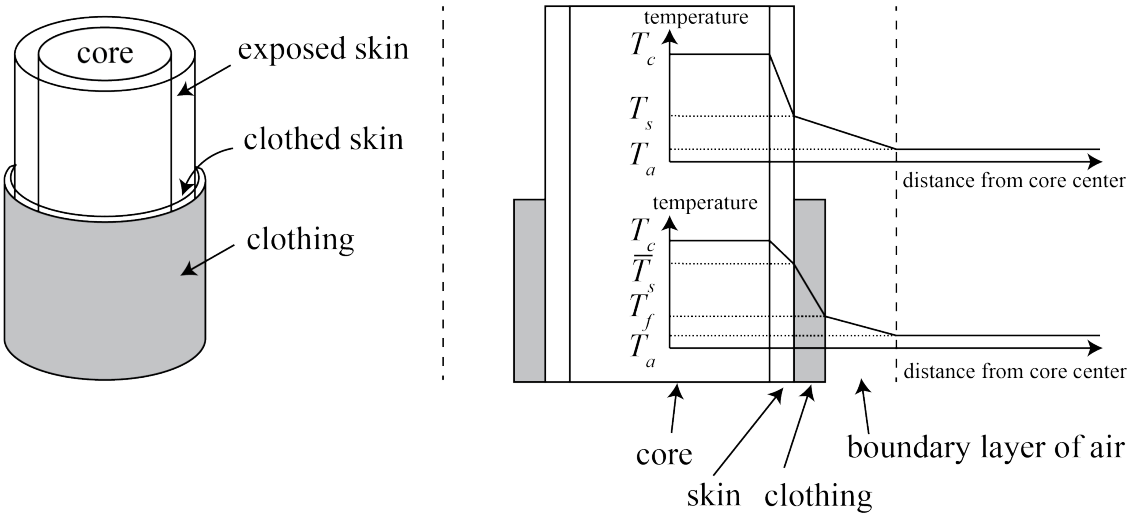

Figure 2.2: (left) The geometry of the human model, with the core, exposed skin, clothed skin and clothing labeled. (right) The cross-sectional view of the human model, with the boundary layer of air drawn explicitly. On top of the cross-sectional view are illustrative temperature distributions along the radial direction of the human model through exposed skin (top axes) and through clothed skin (bottom axes).

In Steadman's model of human thermoregulation, the human is modeled as an interior core (with temperature T_c) covered by a combination of exposed skin (with exterior temperature T_s) and clothed skin (with exterior temperature $\overline{T}_s$), as shown in Figure 2.2. The clothed skin occupies a fraction ϕ of the total skin area, and is covered with clothing (with exterior temperature T_f, whose subscript f denotes "fabric"). Each of these components also has its own vapor pressure at its outermost layer, denoted by p_c, p_s, $\overline{p}_s$ and p_f, where the vapor pressure of the core p_c is understood as the saturation vapor pressure of the saline solution in the human body. The skin, clothing, and boundary layer of air around the human are assumed to be sufficiently thin that their storage (or tendencies) of energy and water can be ignored. (Here and throughout, "boundary layer" refers to the layer of turbulent air in the vicinity of the human's skin and clothing, not the atmospheric boundary layer between

the Earth's surface and free troposphere.) Denoting the air temperature and vapor pressure by T_a and p_a, there are seven equations expressing conservation of energy and water mass,

$$0 = Q - Q_v - \phi\frac{T_c - \overline{T}_s}{R_s} - (1-\phi)\frac{T_c - T_s}{R_s} \quad \text{(energy of steady-state core)} \tag{2.1}$$

$$0 = \frac{T_c - T_s}{R_s} - \frac{T_s - T_a}{R_a} - \frac{p_s - p_a}{Z_a} \quad \text{(energy at exterior of exposed skin)} \tag{2.2}$$

$$0 = \frac{T_c - \overline{T}_s}{R_s} - \frac{\overline{T}_s - T_f}{R_f} - \frac{\overline{p}_s - p_f}{Z_f} \quad \text{(energy at exterior of clothed skin)} \tag{2.3}$$

$$0 = \frac{\overline{T}_s - T_f}{R_f} - \frac{T_f - T_a}{\overline{R}_a} \quad \text{(energy at exterior of clothing)} \tag{2.4}$$

$$0 = \frac{p_c - p_s}{Z_s} - \frac{p_s - p_a}{Z_a} \quad \text{(water at exterior of exposed skin)} \tag{2.5}$$

$$0 = \frac{p_c - \overline{p}_s}{Z_s} - \frac{\overline{p}_s - p_f}{Z_f} \quad \text{(water at exterior of clothed skin)} \tag{2.6}$$

$$0 = \frac{\overline{p}_s - p_f}{Z_f} - \frac{p_f - p_a}{\overline{Z}_a} \quad \text{(water at exterior of clothing)}\,, \tag{2.7}$$

where the R and Z variables denote heat transfer resistance and mass transfer resistance, respectively. Specifically, R_s is the resistance to heat flux by the skin (exposed or clothed), R_f the clothing resistance, R_a the resistance of the air's boundary layer around the exposed skin, and $\overline{R}_a$ is the resistance of the boundary layer around the clothing. Similar definitions apply to Z_s, Z_f, Z_a and $\overline{Z}_a$, which give the resistance to water flux. The convention here is that the barred variables are those pertaining to clothing while exposed skin is represented by unbarred quantities. The expressions of R and Z variables are taken from Steadman [97], and are summarized in Tables 2.2-2.5, with the exception that the exact T^4 longwave radiation expression is used instead of the linearized equation to account for the full range of air temperatures.

The seven governing equations can be understood as follows. Equation (2.1) is the equation for conservation of energy in the steady-state core; if we were not assuming steady state, a term proportional to dT_c/dt would appear on the left-hand side. The sources and sinks of energy for the core are the metabolic rate, ventilative cooling, and the transfer of sensible heat from the core to the clothed and unclothed skin. The constant Q is the metabolic rate per skin area and Q_v is the cooling per skin area within the lungs due to ventilation (a.k.a., breathing) defined by [30, 97]

$$Q_v \equiv \eta Q\Big[c_{pa}(T_c - T_a) + \frac{L\hat{R}_a}{\hat{R}_v p}(p_c - p_a)\Big]\,, \tag{2.8}$$

where η is a constant relating metabolic rate to ventilation rate, the constants $\hat{R}_a$ and $\hat{R}_v$ are the specific gas constants of air and vapor (which are given hats to distinguish them from the resistances), c_{pa} is the heat capacity of air at constant pressure, and L is the latent heat of

vaporization at the core temperature T_c. Equation (2.2) expresses the sensible heat budget of the surface of the exposed skin. The infinitesimally thin surface of the skin has zero heat capacity and zero capacity for storing water, and the skin and boundary layer are likewise assumed to have zero heat capacity and zero capacity for storing water. Therefore, there are no tendency terms and the statement of conservation of energy reduces to the requirement that the fluxes are equal on either side of the skin surface. In this way, the temperature of the exposed skin surface is determined diagnostically, i.e., by solving algebraic equations rather than solving differential equations. Note that the exposed skin has three heat sources that must balance at every moment: heat transferred through the skin (by conduction through tissue and transport by blood), heat lost through the air's boundary layer (by conduction and advection), and evaporative cooling of sweat (by conductive and advection of water vapor through the boundary layer). Equation (2.3) gives a similar governing equation for clothed skin, except that the clothed skin transfers heat and water vapor through the clothing instead of through the boundary layer. Like the skin, the clothing is treated as having zero heat capacity, so its exterior temperature T_f is set diagnostically by equation (2.4), which states that the rate of sensible heat passing through the clothing (from the exterior of the clothed skin at $\overline{T}_s$ to the exterior of the clothing at T_f) must equal the rate of sensible heat passing through the boundary layer (from the exterior of the clothing at T_f to the ambient air at T_a). Equations (2.5–2.7) express continuity of mass fluxes at the exterior surfaces of the exposed skin, clothed skin, and clothing, respectively. As will be discussed later, the fabric resistance R_f and Z_f are proportional to the clothing thickness, and the skin resistance R_s and Z_s are related to the skin blood flow, which controls the heat and mass transfer between the core and the skin.

Table 2.1 defines some of the parameters mentioned above that are used in our extended version of Steadman's model. The parameters describing the thermodynamic properties of water are optimized to give the best fit of the analytical saturation vapor pressure to experimental values [81]. In terms of these constants, the saturation vapor pressure p^* is given by

$$p^*(T) = \begin{cases} p_{\text{trip}} \left(\dfrac{T}{T_{\text{trip}}} \right)^{\frac{c_{pv}-c_{vl}}{\hat{R}_v}} \exp\left[\dfrac{E_{0v} - (c_{vv}-c_{vl})T_{\text{trip}}}{\hat{R}_v} \left(\dfrac{1}{T_{\text{trip}}} - \dfrac{1}{T} \right) \right] & T \geq T_{\text{trip}} \\ p_{\text{trip}} \left(\dfrac{T}{T_{\text{trip}}} \right)^{\frac{c_{pv}-c_{vs}}{\hat{R}_v}} \exp\left[\dfrac{E_{0v} + E_{0s} - (c_{vv}-c_{vs})T_{\text{trip}}}{\hat{R}_v} \left(\dfrac{1}{T_{\text{trip}}} - \dfrac{1}{T} \right) \right] & T < T_{\text{trip}} \end{cases}, \tag{2.9}$$

which replaces the linearized equation used in Steadman [97].

Table 2.1: Constants that are common to all six regions.

Variable	Value	Interpretation
T_{trip}	273.16 K	Triple-point temperature
p_{trip}	611.65 Pa	Triple-point pressure
E_{0v}	2.3740 $\times 10^6$ J kg^{-1}	Difference in energy between vapor and liquid at the triple point
E_{0s}	0.3337 $\times 10^6$ J kg^{-1}	Difference in energy between liquid and solid at the triple point
$\hat{R}_a$	287.04 J kg^{-1} K^{-1}	Specific gas constant of air
$\hat{R}_v$	461 J kg^{-1} K^{-1}	Specific gas constant of vapor
c_{va}	719 J kg^{-1} K^{-1}	Heat capacity of air at constant volume
c_{vv}	1418 J kg^{-1} K^{-1}	Heat capacity of vapor at constant volume
c_{vl}	4119 J kg^{-1} K^{-1}	Heat capacity of liquid at constant volume
c_{vs}	1861 J kg^{-1} K^{-1}	Heat capacity of solid at constant volume
c_{pa}	$c_{va} + \hat{R}_a$	Heat capacity of air at constant pressure
c_{pv}	$c_{vv} + \hat{R}_v$	Heat capacity of vapor at constant pressure
L	$E_{0v} + (c_{vv} - c_{vl})[(310\text{ K}) - T_{\text{trip}}]$	Latent enthalpy of evaporation at 310 K
p_{a0}	1.6 $\times 10^3$ Pa	Reference vapor pressure for the Heat Index [97]
M_c	83.6 kg	Mass of the core, taken as the average of the masses of adult men and women in the United States during 2015-2016 [34]
H	1.69 m	Height, taken as the average of heights of adult men and women in the United States during 2015-2016 [34]
A	$(0.202\text{ m}^2)\left(\frac{M_c}{1\ kg}\right)^{0.425}\left(\frac{H}{1\ m}\right)^{0.725}$	Area of the skin [71]
c_{pc}	3492 J kg^{-1} K^{-1}	Specific heat capacity of the core at constant pressure [36]
Q	180 W m^{-2}	Metabolic rate per skin area for walking [64, 97]
ϕ_{salt}	0.9	Effective relative humidity of saline solution [10, 97]
p	1.013 $\times 10^5$ Pa	Air pressure
η	1.43 $\times 10^{-6}$ kg J^{-1}	Ratio of ventilation rate (kg/s) to metabolic rate (J/s) [30]
σ	5.67$\times 10^{-8}$ W m^{-2} K^{-4}	Stefan-Boltzmann constant

Given T_a, p_a, ϕ, the resistances R_s and R_f, and the fact that $p_c = \phi_{\text{salt}} p^*(T_c)$, there are seven unknowns (T_c, T_s, p_s, $\overline{T}_s$, $\overline{p}_s$, T_f and p_f) and seven equations (2.1–2.7). (As we will see, the variables R_a, $\overline{R}_a$, Z_a, $\overline{Z}_a$, Z_s and Z_f are all functions of some combination of these seven unknowns and/or other specified parameters.) In general, however, solving these seven equations will give a core temperature T_c that is far from the desirable equilibrium value of 310 K. Since human biochemistry functions only when the core temperature is within a narrow range of a few degrees, this is clearly not how the human body works. Instead, the body relies on a combination of behavioral and physiological mechanisms to maintain a stable and standard core temperature. Mathematically, those mechanisms manifest as the introduction of an eighth equation,

$$T_c = 310 \text{ K}\,, \tag{2.10}$$

and, to ensure the system is not overdetermined, the conversion of a constant (e.g., R_s or R_f) to a variable. Solving those eight equations in eight unknowns gives not just the temperatures and vapor pressures of the clothing and skin, but also the ideal behavioral or physiological "choice" for the new variable. For example, in very cold conditions, the ideal behavioral response to a change in temperature would be to add or subtract layers of clothing so that the corresponding value of R_f solves the seven original equations plus $T_c = 310$ K. Or, in very hot and humid conditions, the ideal physiological response to a change in temperature or humidity would be to change the core-to-skin blood flow so that the corresponding value of R_s gives $T_c = 310$ K. In what follows, we will identify the physiological/behavioral adaptations that an ideal human would use in each of six disjoint subsets or "regions" of temperature-humidity pairs spanning temperature-humidity space (i.e., all combinations of temperature and humidity).

The original Heat Index is defined in what we refer to here as regions III and IV, in which an ideal human chooses to be clothed or naked, respectively. As acknowledged in the original paper [97], Steadman's model gives unphysical results when the air temperature becomes too cold (at the cold boundary of region III) or too warm (at the hot boundary of region IV). When the air temperature falls below 287 to 292 K (the precise value depends on the relative humidity), the Heat Index fails because the reference vapor pressure of 1.6 kPa exceeds the saturation vapor pressure at the temperature equal to the Heat Index. When the air temperature rises above 301 to 350 K (again, depending on the relative humidity), the Heat Index fails again, this time because the skin's vapor pressure exceeds its saturation vapor pressure. In the following derivations, we start from region III and extend the Heat Index from its cold end into the new regions II and I. We then move to region IV and extend the Heat Index from its warm end into regions V and VI, which are the main focus of this thesis.

Regions II and III: Clothed

Steadman [97] gave a simplified schematic of the equations of energy and mass conservation using circuits. The analogy to circuits allows for a visualization of the entire equation set

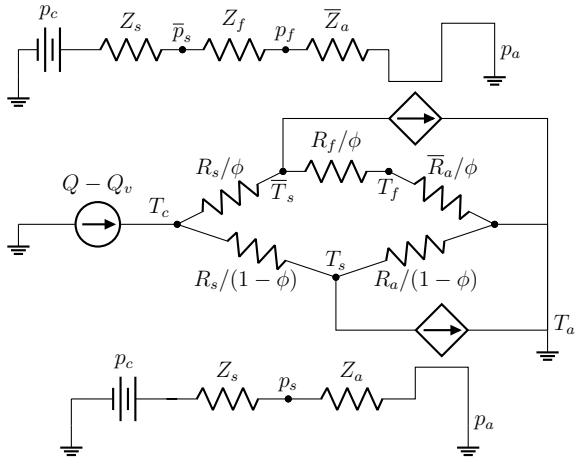

Figure 2.3: Diagram illustrating the potentials and resistances for sensible heat transfer (middle circuit) and water transfer (top and bottom circuits), with all three circuits applying to both regions II and III. Region III is one of the two original cases of Steadman [97]. Region II is where we extend the Heat Index by using $p_a = p^*(T_a)$ instead of $p_a = 1.6$ kPa for the reference pressure. The controlled current sources represent evaporative cooling, which is controlled by the current in the water-transfer circuits. Subscripts c, s, f, and a denote core, skin, fabric, and air, respectively, with temperatures and vapor pressures denoting values at the outermost edges of those components.

in a compact diagram, so we will present the circuit diagrams for each of the six regions. The most complicated of these circuit diagrams represents region III and is shown in Figure 2.3. From top to bottom, the three circuits represent: 1. the transfer of water mass through clothed skin and clothing (where "current" is the rate of vapor mass transfer and "potential" is the vapor pressure), 2. the transfer of sensible heat through both clothed and exposed skin (where "current" is the rate of heat transfer and "potential" is the temperature), and 3. the transfer of water mass through exposed skin. As water passes from skin to either the clothing or the air, it evaporates, generating an evaporative cooling that is represented by a controlled current source in the middle circuit. The current (of sensible heat) passing through those controlled current sources is proportional to the respective current (of water mass); this is represented by the vapor-pressure terms in equations (2.2) and (2.3), which express conservation of energy for the exposed and clothed skin.

In the middle circuit, there is a fixed current source in the core representing the net generation of sensible heat there ($Q - Q_v$). That "current" must pass out to the environment at temperature T_a through some combination of evaporative cooling from the skin (as dictated by the other two circuits) or conduction of sensible heat through either the clothing or exposed skin. The node labeled with temperature T_c is just a point in the circuit and, like a point on a wire in a real electrical circuit, cannot store current. Therefore, Figure 2.3

represents the equilibrated solution to equations (2.1–2.7).

In this circuit, imagine that the potentials p_a and T_a are given and that we also specify the clothing fraction ϕ and the various resistances. In this case, the values of T_c, T_s, p_s, $\overline{T}_s$, $\overline{p}_s$, T_f, p_f in this circuit (which one could measure in a real electrical circuit with a voltmeter) would be the steady-state solution to equations (2.1–2.7). For an arbitrarily chosen values of ϕ and the resistances, however, this would likely to give a core temperature T_c that is incompatible with life.

In region III, the fix is to allow the human to choose R_f by wearing an appropriate number and type of clothing layers. By letting R_f be a free variable, we are free to peg the core temperature to the standard value. In other words, the equation set governing the ideal human in region III is equations (2.1–2.7) and (2.10), and the variables to be solved for are the original seven plus R_f. The parameters used in region III are given in Table (2.2). These are mainly taken directly from Steadman [97] to maintain backwards compatibility of our Heat Index with the one that has been in use for several decades. Minor modifications have been made, however, to allow the Heat Index to be extended to a much wider range of temperatures. For example, as mentioned before, the full non-linear T^4 expression for longwave emission is retained instead of using the linearized expression in Steadman [97]. The Appendix describes how to solve the equations numerically for this region and the others.

In region III, the Heat Index is the value of T_a that would give the same R_f at the reference pressure of $p_a = p_{a0} \equiv 1.6$ kPa. For a T_a that is sufficiently low, p_{a0} will be greater than $p^*(T_a)$, and the Heat Index becomes unphysical. To extend the Heat Index to lower temperatures, we define the reference vapor pressure as $p_a = p^*(T_a)$ in region II. Stated another way, the Heat Index in regions II and III is the T_a that would give the same R_f with $p_a = \min[p_{a0}, p^*(T_a)]$. Given R_f and the requirement that $p_a = \min[p_{a0}, p^*(T_a)]$, we can solve for T_a by using a root solver to find the T_a that gives, using the procedure above, the correct R_f.

Table 2.2: Variables and constants for regions II and III.

Variable	Value	Interpretation
R_f	variable	Resistance to heat transfer through the clothing
T_c	310 K	Core temperature
p_c	$\phi_{\text{salt}} p^*(T_c)$	Core vapor pressure
ϕ	0.84	Fraction of skin covered by clothing [97]
R_s	0.0387 m^2 K W^{-1}	Resistance to heat transfer through the skin [97]
Z_s	52.1 m^2 Pa W^{-1}	Resistance to water transfer through the skin [97]
Z_f	rR_f	Resistance to water transfer through the clothing [97]
r	124 Pa K^{-1}	Ratio of Z_f and R_f [97]
R_a	$\left[\phi_{\text{rad}}\epsilon\sigma(T_s^2+T_a^2)(T_s+T_a)+h_c\right]^{-1}$	Resistance to heat transfer through the boundary layer of air in contact with exposed skin
Z_a	$\left(60.6 \text{ Pa K}^{-1}\right)/h_c$	Resistance to water transfer through the boundary layer of air in contact with exposed skin [97]
h_c	17.4 W K^{-1} m^{-2}	Heat transfer coefficient between surface of exposed skin and air [97]
ϕ_{rad}	0.85	Effective fraction of exposed skin exchanging longwave radiation with air (or surfaces with temperature T_a) [97]
ϵ	0.97	Longwave emissivity of exposed skin [97]
$\overline{R}_a$	$\left[\overline{\phi}_{\text{rad}}\overline{\epsilon}\sigma(T_f^2+T_a^2)(T_f+T_a)+\overline{h}_c\right]^{-1}$	Resistance to heat transfer through the boundary layer of air in contact with clothing
$\overline{Z}_a$	$\left(60.6 \text{ Pa K}^{-1}\right)/\overline{h}_c$	Resistance to water transfer through the boundary layer of air in contact with clothing [97]
$\overline{h}_c$	11.6 W K^{-1} m^{-2}	Heat transfer coefficient between exterior of clothing and air [97]
$\overline{\phi}_{\text{rad}}$	0.79	Effective fraction of clothing exchanging longwave radiation with air (or surfaces with temperature T_a) [97]
$\overline{\epsilon}$	0.97	Longwave emissivity of clothing [97]

Region I: Covering

In conditions that are too cold and dry, we will be unable to find a physical solution in region II. This occurs because the core cannot be maintained at 310 K even with clothing of infinite thickness, i.e., with R_f, and thus also Z_f, equal to infinity. In such cold and dry conditions, the fraction ϕ of the skin covered in clothing must be increased above 0.84. Therefore, we define region I as having $R_f = \infty$ and variable $\phi > 0.84$. In this limit, $T_f = T_a$, $p_f = p_a$, $\overline{T}_s = T_c$, $\overline{p}_s = p_c$, and conservation equations (2.1–2.7) simplify to

$$0 = Q - Q_v - (1-\phi)\frac{T_c - T_s}{R_s} \tag{2.11}$$

$$0 = \frac{T_c - T_s}{R_s} - \frac{T_s - T_a}{R_a} - \frac{p_s - p_a}{Z_a} \tag{2.12}$$

$$0 = \frac{p_c - p_s}{Z_s} - \frac{p_s - p_a}{Z_a}\,. \tag{2.13}$$

As in regions II and III, these are combined with equation (2.10), which ensures that $T_c = 310$ K. The circuit diagram for this region is shown in Figure 2.4. The constants used in region I are given in Table 2.3.

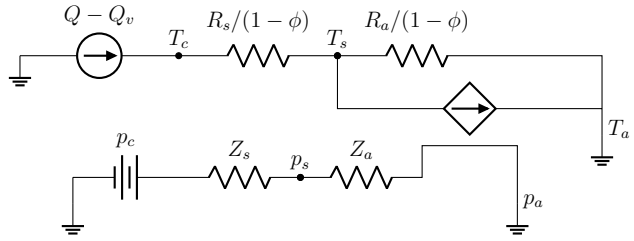

Figure 2.4: Diagram for region I illustrating the potentials and resistances for (top) sensible heat transfer and (bottom) water transfer. In region I, a constant T_c is maintained by varying ϕ between 1 and 0.84, which is the threshold value for region II.

Table 2.3: Variables and constants for region I.

Variable	Value	Interpretation
ϕ	variable	Fraction of skin that is clothed
T_c	310 K	Core temperature
p_c	$\phi_{\text{salt}} p^*(T_c)$	Core vapor pressure
R_s	0.0387 m^2 K W^{-1}	Resistance to heat transfer through the skin [97]
Z_s	52.1 m^2 Pa W^{-1}	Resistance to water transfer through the skin [97]
R_a	$[\phi_{\text{rad}} \epsilon \sigma (T_s^2 + T_a^2)(T_s + T_a) + h_c]^{-1}$	Resistance to heat transfer through the boundary layer of air in contact with the exposed skin
Z_a	$\left(60.6 \text{ Pa K}^{-1}\right) / h_c$	Resistance to water transfer through the boundary layer of air in contact with the exposed skin [97]
h_c	17.4 W K^{-1} m^{-2}	Heat transfer coefficient between surface of exposed skin and air [97]
ϕ_{rad}	0.85	Effective fraction of exposed skin exchanging longwave radiation with air (or surfaces with temperature T_a) [97]
ϵ	0.97	Longwave emissivity of exposed skin [97]

Regions IV and V: Naked

Recall that in region III, the human chooses its clothing thickness so as to maintain its core temperature. In conditions that are too hot and humid, we will be unable to find a physical solution in region III. This occurs because the core cannot be maintained at 310 K even with clothing of zero thickness, i.e., with $R_f = Z_f = 0$. In such hot and humid conditions, the ideal human chooses to be naked ($\phi = 0$) as designed by Steadman [97], and the blood flow to the skin is increased so as to reduce R_s and Z_s as needed. In region IV, the conservation equations (2.1–2.7) simplify to [97]

$$0 = Q - Q_v - \frac{T_c - T_s}{R_s} \tag{2.14}$$

$$0 = \frac{T_c - T_s}{R_s} - \frac{T_s - T_a}{R_a} - \frac{p_s - p_a}{Z_a} \tag{2.15}$$

$$p_s = \frac{Z_a p_c + Z_s p_a}{Z_a + Z_s}\,. \tag{2.16a}$$

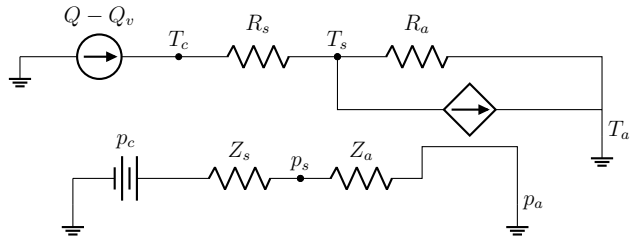

Figure 2.5: Diagram illustrating the potentials and resistances for (top) sensible heat transfer and (bottom) water transfer in region IV, one of the two original cases of Steadman [97].

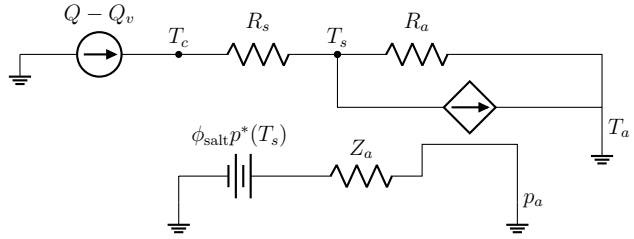

Figure 2.6: Diagram illustrating the potentials and resistances for (top) sensible heat transfer and (bottom) water transfer in region V.

To ensure a healthy human, these are combined with equation (2.10) as before. The circuit diagram for region IV is shown in Figure 2.5. For sufficiently hot and humid conditions, this solution becomes unphysical because p_s exceeds the saturation vapor pressure of sweat $\phi_{\text{salt}} p^*(T_s)$, and the standard Heat Index becomes undefined; see the undefined region in Table 2 of Steadman [97]. To extend the Heat Index into region V, we let sweat drip off the skin, which replaces the mass-balance equation (2.16a) with

$$p_s = \phi_{\text{salt}} p^*(T_s)\,. \tag{2.16b}$$

The circuit diagram for region V is shown in Figure 2.6. In summary, the conservation equations for regions IV and V are (2.14), (2.15), and

$$p_s = \min\left[\frac{Z_a p_c + Z_s p_a}{Z_a + Z_s}, \phi_{\text{salt}} p^*(T_s)\right]\,. \tag{2.16}$$

The constants used in regions IV and V are given in Table 2.4.

Table 2.4: Variables and constants for regions IV and V.

Variable	Value	Interpretation
R_s	variable	Resistance to heat transfer through the skin
T_c	310 K	Core temperature
p_c	$\phi_{\text{salt}} p^*(T_c)$	Core vapor pressure
Z_s	$(6.0 \times 10^8$ Pa W^4 m^{-8} K$^{-5})\, R_s^5$	Resistance to water transfer through the skin [97]
R_a	$[\phi_{\text{rad}} \epsilon \sigma (T_s^2 + T_a^2)(T_s + T_a) + h_c]^{-1}$	Resistance to heat transfer through the boundary layer of air in contact with the exposed skin
Z_a	$\left(60.6 \text{ Pa K}^{-1}\right) / h_c$	Resistance to water transfer through the boundary layer of air in contact with the exposed skin [97]
h_c	12.3 W K^{-1} m^{-2}	Heat transfer coefficient between surface of exposed skin and air [97]
ϕ_{rad}	0.80	Effective fraction of exposed skin exchanging longwave radiation with air (or surfaces with temperature T_a) [97]
ϵ	0.97	Longwave emissivity of exposed skin [97]

Region VI: Warming

In conditions that are too hot and humid, we will be unable to find a physical solution in region V. This occurs because the core cannot be maintained at 310 K even when the circulatory system has driven the skin temperature to that of the core, making $R_s = Z_s = 0$. In such hot and humid conditions, it is necessary to reduce the metabolic rate Q to maintain $T_c = 310$ K; thus Q becomes the free variable. In the limit of $R_s = Z_s = 0$, equations (2.14–2.16) simplify to

$$0 = Q - Q_v - \frac{T_c - T_a}{R_a} - \frac{p_c - p_a}{Z_a}\,. \tag{2.17}$$

The circuit diagram for region VI is shown in Figure 2.7. The constants used in region VI are given in Table 2.5.

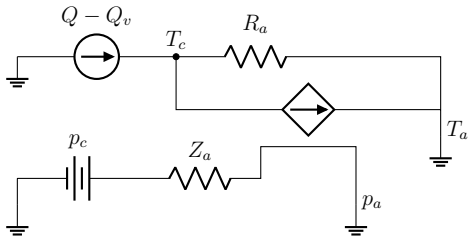

Figure 2.7: Diagram illustrating the potentials and resistances for (top) sensible heat transfer and (bottom) mass transfer in region VI. In this region, it is not possible to maintain a constant T_c, so $dT_c/dt > 0$.

Table 2.5: Variables and constants for region VI using equation (2.17).

Variable	Value	Interpretation
Q	variable	Metabolic rate
T_c	310 K	Core temperature
p_c	$\phi_{\text{salt}} p^*(T_c)$	Core vapor pressure
R_a	$[\phi_{\text{rad}} \epsilon \sigma (T_c^2 + T_a^2)(T_c + T_a) + h_c]^{-1}$	Resistance to heat transfer through the boundary layer of air in contact with skin
Z_a	$\left(60.6 \text{ Pa K}^{-1}\right) / h_c$	Resistance to water transfer through the boundary layer of air in contact with the skin [97]
h_c	12.3 W K^{-1} m^{-2}	Heat transfer coefficient between surface of exposed skin and air [97]
ϕ_{rad}	0.80	Effective fraction of exposed skin exchanging longwave radiation with air (or surfaces with temperature T_a) [97]
ϵ	0.97	Longwave emissivity of exposed skin [97]

In the original regions III and IV, Q is chosen to be equal to 180 W m^{-2} of skin surface, consistent with a person walking outdoors at 1.4 m s^{-1}, or about 3 miles per hour [97]. There are several ways to think about the reduction in Q that is required in region VI. Near the cool edge of region VI, we may think of this reduction in Q as a behavioral choice to reduce the walking pace. This has its limits, however, as even a resting metabolic rate is 51.8 W m^{-2} [71]. Another way to think about the reduction in Q is as a conscious choice to directly cool the core, e.g., by drinking ice water or through some actively powered cooling system. If none of these behavioral choices are available, then a third way to think about region VI

is to dispense with the steady-state assumption and recognize that there will be a positive dT_c/dt. In this case, Q is pegged to the constant value of 180 W m^{-2} and dT_c/dt becomes the free variable through a modified version of equation (2.17), namely

$$C_c \frac{dT_c}{dt} = Q - Q_v - \frac{T_c - T_a}{R_a} - \frac{p_c - p_a}{Z_a}\,. \tag{2.18}$$

Since this is no longer a steady-state equation, there is no simple and analogous circuit diagram. The constants used in region VI with equation (2.18) are given in Table 2.6.

Table 2.6: Variables and constants for region VI using equation (2.18).

Variable	Value	Interpretation
dT_c/dt	variable	Tendency of core temperature
T_c	310 K	Initial core temperature
C_c	$M_c c_{pc}/A$	Heat capacity of the core per skin area
p_c	$\phi_{\text{salt}} p^*(T_c)$	Core vapor pressure
R_a	$[\phi_{\text{rad}} \epsilon \sigma (T_c^2 + T_a^2)(T_c + T_a) + h_c]^{-1}$	Resistance to heat transfer through the boundary layer of air in contact with the skin
Z_a	$\left(60.6 \text{ Pa K}^{-1}\right)/h_c$	Resistance to water transfer through the boundary layer of air in contact with the skin [97]
h_c	12.3 W K^{-1} m^{-2}	Heat transfer coefficient between surface of exposed skin and air [97]
ϕ_{rad}	0.80	Effective fraction of exposed skin exchanging longwave radiation with air (or surfaces with temperature T_a) [97]
ϵ	0.97	Longwave emissivity of exposed skin [97]

Summary of the Derivations

Here, we summarize the preceding derivations. Recall that R_f is proportional to the clothing thickness and R_s is inversely related to the skin blood flow. We refer to Steadman's clothed solutions (with variable clothing thickness and constant skin blood flow) as region III and Steadman's naked solutions (with variable skin blood flow) as region IV. The transition from region III to IV happens at a Heat Index of about 298 K, at which the clothing thickness becomes zero. Moving from region III into colder temperatures, the existing Heat Index becomes undefined because Steadman assumes a fixed reference vapor-pressure of 1.6 kPa, which would exceed the saturation pressure at an air temperature less than $p^{*-1}(1.6\text{kPa}) = 287$ K, where p^{*-1} is the inverse function of the saturation vapor pressure given by equation

(2.9). To extend the Heat Index to cold regimes, we define a region II where the clothing thickness is still variable, but the reference vapor pressure is set to the Heat Index's saturation vapor pressure rather than 1.6 kPa. The transition from region III to II thus occurs at a Heat Index of 287 K. At sufficiently low air temperatures, the clothing thickness becomes infinite, indicating that the clothing (which covers only 84% of the skin) becomes so thick as to be perfectly insulating; we define this as the boundary between regions II and I, at which the Heat Index is about 238 K. In region I, we hold the clothing thickness fixed at infinity and let the clothed skin fraction vary; in this region, the Heat Index is defined as the temperature of saturated air that would solve the equations with the same clothed fraction. In region I, the Heat Index is very nearly equal to the air temperature, regardless of the relative humidity.

Moving from region IV into hotter temperatures, the existing Heat Index becomes undefined because Steadman equates the skin's evaporation rate to the sweating rate. When the air temperature is sufficiently high, this causes the skin's vapor pressure to exceed its saturation value. By allowing sweat to drip off the skin, we are able to extend the definition of the Heat Index into higher-temperature regimes. To do so, we define a region V where the skin blood flow is still variable, but the skin's vapor pressure is equal to its saturation vapor pressure. To accommodate this new constraint in region V, we remove the mass-conservation equation for the skin's water budget; physically, this allows excess water to drip off the sweat-soaked skin. Note that the transition from region IV to V occurs when equations (2.16a) and (2.16b) give the same skin vapor pressure, and this does not corresponds to a single Heat Index, but a range of Heat Indices from 308 K to 333 K. For sufficiently hot and humid conditions, the skin blood flow becomes infinite, making the temperature of the skin equal to that of the core. We call this the boundary between regions V and VI, which occurs at a Heat Index of 345 K[1]. In region VI, it is impossible to maintain a healthy core temperature without a reduction in the metabolic rate Q, a new source of internal cooling, or growth in the core temperature. The Heat Index is then defined as the temperature (at the reference pressure of 1.6 kPa) that would give the same variable Q with $dT_c/dt = 0$ or, equivalently, the temperature at the reference pressure that would give the same dT_c/dt with the reference Q. Sample values of the extended Heat Index in regions IV through VI are shown in Figure 2.8.

Comparisons with the Polynomial Fit

For compatibility with Steadman's Heat Index, we use all of the same parameter values, except that we replace some of Steadman's linearized equations with the full T^4 dependence for longwave radiation, a formal expression of ventilation cooling (equation 2.8), and a more accurate formula for saturation vapor pressure of water (or of ice, when the temperature is below freezing) (equation 2.9). These improvements, which are necessary at very high

[1]To hundredths of a degree, the Heat Index values separating regions I through VI are 238.49, 287.16, 298.44, a range from 308.23 to 333.39, and 344.65 K, respectively. Although the Heat Index can be calculated to this precision or higher, we will henceforth report the Heat Index as an integer value.

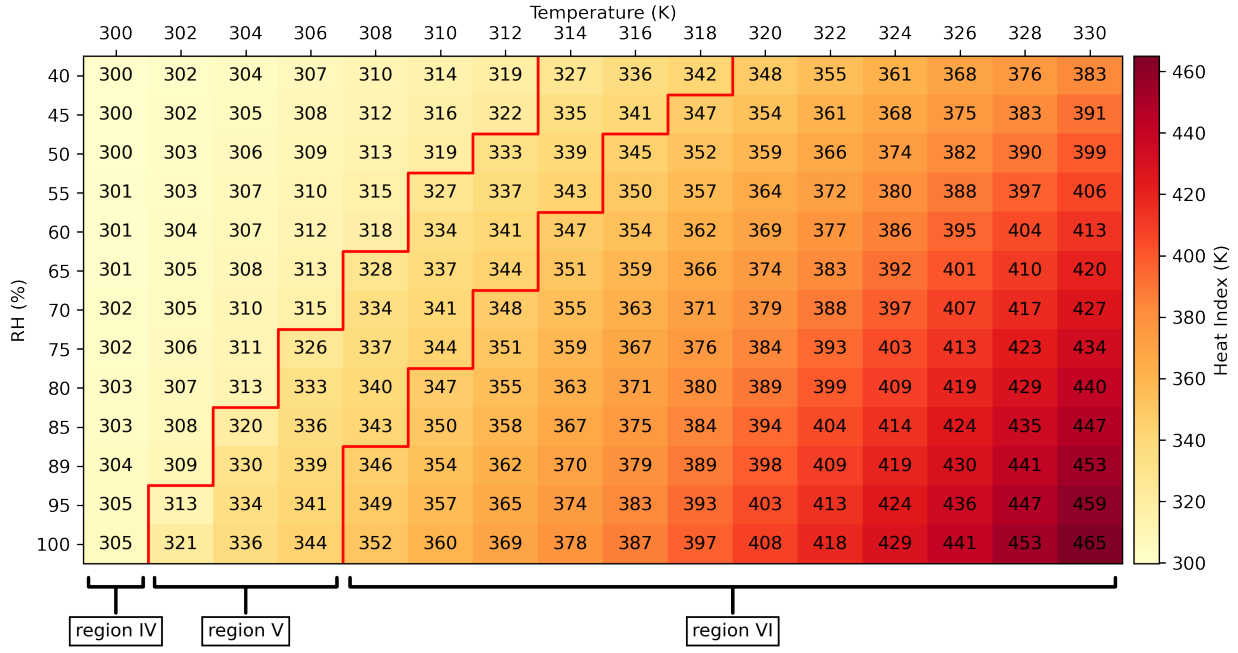

Figure 2.8: The Heat Index as a function of the air temperature and relative humidity. Red lines separate regions IV, V, and VI. The Heat Index was previously undefined in regions I and II (not shown here) and in regions V and VI.

temperatures, cause deviations from the original Heat Index of less than 1 K throughout regions III and IV where the original Heat Index is defined, ensuring backwards compatibility. This can be verified from the right panel of Figure 2.9, which shows the difference between Steadman's Heat Index [taken directly from Table 2 of 97] and the Heat Index computed using our formalism, sampled over 293 K $\leq T_a \leq$ 323 K with increments of 1 K and $0 \leq$ RH ≤ 1 with increments of 0.1. In Figure 2.9, pairs of temperature and humidity for which Steadman's Heat Index was not defined [including the value in parenthesis in Table 2 of 97] are excluded. For comparison, an oft-used polynomial fit [83] has errors with respect to Steadman's original Heat Index as large as 7 K (see the left panel of Figure 2.9). Even with the National Weather Service's adjustments to the polynomial fit [63, replicated in the Appendix], the polynomial fit still has errors as large as 2 K compared to Steadman's published values (see the middle panel).

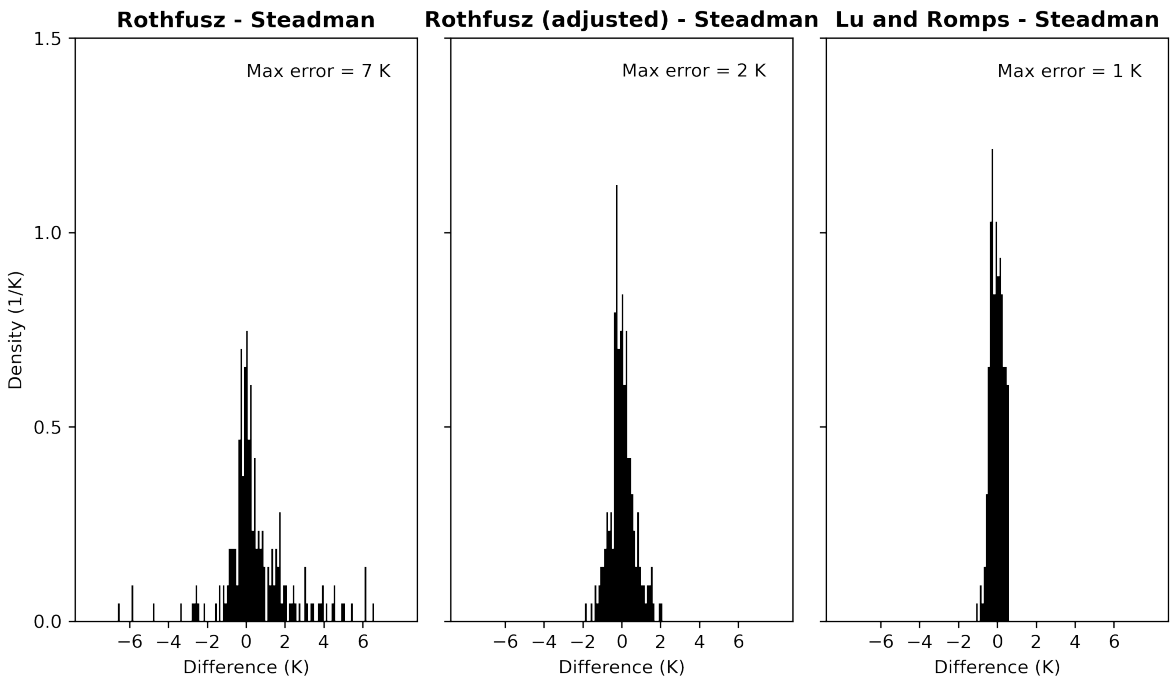

Figure 2.9: The differences between Steadman's Heat Index and (left) the polynomial fit of Rothfusz [83], (middle) the Rothfusz polynomial fit with adjustments [63], and (right) our extended Heat Index. Steadman's Heat Index is taken directly from Table 2 of Steadman [97], omitting the undefined Heat Index (including the value given there in parentheses).

Furthermore, the National Weather Service (NWS) uses its polynomial fit not just to interpolate the Heat Index values given by Steadman, but also to extrapolate them into the undefined regions, i.e., into what we refer to here as regions V and VI. The top panel of Figure 2.10 replicates the "Heat Index Chart" displayed on the NWS web site [60], which displays the polynomial fit in degrees Fahrenheit. In the original chart, the four colors, from yellow to red, are labeled by the NWS with "caution", "extreme caution", "danger", and "extreme danger". The middle panel of Figure 2.10 shows the errors in that chart, as compared to the extended Heat Index calculated here. We see that the NWS values are biased low by as much as 28 degrees Fahrenheit (16 K). Therefore, studies relying on this extrapolation will have underestimated the risk of high heat. The bottom panel of Figure 2.10 displays a corrected version of the NWS chart using the same numerical boundaries between the four colors. Since 161 °F (345 K) is the Heat Index that separates regions V and VI, we learn that the edge of the labeled region in this NWS chart corresponds closely with the boundary between regions V and VI, i.e., the unlabeled region is where ill effects are unavoidable even for an ideal human under ideal circumstances. In another NWS chart, polynomial extrapolation is used well into region VI [61].

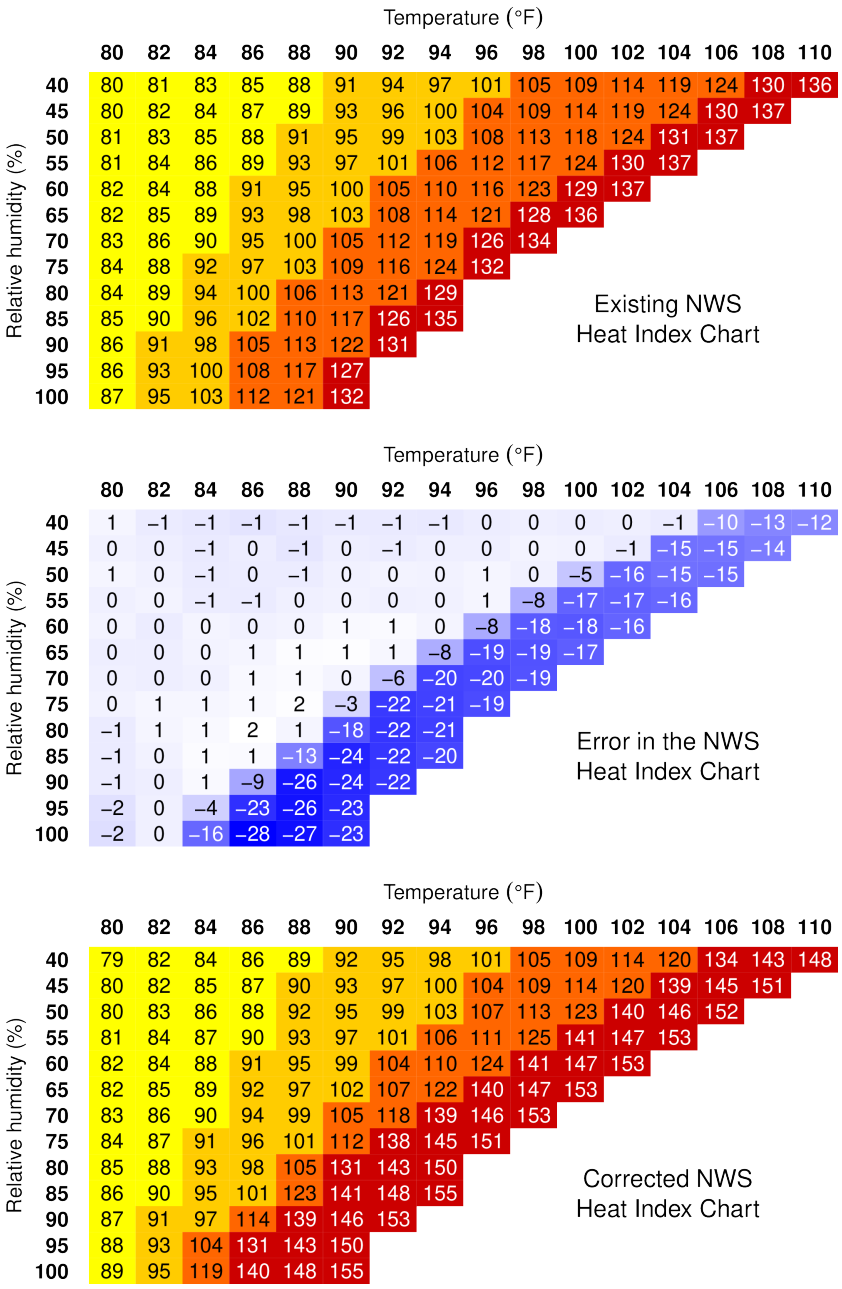

Figure 2.10: (top) The Heat Index chart displayed on the web site of the National Weather Service (NWS) with values in degrees Fahrenheit [60]. (middle) The errors in that chart, defined by subtracting the extended Heat Index. (bottom) The corrected version of the NWS chart.

2.3 Physical Interpretation of the Heat Index

By construction, each value of the Heat Index maps to a unique value of a physical variable. In region I, that variable is ϕ, which describes the fraction of the body that must be fully insulated to maintain a core temperature of 310 K. In regions II and III, the variable is R_f, which describes the thickness of clothing required (over 84% of the body) to keep the core temperature at 310 K; R_f is proportional to the clothing thickness d via [97]

$$R_f = \left(16.7 \text{ m K W}^{-1}\right) d \,. \tag{2.19}$$

In regions IV and V, the variable is R_s, which describes the skin blood flow required to keep the core at 310 K; the relation between R_s and the skin blood flow $\dot{V}$ is [36]

$$\frac{1}{R_s} = \frac{1}{R_{s0}} + \rho c \dot{V} / A \,, \tag{2.20}$$

where $R_{s0} = 0.189$ m^2 K W^{-1} is the heat transfer resistance of the tissue per skin area, $\rho = 1000$ kg m^{-3} is the density of blood, $c = 4184$ J kg^{-1} K^{-1} is the specific heat capacity of blood, and A is the skin area as given in Table 2.1. In region VI, the variable is dT_c/dt, which describes how quickly the core temperature is rising above its ideal value of 310 K.

The first three rows of Figure 2.11 plot the clothing fraction, clothing thickness, and skin blood flow as functions of the Heat Index in regions I to V. At the hot end of region V, the blood flow is so high that it pegs the skin temperature to that of the core. At this point, the cooling effects of perspiration and blood flow have been maxed out. In region VI, it is not possible to maintain a healthy core temperature of 310 K with the walking metabolic rate of 180 W m^{-2}, and so dT_c/dt is positive. While unhealthy, a positive dT_c/dt is not necessarily fatal in a young, healthy adult if the core temperature equilibrates below the critical thermal maximum of 315 K, which is commonly used as the threshold for heat death [9, 31]. As shown in the next subsection, the equilibrated T_c is a function only of the Heat Index, as opposed to a more general function of air temperature and humidity. As shown in the fourth row of Figure 2.11, the equilibrium core temperature enters the range for heat exhaustion, heat stroke, and heat death ($T_c > 310$, 313, and 315 K) [9] at Heat Indices of 345, 357, and 366 K[2]. For a sustained Heat Index above 366 K, it is not a question of whether a fatal core temperature will be reached, but how soon it will be reached. As also shown in the next subsection, the time it takes T_c to rise from 310 to 315 K is also a function only of the Heat Index; this duration is plotted in the fifth row of Figure 2.11. Many studies have used a wet-bulb temperature of 35 °C as a threshold value that is fatal to humans [33, 70, 78, 93]. In reality, each Heat Index corresponds to a range of wet-bulb temperatures: the fatal Heat Index of 366 K corresponds to wet-bulb temperatures from 32 to 38 °C.

[2]More precise values are 344.65, 357.42, and 366.44 K, respectively.

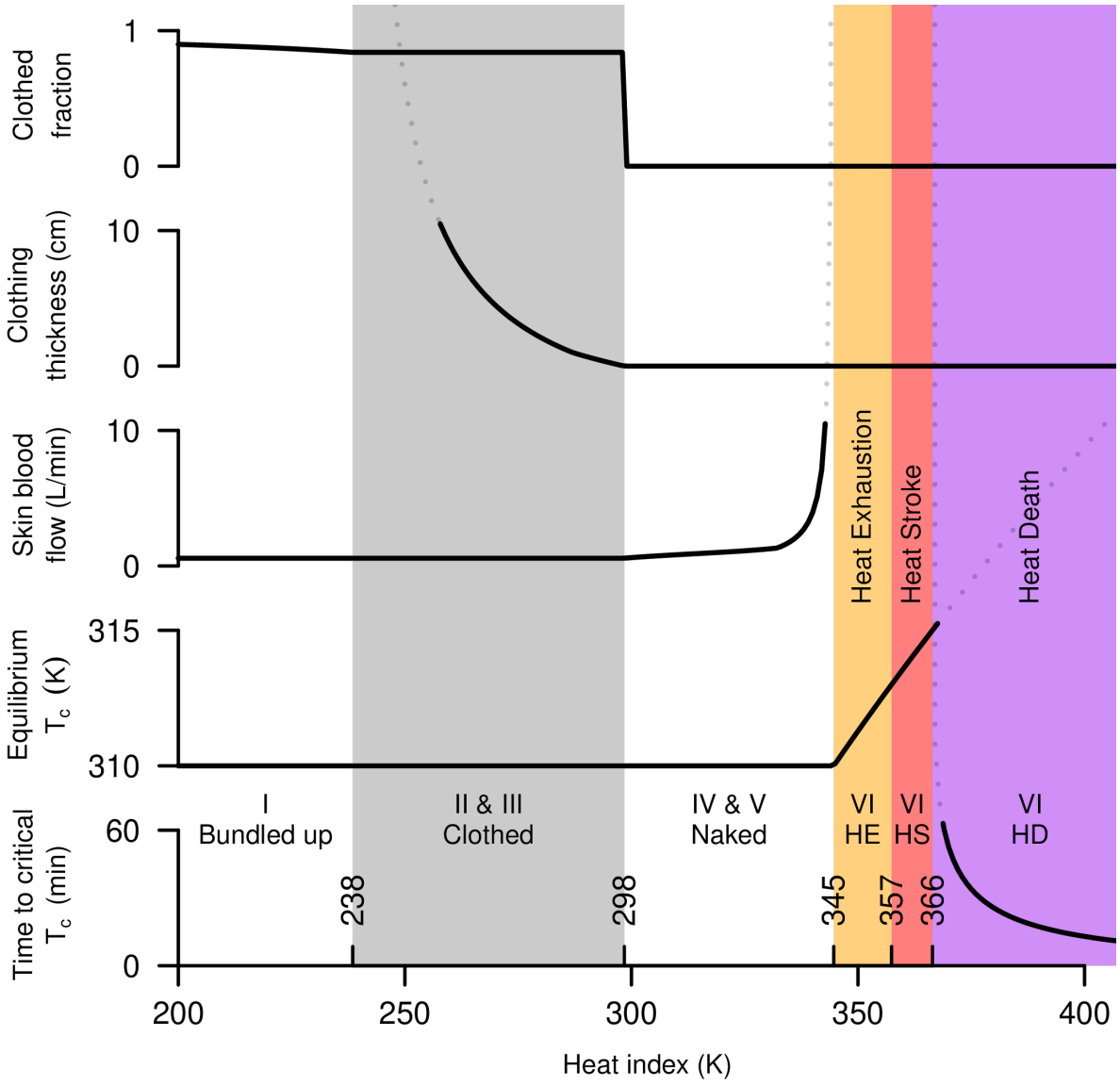

Figure 2.11: The human condition as a function of the Heat Index.

Functions of the Heat Index in region VI

Here, we show that, in region VI, the equilibrium core temperature $\widetilde{T}_c$ and the time τ it takes the core to get to the critical thermal maximum of 315 K are functions only of the Heat Index. Previous work has shown that the polynomial extrapolated Heat Index is highly correlated to the equilibrium core temperature [86]. With the analytic extension of the Heat Index as done in this thesis, the relation is made exact.

We start with equation (2.18), which can be written as

$$f(T_c, T_a, p_a) \equiv C_c \frac{dT_c}{dt} \tag{2.21}$$

$$= Q - \eta Q \left\{ c_{pa}(T_c - T_a) + \frac{L\hat{R}_a}{\hat{R}_v p}\Big[\phi_{\text{salt}} p^*(T_c) - p_a\Big] \right\} \tag{2.22}$$

$$- \phi_{\text{rad}} \epsilon \sigma (T_c^4 - T_a^4) - h_c(T_c - T_a) - \frac{\phi_{\text{salt}} p^*(T_c) - p_a}{Z_a} \tag{2.23}$$

$$= \underbrace{Q - \eta Q c_{pa} T_c - \eta Q \frac{L\hat{R}_a}{\hat{R}_v p} \phi_{\text{salt}} p^*(T_c) - \phi_{\text{rad}} \epsilon \sigma T_c^4 - h_c T_c - \frac{\phi_{\text{salt}} p^*(T_c)}{Z_a}}_{g(T_c)} \tag{2.24}$$

$$+ \underbrace{\eta Q c_{pa} T_a + \phi_{\text{rad}} \sigma T_a^4 + h_c T_a}_{h(T_a)} + \underbrace{\eta Q \frac{L\hat{R}_a}{\hat{R}_v p} p_a + \frac{p_a}{Z_a}}_{k(p_a)} \tag{2.25}$$

$$= g(T_c) + h(T_a) + k(p_a)\,. \tag{2.26}$$

We see that dT_c/dt is equal to the sum of three functions, each of which depends only on T_c, T_a, and p_a, respectively. Now, consider a given T_a and p_a. For the purposes of the derivation here, let us define $T_{c0} = 310$ K and let us denote the Heat Index by T. By the definition of the Heat Index in region VI,

$$f(T_{c0}, T_a, p_a) = f(T_{c0}, T, p_{a0})\,,$$

which implies that

$$g(T_{c0}) + h(T_a) + k(p_a) = g(T_{c0}) + h(T) + k(p_{a0})\,.$$

Adding $g(T_c) - g(T_{c0})$ to both sides, we get

$$f(T_c, T_a, p_a) = f(T_c, T, p_{a0})\,, \tag{2.27}$$

which holds for arbitrary T_c. Next, by definition, the equilibrium core temperature $\widetilde{T}_c$ satisfies $f(\widetilde{T}_c, T_a, p_a) = 0$, so using equation (2.27), we can write this as $f(\widetilde{T}_c, T, p_{a0}) = 0$, which can be solved for $\widetilde{T}_c$ in terms of T. In other words, $\widetilde{T}_c$ is a function only of the Heat Index T, as

opposed to having some other functional dependence on T_a and p_a. Similarly, let us define τ to be the time its takes the core to increase in temperature from $T_{c0} = 310$ K to the critical thermal maximum of $T_{c1} = 315$ K. By rearrangement of equation (2.21), we can write this as

$$\tau = \int_{T_{c0}}^{T_{c1}} \frac{C_c dT_c}{f(T_c, T_a, p_a)} \tag{2.28}$$

$$= \int_{T_{c0}}^{T_{c1}} \frac{C_c dT_c}{f(T_c, T, p_{a0})}\,, \tag{2.29}$$

where we have used (2.27) in the last line. Therefore, τ is a function only of the Heat Index T.

2.4 Validity of the Ideal-Human Assumption

Steadman's model is idealized in many ways: it assumes that the human is doing no heavy labor, has unrestricted access to drinking water, has a perfect system of thermal regulation, and has no modesty (disrobing as needed to maximize thermal comfort). Since the Heat Index is constructed from a best-case scenario – a perfect human responding in an ideal way – it serves as a robust lower bound on the physiological consequences of high heat and humidity. In our extension of the Heat Index, we maintain this "best-case scenario" approach by imposing no limits on the skin blood flow or sweat rate. As shown in the next two subsections, imposing realistic bounds on the skin blood flow and sweat rate changes the apparent temperature by no more than a few degrees.

Similarly, the ambient condition of the Steadman model is also idealized: it assumes the human is under the shade with a constant breeze. When the human stays under the sunlight with a lower wind speed, the body can be warmed up significantly, depending on the amount of shortwave radiation absorbed and the amount of reduced evaporation rate. Therefore, 366 K can be considered a conservative upper bound on the Heat Index that can be survived with sustained exposure. In reality, with a diverse population in diverse circumstances, the fatality rate will climb to unacceptable levels well before the Heat Index reaches such a value.

Finite Skin Blood Flow

In the model of thermoregulation, we assume the skin blood flow can be made as large as needed, all the way up to infinite flow (equivalently, $R_s = 0$). In reality, the largest skin blood flow recorded in the literature is 7.8 L min^{-1} [84, 95], which, using equation 2.20, corresponds to $R_s = 0.004$ m^2 K W^{-1}. Although our extension of Steadman's model has intentionally maintained its ideal nature, we could have imposed this upper bound on the skin blood flow and defined the extended Heat Index accordingly. This would make the hot boundary of region V retreat to lower temperatures, albeit subtly as shown in Figure 2.12.

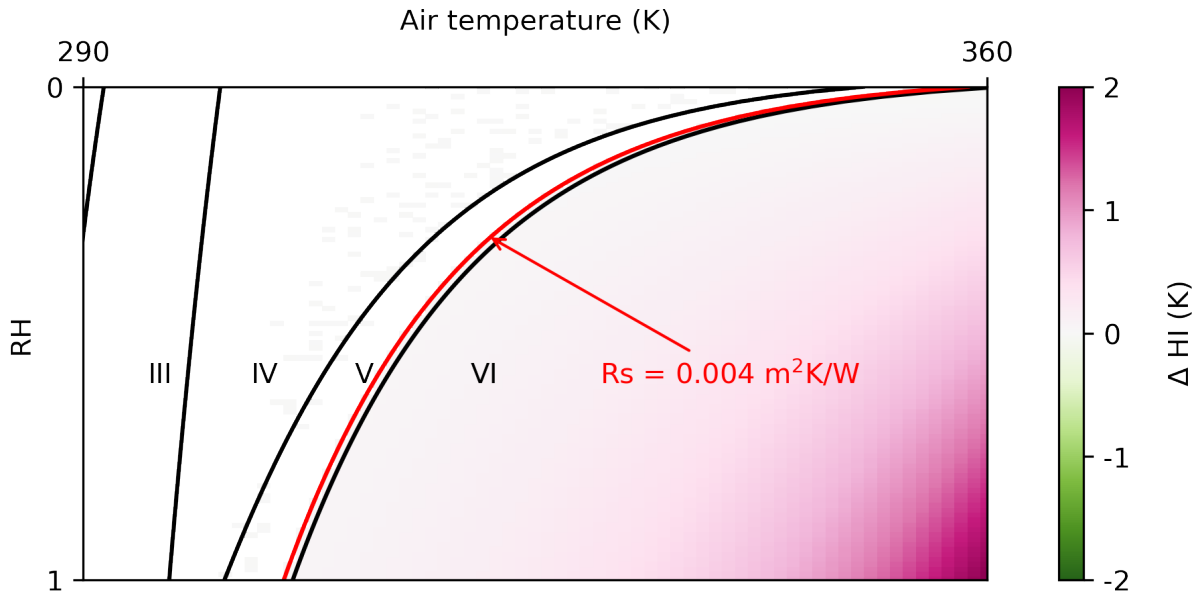

Figure 2.12: Change in the Heat Index if we set an upper bound of 7.8 L min^{-1} ($R_s = 0.004$ m^2 K W^{-1}) on the skin blood flow. The black curves separate the extended Heat Index regions with unbounded skin blood flow. Note that the right-most black curve separating regions V and VI is the constant $R_s = 0$ curve. The red curve is the constant $R_s = 0.004$ m^2 K W^{-1} curve, corresponding to a skin blood flow of 7.8 L min^{-1}. The color scale shows the change in the Heat Index, which only reaches as high as 2 K for saturated air of a temperature of 360 K (87 °C, 188 °F).

From equation 2.14, a non-zero R_s implies there must exist a finite temperature difference between the core and the skin, and so in region VI, equation 2.18 is replaced with

$$C_c \frac{dT_c}{dt} = Q - Q_v - \frac{T_c - T_s}{R_s} \tag{2.30}$$

$$0 = \frac{T_c - T_s}{R_s} - \frac{T_s - T_a}{R_a} - \frac{\phi_{\text{salt}} p^*(T_s) - p_a}{Z_a}, \tag{2.31}$$

where R_s is fixed at 0.004 m^2 K W^{-1}. We can solve the two equations for dT_c/dt, and the Heat Index is defined as the air temperature T_a that would give the same dT_c/dt at $p_a = p_{a0}$. With the modification, the Heat Index changes, but by less than 2 K, and with changes approaching 2 K only at the otherworldly conditions of saturated air at a temperature of 360 K (87 °C, 188 °F) (see Figure 2.12). Therefore, we conclude that using infinite skin blood flow does not make a significant difference compared to using a realistic bounded skin blood flow.

Finite Sweat Rate

Steadman's human model also assumes that the sweat rate can reach any desired value to keep the body cool. However, a human has a maximum sweat rate of about $2 - 4$ L hour^{-1} [52]. We can check, however, if the model would ever require a sweat rate higher than this limit. Using the mass transfer term $(p_s - p_a)/Z_a$ in each region, we can plot contours of the sweat rate on temperature-humidity space. Referring to Figure 2.13, we see that the maximum sweat rate occurs at around $T_a = 360$ K and RH $= 0$, and has the value of 3.3 L hour^{-1}. Therefore, only in this extreme circumstance does the model generate a sweat rate that is in the vicinity of the documented maximum of 2-4 L hour^{-1}. Note that the negative sweat rate in other circumstances means that the environmental vapor condenses onto the skin, releasing latent heat to the human body. In these situations, sweat is unable to cool the body since the ambient vapor pressure is higher than that at the skin.

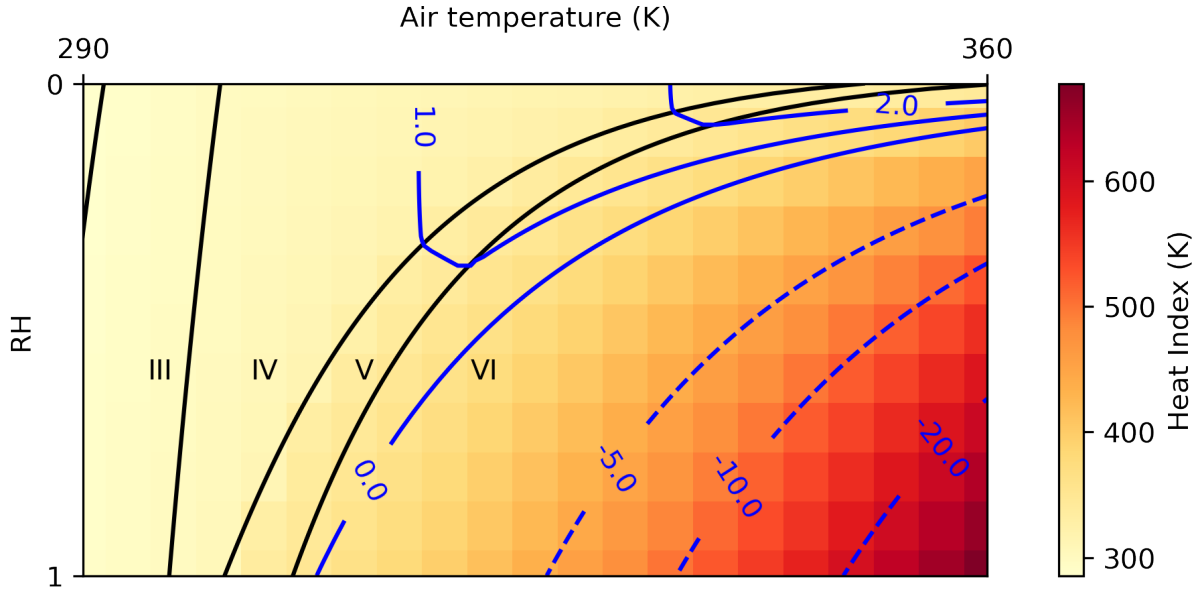

Figure 2.13: The blue contours show the sweat rate of the human model with units of liters per hour. Negative values represent condensation rates of the ambient vapor onto the skin. Black curves separate the regions of the Heat Index as defined before. The color scale shows the value of the Heat Index within $0 \leq T_a \leq 360$ K and $0 \leq \text{RH} \leq 1$.

2.5 Change in the Heat Index in Warming Scenarios

For the summer time at the ARM SGP site with a previously undefined Heat Index (due to high temperature and humidity) as shown in Figure 2.1, we can now calculate the Heat Index and its distribution, which is shown in Figure 2.14. Note that the transition from

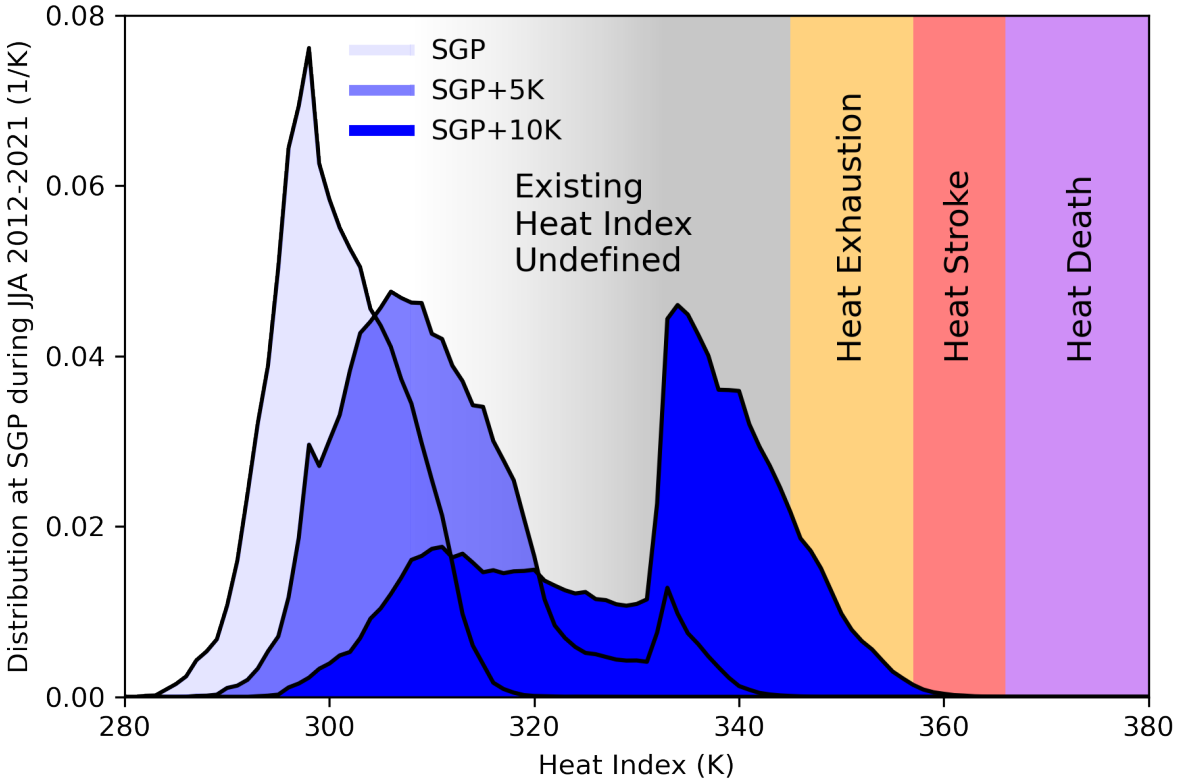

Figure 2.14: (light blue) Distribution of the Heat Index at the ARM SGP site from one-minute measurements of temperature and humidity during JJA 2012-2021. (blue and dark blue) Same, but adding 5 K and 10 K to the temperatures while keeping the relative humidities unchanged. The grey region with gradient shows the range of Heat Indices where region IV transitions to region V. (The transition occurs within a finite range of Heat Index from 308 K to 333 K, and therefore is represented by the grey color with gradient.)

region IV to the previously undefined region V occurs at Heat Indices from 308 K to 333 K, and this range is thus shaded in grey color with gradient. In the current climate from year 2012 to 2021, inclusive, the maximum Heat Index in the summer time is right around the boundary of region V, where the body has maximized its capacity for evaporative cooling, with excess sweat dripping off the skin.

To illustrate the change in the Heat Index under different warming scenarios, two other distributions are plotted by adding either 5 K (blue) or 10 K (dark blue) to the SGP summertime temperatures while keeping the relative humidities fixed. The change in the Heat Index is not a simple translation as the distribution in temperature-humidity space (see Figure 2.1), but has a nonlinear response to warming. In region V, the only thermoregulatory mechanism left to the body is to crank up the skin blood flow, altering the temperature

of its skin, which is, in practice, limited to a range of only a few Kelvin. Therefore, this adaptation is exhausted within only a few Kelvin of warming, throwing the body into region VI. As a consequence, warming the SGP air temperatures by 10 K increases the maximum Heat Index by 40 K. In this scenario, 12% of the time has a Heat Index above 345 K, which guarantees heat exhaustion: even for an ideal human at rest in the shade with ample water, their core temperature would be forced to rise above 310 K.

2.6 Conclusion

We have extended the definition of the Heat Index so that it applies to a much wider range of temperature and humidity, while retaining backwards compatibility. As in Steadman's original definition, the underlying model of thermoregulation represents a human with optimal physiology (e.g., unlimited rates of sweating and skin blood flow) and behavior (e.g., seeking shade and disrobing as needed). Each Heat Index value corresponds to a unique physiological state that specifies the clothing fraction, clothing thickness, skin blood flow rate, and the rate of change in the core temperature. In physiological states for which the time derivative of the core temperature is positive, that rate can be mapped to an equilibrium core temperature or the time needed to reach the fatal core temperature.

The correspondence between the Heat Index and the physiological state allows us to assess future habitability under different warming scenarios. Even for a very fit individual (approaching the optimal human being assumed in the thermoregulation model), the rate at which a human can expel heat is still constrained by physical laws that govern, for example, heat conduction and the evaporation of water. In a sufficiently hot and humid environment, the human body runs out of tricks for regulating its core temperature, leading to sickness or death.

Both the original Heat Index and the extended Heat Index presented here are constructed from a model of a human with optimal physiology and behavior. Therefore, a suitable interpretation of the Heat Index is that it approximates the apparent temperature for a young, healthy adult. In this regard, the mapping given here from Heat Index to physiological response (e.g., exhaustion, stroke, or death) should be considered a best-case scenario that serves as a lower bound on the health effects for any real individual. It should be anticipated that Heat Index values below the nominally fatal value of 366 K may be fatal for a large fraction, if not a majority, of the population.

Acknowledgments

This work was supported by the U.S. Department of Energy's Atmospheric System Research program through the Office of Science's Biological and Environmental Research program under Contract DE-AC02-05CH11231. Observational data were obtained from the Atmospheric Radiation Measurement (ARM) user facility, a U.S. Department of Energy (DOE) Office of Science user facility managed by the Biological and Environmental research program.

Data availability statement

Code for calculating the heat index is available in R, Python, and Fortran at `https://romps.berkeley.edu/papers/pubs-2020-heatindex.html`. The DOE ARM data can be downloaded from `https://www.arm.gov/capabilities/observatories/sgp`.

Appendix A: Numerical solutions in regions I-VI

To solve the algebraic equations presented in the thesis, the following procedures are used.

Numerical solution in regions II and III

We use the equations (2.1–2.7) to solve for R_f as follows. First, use (2.5) to solve for p_s,

$$p_s = \frac{Z_a p_c + Z_s p_a}{Z_a + Z_s}\,.$$

Substituting into equation (2.2) and noting that R_a has a nonlinear dependence on T_s (see Table 2.2), we can solve (2.2) for T_s using a root solver. We then solve for $\overline{T}_s$ using equation (2.1). The remaining unknowns are p_f, T_f, $\overline{p}_s$, and R_f. Using equation (2.4), we can write R_f in terms of T_f as

$$R_f = \overline{R}_a \frac{\overline{T}_s - T_f}{T_f - T_a}\,.$$

We can use equations (2.6) and (2.7) to write $\overline{p}_s$ and p_f in terms of R_f as

$$\overline{p}_s = \frac{(\overline{Z}_a + rR_f)p_c + Z_s p_a}{\overline{Z}_a + rR_f + Z_s} \tag{2.32}$$

$$p_f = \frac{\overline{Z}_a p_c + (rR_f + Z_s)p_a}{\overline{Z}_a + rR_f + Z_s}\,. \tag{2.33}$$

Substituting the expression for R_f into these last two equations, we now have R_f, $\overline{p}_s$, and p_f as functions of T_f. Substituting all three of these expressions into equation (2.3), we can solve for T_f using a root solver. That then gives us R_f, $\overline{p}_s$, and p_f.

Numerical solution in region I

We can solve equations (2.11–2.13) for ϕ as follows. First, use (2.13) to solve for p_s,

$$p_s = \frac{Z_a p_c + Z_s p_a}{Z_a + Z_s}\,.$$

Substituting into equation (2.12), we get

$$0 = \frac{T_c - T_s}{R_s} - \frac{T_s - T_a}{R_a} - \frac{p_c - p_a}{Z_a + Z_s}\,. \tag{2.34}$$

Since R_a depends on T_s, this must be solved for T_s using a root solver. Once T_s is obtained in this way, ϕ can be obtained from equation (2.11) as

$$\phi = 1 - R_s \frac{Q - Q_v}{T_c - T_s} \,.$$

We define the Heat Index as the T_a that gives the same ϕ for $p_a = \min[p_{a0}, p^*(T_a)]$, which, since $p^*(T_a)$ is always less than p_{a0} in region I, is simply $p^*(T_a)$. This is calculated by using a root solver to find the T_a that gives, using the procedure above, the correct ϕ.

Numerical solution in regions IV and V

We can solve equations (2.14–2.16) for R_s as follows. First, we solve (2.14) for T_s, which gives T_s as a function of R_s,

$$T_s = T_c - (Q - Q_v) R_s \,.$$

Plugging this into (2.16), and noting that Z_s is a function of R_s, we get p_s as an explicit function of R_s. Therefore, we can write all the terms of (2.15) as explicit functions of R_s, for which we can then find using a root solver. We then define the Heat Index as the T_a that gives the same R_s for $p_a = p_{a0}$ at $T_c = 310$ K. This is calculated by using a root solver to find the T_a that gives, using the procedure above, the correct R_s.

Numerical solution in region VI

Given T_a and p_a, equation (2.17) provides an explicit expression for dT_c/dt. We then define the Heat Index as the T_a that gives the same dT_c/dt for $p_a = p_{a0}$. Since R_a depends nonlinearly on T_a, equation (2.17) is solved for this T_a using a root solver.

Appendix B: Text of National Weather Service [63]

The following is the content of the web site that gives the polynomial fit used by the NWS for calculating the Heat Index [63]. The web site was described as last modified on May 28, 2014 when it was accessed on February 16, 2022. The content has been lightly edited to present the equations with standard mathematical formatting.

> The computation of the heat index is a refinement of a result obtained by multiple regression analysis carried out by Lans P. Rothfusz and described in a 1990 National Weather Service (NWS) Technical Attachment (SR 90-23). The regression equation of Rothfusz is

$$\begin{aligned} \mathrm{HI} = {} & -42.379 + 2.04901523\,T + 10.14333127\,\mathrm{RH} - 0.22475541\,T\,\mathrm{RH} - 0.00683783\,T^2 \\ & - 0.05481717\,\mathrm{RH}^2 + 0.00122874\,T^2\,\mathrm{RH} + 0.00085282\,T\,\mathrm{RH}^2 - 0.00000199\,T^2\,\mathrm{RH}^2 \,, \end{aligned}$$

where T is temperature in degrees F and RH is relative humidity in percent. HI is the heat index expressed as an apparent temperature in degrees F. If the RH is less than 13% and the temperature is between 80 and 112 degrees F, then the following adjustment is subtracted from HI:

$$\text{ADJUSTMENT} = \frac{13 - \text{RH}}{4} \sqrt{\frac{17 - |T - 95|}{17}} \, .$$

On the other hand, if the RH is greater than 85% and the temperature is between 80 and 87 degrees F, then the following adjustment is added to HI:

$$\text{ADJUSTMENT} = \frac{RH - 85}{10} \frac{87 - T}{5} \, .$$

The Rothfusz regression is not appropriate when conditions of temperature and humidity warrant a heat index value below about 80 degrees F. In those cases, a simpler formula is applied to calculate values consistent with Steadman's results:

$$\text{HI} = 0.5 \Big[T + 61.0 + 1.2(T - 68.0) + 0.094 \, \text{RH} \Big] \, .$$

In practice, the simple formula is computed first and the result averaged with the temperature. If this heat index value is 80 degrees F or higher, the full regression equation along with any adjustment as described above is applied. The Rothfusz regression is not valid for extreme temperature and relative humidity conditions beyond the range of data considered by Steadman.

Chapter 3

Chronically Underestimated: A Reassessment of US Heat Waves Using the Extended Heat Index

3.1 Introduction

Among meteorological phenomena, heat waves are the number one cause of death in the United States [14]. Heat waves pose a particular threat to the elderly [13], those without access to air conditioning [66], and outdoors workers [1]. As the Earth warms, the frequency and severity of heat waves is expected to increase [28]. It is important, therefore, to have accurate metrics for heat waves, both to issue operational warnings and to plan adaptations for the future.

Many different metrics have been used to define, identify, and measure heat waves [116]. Defined as having an anomalously high air temperature, heat waves in the contiguous United States (CONUS) are found to be most severe in the South [28, 54]. Heat waves have also been defined using the heat index, also known as the apparent temperature, which is a metric that maps one-to-one onto physiological states (different rates of skin blood flow) in hot conditions [97]. Most studies that define heat waves in terms of the heat index also find that the frequency of heat waves peaks in the South [e.g., 51, 96]. An exception is the study of Robinson [79], who found that heat waves are comparably frequent in the South, Midwest, and Mid-Atlantic.

It is notable, however, that these studies – and all other studies that have used Steadman's heat index to study heat waves – have used not the actual heat index, but a functional approximation to the heat index. Of the many different approximations [5], the most widely used is the polynomial fit developed by the United States National Weather Service [63, 83]. The National Weather Service (NWS) approximation is used on a regular basis to issue warnings to the public and to study past severe heat [e.g., 45, 51, 72, 79, 96, 104, 114, 117] and future severe heat [e.g., 4, 19, 21, 25, 26, 56, 69, 75, 77]. Even in the current

climate, there are conditions hotter and more humid than were considered and tabulated by Steadman [97], and so the NWS approximation is used to extrapolate the heat index beyond those tabulated values. That extrapolation is used extensively in operational warnings and in the aforementioned research studies.

From the perspective of social impacts, heat waves would ideally be identified and quantified using not an extrapolation but an accurate measure of physiological stress. Recently, Lu and Romps [49] extended Steadman's heat index to all combinations of temperature and humidity, providing such a measure. The objectives of this thesis are threefold: 1. to use the extended heat index to define and rank the most severe heat waves experienced over the United States during recent decades, 2. to evaluate the extent to which the NWS approximation errs in reporting the heat index during those heat waves, and 3. to evaluate the physiological state required of humans exposed to conditions during the most severe of those heat waves.

3.2 The heat index

To motivate the use of the heat index, we give here a brief review. As is well known, sweating is a physiological adaptation to high temperatures, with the evaporation of sweat providing a cooling effect. But this adaptation has limits: if the air is sufficiently hot and humid, evaporative cooling is unable to compensate for the inputs of metabolic heat, sensible heat, and infrared radiation, and the core temperature rises. In general, in hot and humid conditions, humans are subjected to greater physiological stress if either the temperature or humidity increases.

To capture these effects, Steadman [97] developed a model of thermoregulation with parameters chosen to represent a healthy adult walking in the shade with ample access to drinking water. The model quantifies the behavior (clothing thickness) and physiology (skin blood flow) in response to a combination of temperature and humidity. An important aspect of this model is that the human responds to changes in temperature and humidity by adjusting only one parameter at a time. For example, in relatively cold conditions, the human responds to changes in temperature by adjusting the thickness of the clothing being worn. Once that response has been exhausted (i.e., the clothing thickness has been driven to zero), the human responds to adjusting its skin blood flow. As a consequence, all states form a one-dimensional family, i.e., the states can be parameterized by a single variable. For example, in the original Steadman model, the states could be parameterized by ζ with the clothing thickness in millimeteres equal to $-\zeta$ for $\zeta < 0$ and the skin blood flow, in liters per minute, elevated by an amount of ζ for $\zeta \geq 0$.

Since the space of states is one-dimensional, whereas the space of all possible temperature and humidity is two-dimensional, each state corresponds to a one-dimensional isopleth in temperature-humidity space. For example, all pairs of temperature and humidity corresponding to a clothing thickness of five millimeters form a continuous one-dimensional curve with $\zeta = -5$. So long as the actual air temperature and humidity remain on an isopleth, a

human's experience of those conditions does not change (e.g., the choice of clothing or the skin blood flow remains the same). The heat index, which is a function of temperature and humidity, is simply a convention for assigning a unique temperature to each isopleth: the heat index is defined to be the temperature of the isopleth at 1600 Pa [97].

For illustration, Figure 3.1 shows the curve corresponding to $\zeta = 0.88$ (the state with an extra 0.88 l min^{-1} of skin blood flow), which intercepts a vapor pressure of 1600 Pa at a temperature of 60 °C (140 °F). All pairs of temperature and humidity lying on this curve have a heat index of 60 °C and induce identical behavioral and physiological responses (minimization of clothing and an extra skin blood flow of 0.88 l min^{-1}). In this way, every pair of temperature and humidity can be mapped to a value of the heat index and a thermoregulatory state. This is useful for communicating the hazard posed by high heat and humidity. For example, a heat index of 60 °C (140 °F) corresponds to a skin blood flow that is about two and a half times its value at room temperature. Maintaining a high skin blood flow can stress the cardiovascular system, even leading to death by heart failure. On the other hand, failing to maintain the required skin blood flow would lead to an elevated core temperature, which, if elevated by only a few degrees, can lead to death by hyperthermia.

Unfortunately, the heat index defined by Steadman [97] was defined only up to certain combinations of heat and humidity, beyond which the heat index was undefined. Those originally undefined regions are labeled V and VI in Figure 8 of Lu and Romps [49]. For example, Steadman was unable to define the heat index for 30 °C (86 °F) at 90% relative humidity, or for 35 °C (95 °F) at 65% relative humidity. The heat index was left undefined in those conditions due to an apparent failure of the underlying model of thermoregulation: the vapor pressure at the skin surface exceeded the saturation value. To allow for extrapolation beyond this point of apparent failure, the NWS developed and adopted a polynomial fit to the heat index as a function of temperature and humidity [63, 83]. But without a model of thermoregulation at the high values of temperature and humidity, those extrapolated values have no interpretation with respect to a thermoregulatory state. Furthermore, as will be shown below, the extrapolated values used by the NWS are biased low by ∼10 °C (∼20 °F) during the peaks of severe heat waves.

Recently, Lu and Romps [49] showed that Steadman's model, and therefore the heat index, could be extended in a physical way. One of the keys to extending the model to high heat and humidity is to allow sweat to drip off the skin; this simple fix avoids any water-vapor supersaturation. This extension is backwards compatible – it gives the same values as the model of Steadman [97] where the original model was defined – but extends the definition of the heat index to all combinations of temperature and humidity. And, as with the original heat index, every value maps one-to-one to a one-dimensional family of thermoregulatory states, which are parameterized by the fraction of skin covered by clothing in very cold conditions, the thickness of clothing in cold-to-mild conditions, the skin blood flow in hot conditions, and the rate of core-temperature rise in dangerously hot or lethal conditions.

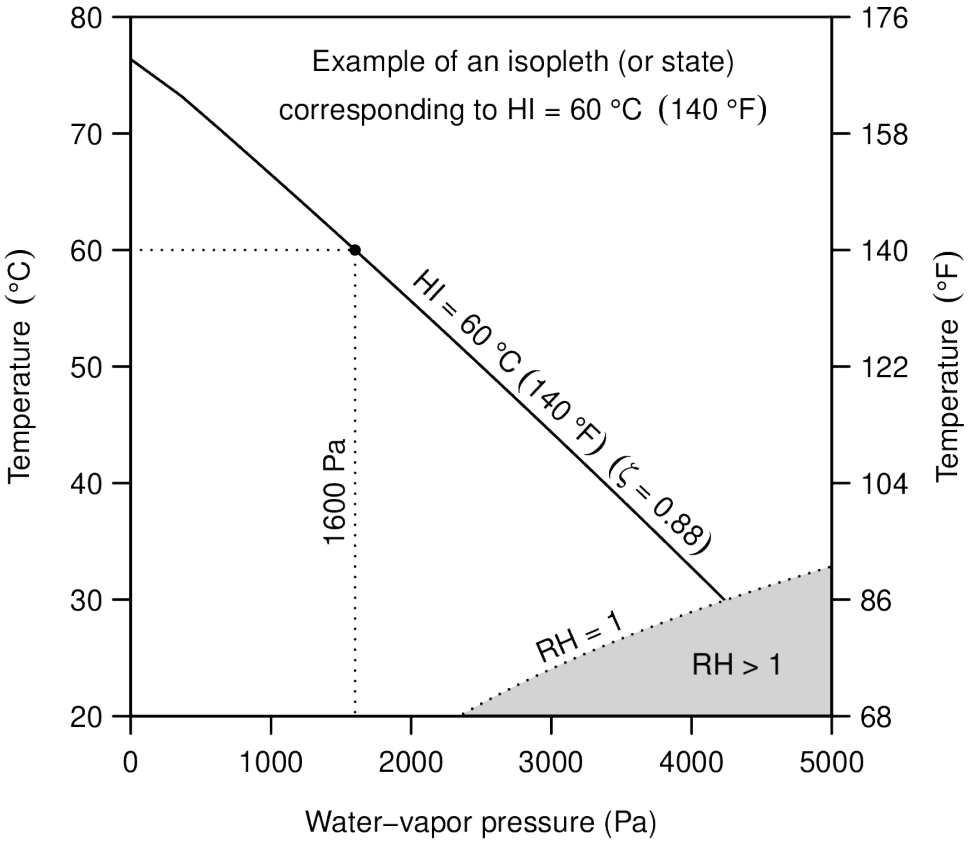

Figure 3.1: The curve, in temperature-humidity space, corresponding to the state with an extra 0.88 liters per minute of skin blood flow. The small circle indicates where the curve intercepts the reference vapor pressure of 1600 Pa. The temperature of that point is 60 °C (140 °F), which defines the heat index (HI) for all points on the curve.

3.3 Methods

To calculate the heat index (HI), we use the instantaneous two-meter temperature and humidity from the National Centers for Environmental Prediction (NCEP) North American Regional Reanalysis [NARR; 55], which provides data at a grid spacing of 32 km every three hours. We calculate the extended heat index [49] for each three hourly snapshot from January 1, 1984 to December 31, 2020. We also calculate the polynomial fit to the heat index developed by the National Weather Service [63, 83] with one minor modification made here to avoid bad behavior at cold temperatures (see the appendix).

We will identify and quantify heat waves using the spatially integrated exceedance of the daily maximum heat index beyond its local 99.9th percentile of daily maxima. This

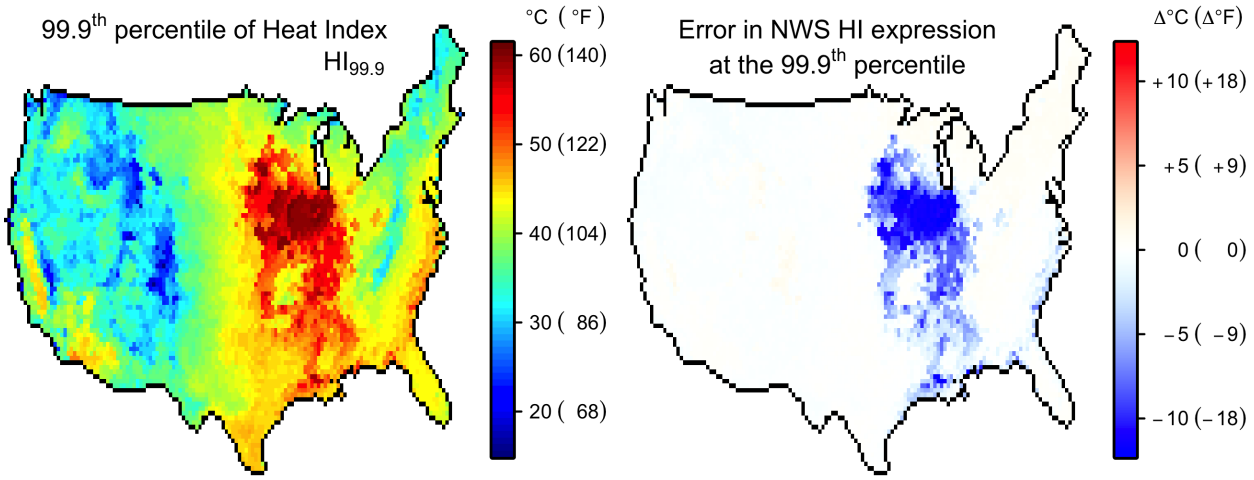

Figure 3.2: (left) The 99.9th percentile of the daily maximum heat index $\mathrm{HI}_{99.9}$. (right) The 99.9th percentile of the daily maximum heat index calculated by the NWS approximation minus the actual $\mathrm{HI}_{99.9}$.

choice defines heat waves in terms of their severity as perceived by humans, although there are other choices that could be made (e.g., weighting the exceedance by population density). The 99.9th percentile is chosen to isolate the most extreme events, i.e., those events comprised of values with a ∼3-year (1000-day) return period.

We first define a grid cell's daily maximum heat index $\mathrm{HI}_{\mathrm{dm}}$ as the highest HI among UTC 12, 15, 18, and 21 on the same date and UTC 0, 3, 6, and 9 of the following day. During spring, summer, and early fall, when CONUS is observing daylight saving, this captures all available NARR data from 5am to 2am (next day) local time on the West Coast and 8am to 5am (next day) local time on the East Coast. With 37 years of data, this gives 13,515 daily maximum values. The next step is to calculate, separately for each grid cell, the 99.9th percentile of $\mathrm{HI}_{\mathrm{dm}}$ over all 13,515 days, which we denote by $\mathrm{HI}_{99.9}$.

The map of $\mathrm{HI}_{99.9}$ is shown in the left panel of Figure 3.2. We see that the most extreme values of the heat index do not occur in the South as one might expect, but in the Midwestern states of Illinois, Iowa, and Missouri. In those states, the 99.9th percentile of the daily maximum heat index reaches up to and beyond 60 °C (140 °F). As seen in the right panel of Figure 3.2, these extreme values are not captured by the polynomial extrapolation used by the NWS. In those midwestern states, the 99.9th percentile is underestimated by the NWS polynomial by as much as ∼10 °C (∼20 °F).

To prepare to identify heat waves, we first calculate the daily time series of the integral over CONUS of the number of degrees that $\mathrm{HI}_{\mathrm{dm}}$ is in excess of the 99.9th percentile,

$$\int_{\mathrm{CONUS}} \mathrm{d}x\,\mathrm{d}y\ \max\left[0, \mathrm{HI}_{\mathrm{dm}}(x,y,d) - \mathrm{HI}_{99.9}(x,y)\right],$$

where x and y denote east-west and north-south distance and d denotes the day. This time series has 13,515 values: one for each day from January 1, 1984 to December 31, 2020. To find the first heat wave, we identify the maximum value in this time series. To find the start and end of that heat wave, we find the largest contiguous interval in that time series containing that maximum for which all values are at least 25% as large as that maximum; this defines the heat wave. We then find the two nearest local minima that bracket that heat wave and set to zero the interval that starts and ends with those two local minima. We then repeat the process to find the second heat wave, and so on. This identifies heat waves naturally ranked by the peak of their area-integrated exceedance of $\mathrm{HI}_{99.9}$. The sensitivity of this ranking to the threshold, chosen here to be 25%, is explored in Figures 3.6 and 3.7. A lower threshold would result in longer-duration heat waves, but would not substantially alter the ranking of the most severe heat waves: for threshold values ranging from 4% to 34%, the ranking of the top 5 heat waves is unchanged.

3.4 Results

For visualization of a heat wave, we define $\mathrm{HI}_{\mathrm{max}}$ for each grid cell as the largest $\mathrm{HI}_{\mathrm{dm}}$ in that grid cell during the days of the heat wave. For each of the top nine heat waves identified by the algorithm described above, Figure 3.3 displays $\mathrm{HI}_{\mathrm{max}}$ minus $\mathrm{HI}_{99.9}$. The most severe heat wave (heat wave #1) is found to be centered on the Midwest during July 17-22, 2011. This time and place corresponds to a heat wave that generated a raft of news coverage and a dramatic spike in heat-related illness [8, 35, 101]. The second most severe heat wave (heat wave #2) is identified as occurring over the same region during July 12-15, 1995. This again corresponds to a well-known heat wave that hit the city of Chicago especially hard, leading to hundreds of heat-related deaths [22, 90, 91, 110]. A list of the top 20 heat waves is given in Table 3.1. Although the Midwest occupies only 26% of the area of the contiguous United States, it contains the peak heat index during 7 of the top 10 heat waves. This is particularly notable in comparison to the South, which occupies 29% of the area, but contains the peak heat index during only 3 of the top 10 heat waves. A list of the top 100 heat waves identified by this algorithm is given in Tables 3.2 and 3.3 and maps of their $\mathrm{HI}_{\mathrm{max}} - \mathrm{HI}_{99.9}$ are shown in Figure 3.8.

The top row of Figure 3.4 displays $\mathrm{HI}_{\mathrm{max}}$ during the top two heat waves. In both cases, the heat index reaches values well in excess of 60 °C (140 °F), reaching 70 °C (157 °F) during the 2011 heat wave and 68 °C (154 °F) during the 1995 heat wave. Compared to $\mathrm{HI}_{\mathrm{max}} - \mathrm{HI}_{99.9}$, $\mathrm{HI}_{\mathrm{max}}$ is more tightly peaked in the Midwest with typical values of ∼130-150 °F. Since Steadman's original model fails for such high heat and humidity, the NWS has used its polynomial fit to report a heat index by extrapolation. The values resulting from that extrapolation are shown in the middle row of Figure 3.4. The peak values of the heat index are noticeably muted in the NWS extrapolation. The error in the NWS extrapolation, shown in the bottom row of Figure 3.4, is ∼10 °C (∼20 °F) for the peak values of the heat index.

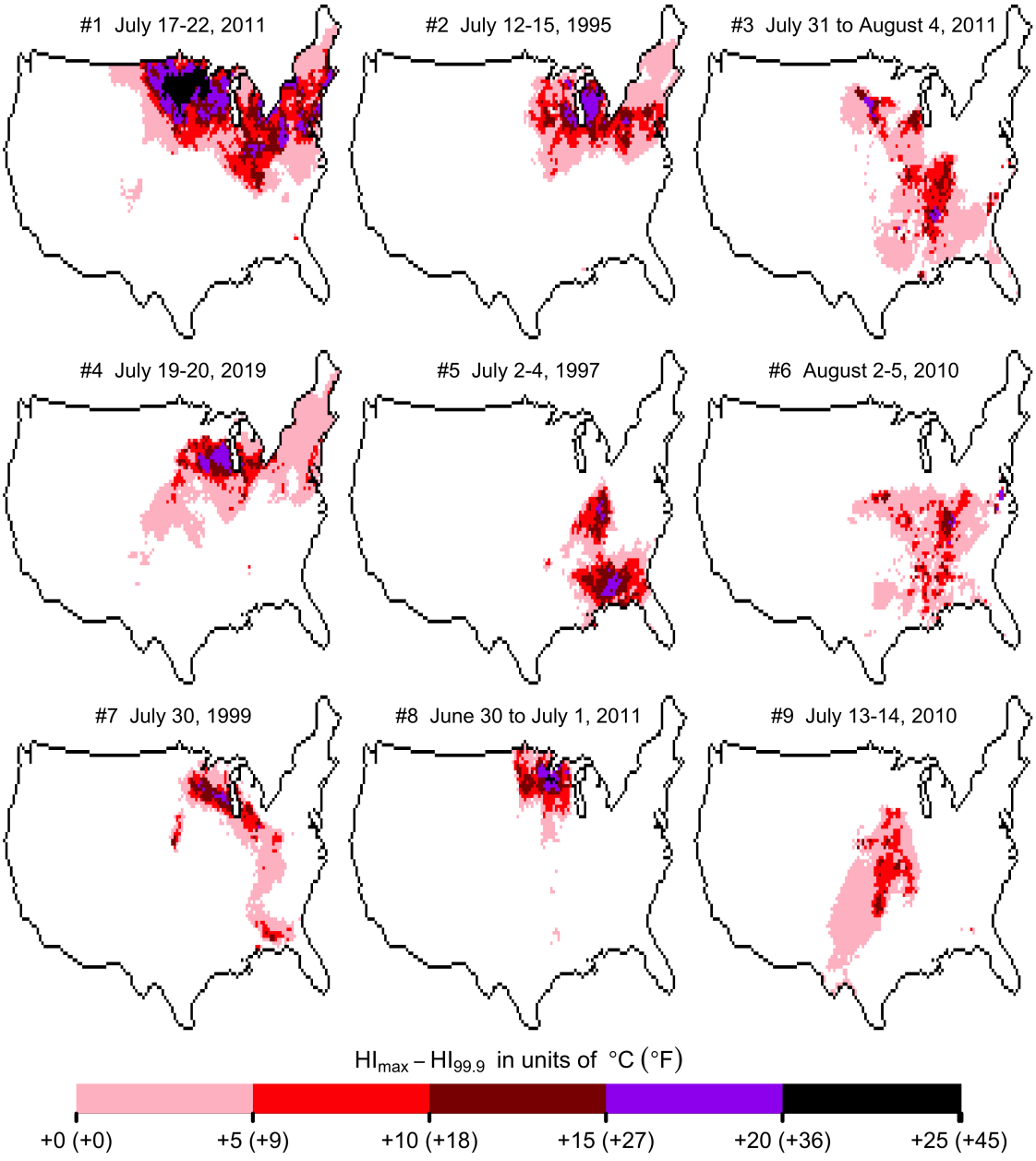

Figure 3.3: The top nine heat waves from January 1, 1984 to December 31, 2020 as identified using the spatially integrated map of $HI_{99.9}$ exceedance.

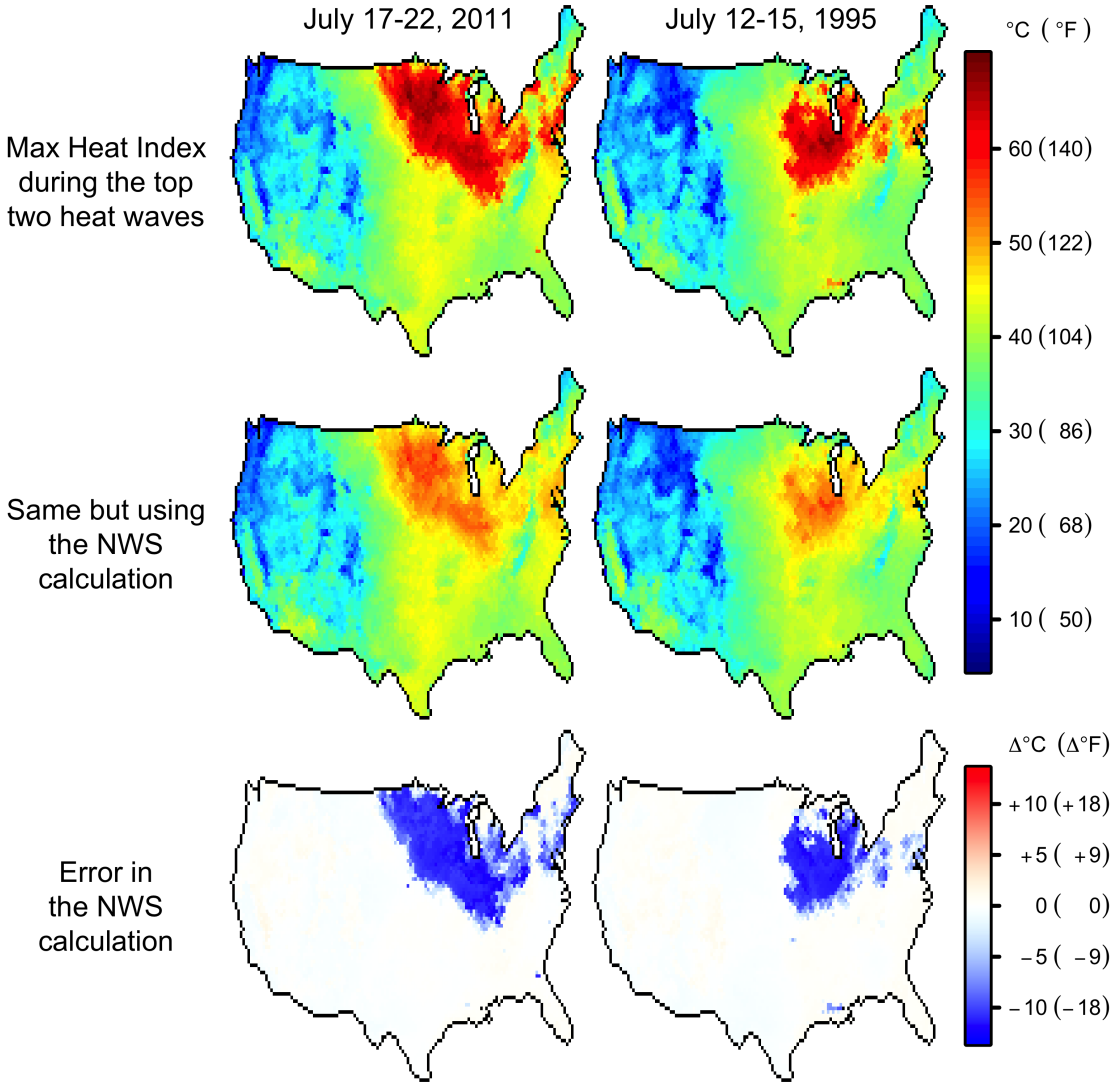

Figure 3.4: (top) Actual HI_{max} for the top two heat waves. (middle) The HI_{max} according to the NWS approximation. (bottom) The error in the NWS approximation.

Rank	Dates	State with max HI	Max HI in °C (°F)	Max NWS value in °C (°F)
1	July 17-22, 2011	North Dakota	70 (157)	59 (139)
2	July 12-15, 1995	Illinois	68 (154)	57 (135)
3	July 31 to August 4, 2011	Mississippi	70 (158)	59 (139)
4	July 19-20, 2019	Iowa	68 (155)	58 (136)
5	July 2-4, 1997	Alabama	63 (145)	51 (124)
6	August 2-5, 2010	Iowa	65 (149)	54 (129)
7	July 30, 1999	Wisconsin	63 (146)	51 (124)
8	June 30 to July 1, 2011	Wisconsin	66 (150)	54 (129)
9	July 13-14, 2010	Iowa	65 (149)	53 (127)
10	July 23-27, 2005	Mississippi	61 (141)	50 (121)
11	July 10-11, 2011	Indiana	64 (147)	52 (126)
12	July 1-3, 2002	Maine	61 (141)	48 (119)
13	August 11-16, 2010	Illinois	64 (147)	52 (126)
14	July 10-14, 2002	Kentucky	47 (117)	43 (109)
15	July 1, 2012	South Carolina	69 (155)	57 (135)
16	July 1-2, 2020	Oklahoma	62 (144)	51 (125)
17	July 13-15, 2015	Tennessee	65 (149)	52 (126)
18	August 12-14, 2019	Louisiana	61 (143)	49 (120)
19	June 30 to July 3, 2018	Texas	59 (139)	46 (114)
20	July 30 to August 3, 2006	Illinois	62 (144)	51 (123)

Table 3.1: Top 20 most severe CONUS heat waves from 1984 to 2020.

During the July 1995 heat wave, the NWS reported a peak heat index of 119 °F at O'Hare airport and 125 °F at Midway airport. Those values were subsequently referenced by major newspapers [43, 47, 59, 99], the Disease Control and Prevention [CDC; 27], and research studies [22, 38, 90, 110]. Using the hourly temperature and relative humidity recorded at O'Hare and Midway, we find that the NWS extrapolation yields a peak HI of 118 °F at O'Hare airport at 1pm local time (when the temperature was 100 F and the relative humidity was 50%) and 124 °F at Midway airport at 12pm (temperature of 100 F and relative humidity of 55%), consistent with the reported values. Using these same temperature and humidity values, we can calculate the actual heat index to have been 123 °F at O'Hare (5 °F higher than reported by the NWS) and 141 °F at Midway (17 °F higher than reported by the NWS).

Like the original heat index, each value of the extended heat index maps one-to-one to thermoregulatory states [49]. For the extreme HI values in the Midwest during the July 2011 and July 1995 heat waves, a healthy adult walking in the shade would have been stressed physiologically in an effort to maintain a healthy core temperature: their body would need to sweat profusely (dripping sweat) and maintain a rapid rate of blood flow to the skin. This

high blood flow would be needed to maintain an elevated skin temperature to ensure that the skin loses net energy to the environment at the same rate that metabolic heat is added to the core.

The right column of Figure 3.5 shows the skin blood flow required to maintain a healthy core temperature at the times of the maximum heat index during the top two heat waves. Combining the model of Steadman [97] with the skin blood flow relation from Gagge et al. [36] [see 49], the normal skin blood flow (i.e., in mild conditions) is 0.57 liters per minute. Therefore, the dark red colors in Figure 3.5 correspond to skin blood flows that are severalfold higher than usual, indicating a high state of physiological stress. The highest rate of skin blood flow measured in the laboratory, achieved by inducing severe thermal stress, is estimated to be around 7.8 l min^{-1} [84, 95]. In the 2011 heat wave, there are a handful of grid cells of the reanalysis that report a required skin blood flow approaching 7.8 l min^{-1} and one grid cell that exceeds that value. In contrast, the required skin blood flow implied by the NWS approximation to the heat index, shown in the left column of Figure 3.5, never exceeds 1.3 l min^{-1} during either heat wave.

3.5 Discussion

Using the heat index, which has recently been extended to high heat and humidity [49], the most physiologically stressful heat waves in the contiguous United States occur most often in the Midwest, not in the South as might be expected or previously reported [e.g., 51, 96]. The finding that the Midwest is home to the most hazardous heat and humidity is manifested both in the map of the 99.9th percentile of the daily maximum heat index $\text{HI}_{99.9}$ (Figure 3.2) and in the locations of the most severe heat waves as ranked by their exceedance of $\text{HI}_{99.9}$ (Figure 3.3). In both the July 1995 and July 2011 heat waves, the soils of the Midwest were moist when the high pressure arrived, trapping heat and humidity in a shallow boundary layer [46, 58]. Although the ingredients of individual events can be described in this way, we are not aware of any first-principles theory for why the most severe US heat waves tend to occur preferentially in the Midwest.

The calculation used by the US National Weather Service underestimates the apparent temperature in extreme heat waves by as much as twenty degrees Fahrenheit. This has real consequences for our understanding of physiological impacts. For example, during the July 1995 heat wave, the heat index at the Midway airport hit a high of 141 °F. In other words, conditions in the shade at the airport felt the same as being in a room at 141 °F with 1.6 kPa of water-vapor pressure (8% relative humidity at that temperature). The physiological consequence of this exposure is that the cardiovascular system must maintain a skin blood flow that is elevated by 170%. In contrast, the heat index of 124 °F calculated by the NWS would imply a skin blood flow that is elevated by only 90%. As seen in the reanalysis, the discrepancy was even larger elsewhere in Illinois during the July 1995 heat wave, with the required skin blood flow elevated by 120% according to the NWS approximation, but elevated by 820% according to the actual heat index. Thus, the approximate calculation

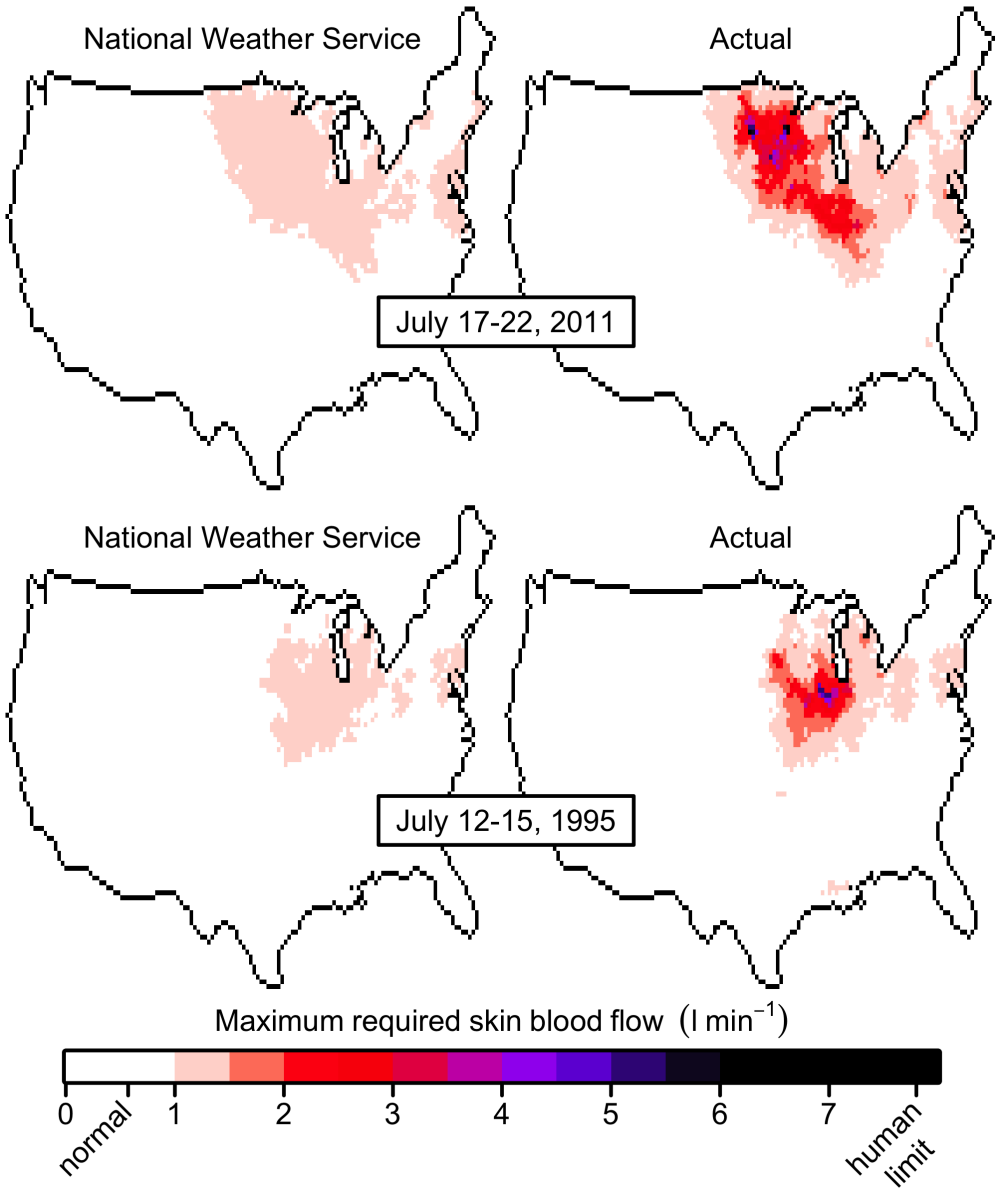

Figure 3.5: The maximum skin blood flow required to maintain a healthy core temperature during the heat waves of (top) July 17-22, 2011 and (bottom) July 12-15, 1995 as calculated using the National Weather Service's approximation to the heat index (left) and the actual heat index (right). On the color bar, "normal" corresponds to 0.57 l min^{-1}, the resting value, and "human limit" corresponds to 7.8 l min^{-1}, the physiological limit estimated from laboratory experiments.

used by the NWS, and widely adopted, inadvertently downplays the health risks of severe heat waves.

Acknowledgments

This work was supported by the U.S. Department of Energy's Atmospheric System Research program through the Office of Science's Biological and Environmental Research program under Contract DE-AC02-05CH11231.

Appendix A: The NWS approximation

The NWS approximation to the heat index is

$$\mathrm{HI} = \begin{cases} X & X \geq 80 \\ Y & X < 80 \end{cases}$$

with

$$\begin{aligned} X = {} & -42.379 + 2.04901523\,T + 10.14333127\,\mathrm{RH} - 0.22475541\,T\,\mathrm{RH} \\ & - 0.00683783\,T^2 - 0.05481717\,\mathrm{RH}^2 + 0.00122874\,T^2\,\mathrm{RH} \\ & + 0.00085282\,T\,\mathrm{RH}^2 - 0.00000199\,T^2\,\mathrm{RH}^2 \\ & - \mathcal{H}(13 - \mathrm{RH})\mathcal{H}(T - 80)\mathcal{H}(112 - T)\frac{13 - \mathrm{RH}}{4}\sqrt{\frac{17 - |T - 95|}{17}} \\ & + \mathcal{H}(\mathrm{RH} - 85)\mathcal{H}(T - 80)\mathcal{H}(87 - T)\frac{RH - 85}{10}\frac{87 - T}{5} \\ Y = {} & 0.5\Big[T + 61.0 + 1.2(T - 68.0) + 0.094\,\mathrm{RH}\Big], \end{aligned}$$

where $\mathcal{H}$ is the Heaviside unit step function and the variables T, RH, and HI in this expression are dimensionless: T is the temperature in degrees Fahrenheit, RH is the relative humidity in percent, and HI is the heat index in degrees Fahrenheit [63, 83]. In the NWS implementation, HI is set equal to X or Y depending on whether X is greater than or less than 80. That leads to some very bad behavior at low temperatures. For example, at 0 °C (32 °F) and 70% relative humidity, the heat index would be given as 74 °C (166 °F). To avoid this problem, we modify the NWS approximation to use $T = 80$ as the dividing line between these two expressions:

$$\mathrm{HI} = \begin{cases} X & T \geq 80 \\ Y & T < 80 \end{cases}.$$

This eliminates the poor behavior at cooler temperatures and does not affect the performance of the approximation at warmer temperatures.

Appendix B: Supplementary Material

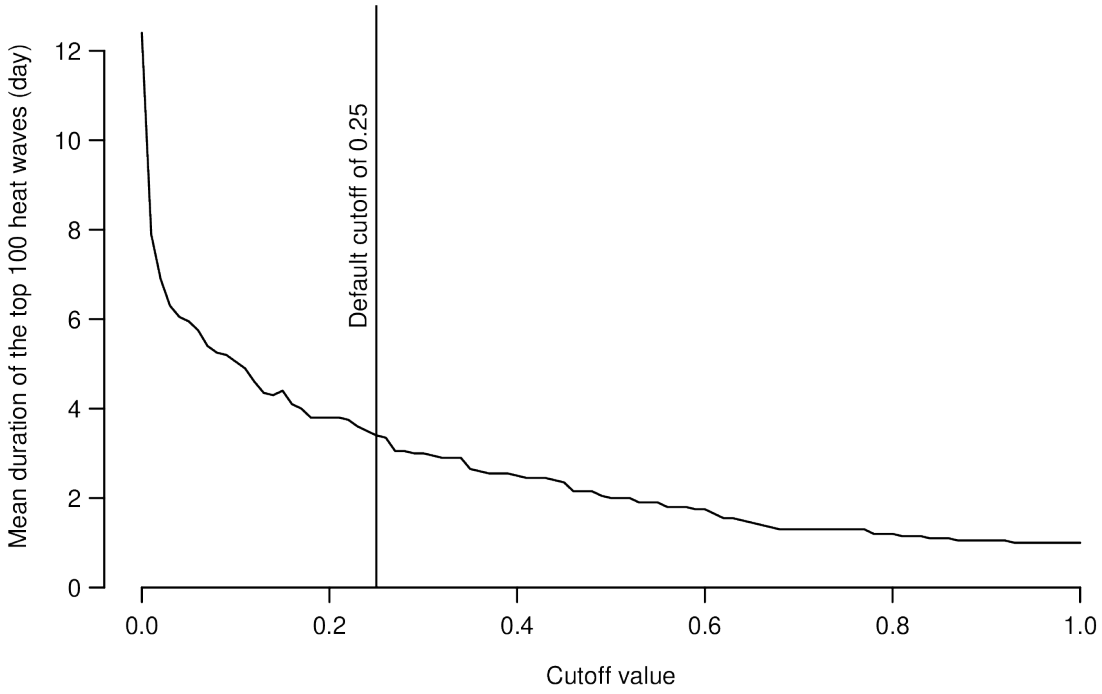

Figure 3.6: The mean duration of the top 100 heat waves identified using the corresponding cutoff. With the cutoff of 0.25 used in the manuscript, the mean duration of the top 100 heat waves is 3.4 days.

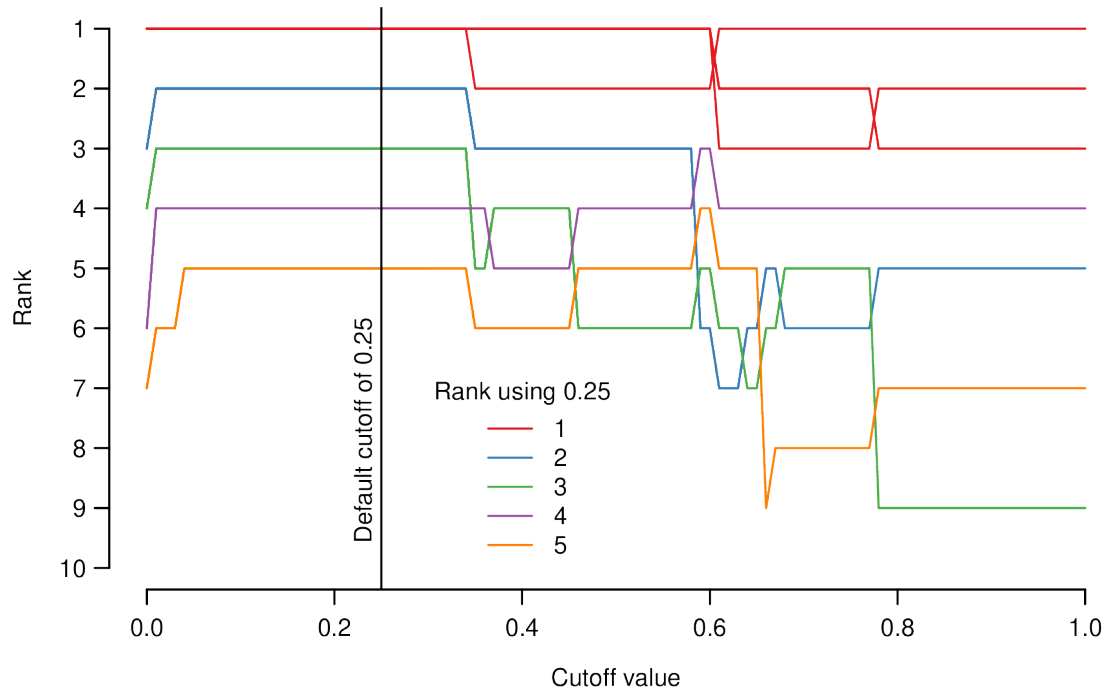

Figure 3.7: For days within the top 5 heat waves identified using the default cutoff of 0.25 (colors), the rank (ordinate) of heatwaves, identified using the cutoff (abscissa), that contain those days. Note that the top heat wave identified with a cutoff of 0.25 is composed of six contiguous days, which get split into two or three separate heat waves when the cutoff equals or exceeds 0.35.

Rank	Dates	State with max HI	Max HI in °C (°F)	Max NWS value in °C (°F)
1	July 17-22, 2011	North Dakota	70 (157)	59 (139)
2	July 12-15, 1995	Illinois	68 (154)	57 (135)
3	July 31 to August 4, 2011	Mississippi	70 (158)	59 (139)
4	July 19-20, 2019	Iowa	68 (155)	58 (136)
5	July 2-4, 1997	Alabama	63 (145)	51 (124)
6	August 2-5, 2010	Iowa	65 (149)	54 (129)
7	July 30, 1999	Wisconsin	63 (146)	51 (124)
8	June 30 to July 1, 2011	Wisconsin	66 (150)	54 (129)
9	July 13-14, 2010	Iowa	65 (149)	53 (127)
10	July 23-27, 2005	Mississippi	61 (141)	50 (121)
11	July 10-11, 2011	Indiana	64 (147)	52 (126)
12	July 1-3, 2002	Maine	61 (141)	48 (119)
13	August 11-16, 2010	Illinois	64 (147)	52 (126)
14	July 10-14, 2002	Kentucky	47 (117)	43 (109)
15	July 1, 2012	South Carolina	69 (155)	57 (135)
16	July 1-2, 2020	Oklahoma	62 (144)	51 (125)
17	July 13-15, 2015	Tennessee	65 (149)	52 (126)
18	August 12-14, 2019	Louisiana	61 (143)	49 (120)
19	June 30 to July 3, 2018	Texas	59 (139)	46 (114)
20	July 30 to August 3, 2006	Illinois	62 (144)	51 (123)
21	July 26-27, 1997	Illinois	63 (145)	51 (123)
22	August 1-4, 2008	Missouri	62 (143)	50 (121)
23	August 8-9, 2010	Iowa	64 (148)	52 (126)
24	July 21-22, 2016	Iowa	66 (151)	54 (130)
25	June 29, 2012	West Virginia	65 (150)	52 (126)
26	August 22, 2010	Mississippi	64 (147)	51 (123)
27	June 15, 2016	Oklahoma	63 (145)	52 (126)
28	July 4, 2012	Minnesota	62 (143)	49 (120)
29	July 24-25, 2015	Arkansas	67 (153)	56 (133)
30	July 21-23, 2007	North Dakota	46 (114)	46 (114)
31	July 6-8, 2012	Indiana	61 (141)	50 (122)
32	August 3-7, 2001	Minnesota	62 (144)	50 (122)
33	July 21-24, 2006	Kentucky	53 (127)	45 (112)
34	July 17, 2010	Kansas	61 (142)	51 (123)
35	June 22-24, 2009	Iowa	67 (152)	55 (131)
36	July 10-13, 2020	Louisiana	60 (140)	48 (118)
37	August 8-11, 2007	Indiana	59 (139)	48 (119)
38	June 30 to July 2, 2013	California	48 (118)	48 (119)
39	July 4-5, 1999	Michigan	60 (139)	47 (117)
40	August 6-11, 2015	Louisiana	62 (143)	49 (121)
41	June 20-22, 2019	Mississippi	60 (140)	47 (116)
42	July 23-25, 2010	Illinois	61 (141)	49 (120)
43	July 24, 2016	Illinois	63 (145)	51 (124)
44	July 29-30, 2015	Louisiana	62 (143)	50 (121)
45	June 19, 1998	Oklahoma	62 (144)	51 (124)
46	June 9, 2020	Arkansas	60 (140)	48 (118)
47	August 23-24, 2011	Nebraska	63 (146)	52 (126)
48	June 26-28, 1994	Oklahoma	55 (132)	47 (116)
49	June 26-28, 2013	Missouri	60 (141)	48 (119)
50	August 7, 2011	Tennessee	61 (142)	51 (123)

Table 3.2: First half of the top 100 most severe CONUS heat waves from 1984 to 2020.

Rank	Dates	State with max HI	Max HI in °C (°F)	Max NWS value in °C (°F)
51	July 22-23, 2003	Arizona	44 (110)	44 (111)
52	July 29, 1993	Georgia	60 (140)	47 (117)
53	July 31, 2010	Florida	64 (147)	53 (127)
54	August 9-10, 2018	California	44 (111)	44 (112)
55	August 27, 2011	Florida	59 (138)	47 (117)
56	June 23, 2015	Missouri	60 (139)	47 (117)
57	August 19, 2019	Kansas	61 (141)	50 (121)
58	July 30 to August 1, 2000	California	46 (114)	46 (114)
59	August 15-16, 1995	Florida	61 (141)	46 (115)
60	August 16, 2020	Louisiana	60 (139)	48 (118)
61	July 5-8, 2016	Missouri	61 (142)	48 (118)
62	August 21-22, 2005	Alabama	60 (141)	47 (116)
63	July 14-16, 1988	Illinois	62 (144)	52 (125)
64	July 20-21, 2005	Illinois	57 (134)	46 (114)
65	June 27, 1998	Iowa	61 (142)	50 (122)
66	June 24-26, 2012	Louisiana	54 (129)	46 (115)
67	August 26, 2019	Oklahoma	59 (139)	48 (118)
68	August 10-11, 2016	Louisiana	64 (147)	51 (125)
69	June 17-18, 2016	Oklahoma	59 (138)	49 (120)
70	June 13-15, 1998	Oklahoma	60 (140)	49 (120)
71	August 20, 2011	Mississippi	63 (145)	51 (124)
72	August 14, 1999	Florida	63 (146)	50 (122)
73	July 18-19, 1998	Iowa	56 (133)	46 (114)
74	August 9-11, 2011	Mississippi	58 (137)	48 (118)
75	June 28-29, 2015	California	44 (111)	44 (112)
76	August 1, 2012	Mississippi	62 (143)	50 (121)
77	August 18, 1995	South Carolina	61 (142)	47 (117)
78	August 8, 1995	Iowa	60 (140)	46 (116)
79	August 6, 2016	Mississippi	64 (146)	51 (124)
80	June 4-5, 1998	Texas	50 (121)	45 (114)
81	May 25, 2016	Oklahoma	60 (140)	48 (118)
82	June 24-25, 1988	Minnesota	46 (115)	45 (112)
83	July 27-29, 2009	California	45 (114)	46 (114)
84	July 20-21, 2002	Minnesota	63 (146)	51 (124)
85	July 1-2, 1992	Oklahoma	59 (138)	48 (119)
86	August 18-19, 2020	California	48 (119)	49 (120)
87	June 28-29, 1990	Iowa	47 (116)	44 (111)
88	July 17, 2015	Mississippi	63 (146)	50 (123)
89	August 14-15, 2003	California	44 (112)	44 (112)
90	June 21, 2011	Texas	48 (118)	48 (118)
91	June 27-28, 2018	Georgia	61 (142)	47 (117)
92	September 6-7, 2020	California	50 (122)	50 (122)
93	June 19, 2007	Texas	52 (125)	46 (115)
94	June 28, 2009	Mississippi	60 (141)	48 (119)
95	July 27, 2012	North Carolina	61 (142)	47 (117)
96	August 29, 2020	Arkansas	60 (140)	47 (117)
97	July 21, 2014	Minnesota	60 (139)	47 (117)
98	September 23, 2006	Texas	53 (127)	46 (116)
99	July 17, 2001	Iowa	60 (141)	49 (120)
100	June 7, 1995	Oklahoma	60 (141)	48 (119)

Table 3.3: Second half of the top 100 most severe CONUS heat waves from 1984 to 2020.

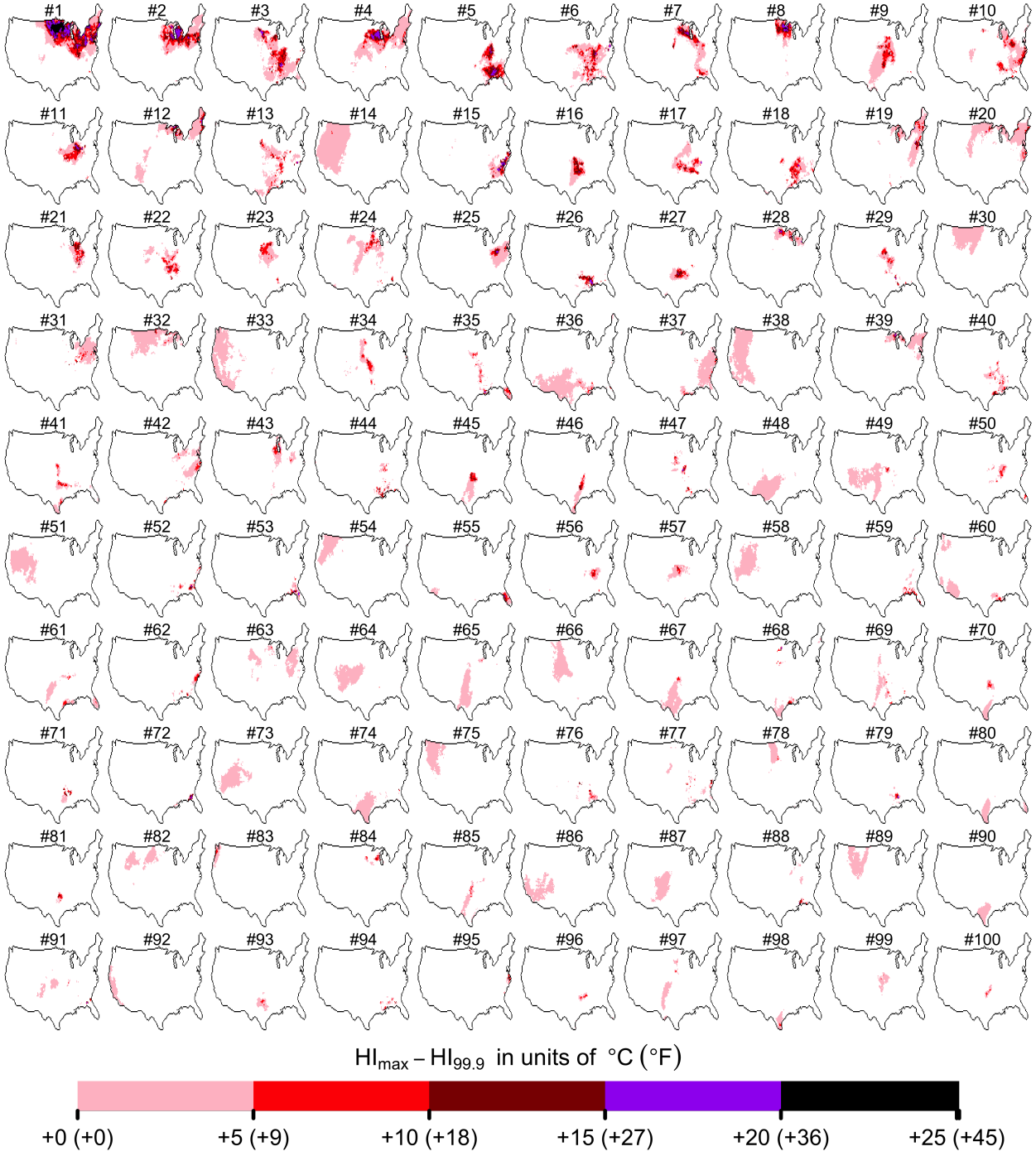

Figure 3.8: The top 100 heat waves from January 1, 1984 to December 31, 2020.

Chapter 4

Predicting Fatal Heat and Humidity Using the Heat-Index Model

As a publication in a physiology journal, this chapter will use temperatures in Celsius (°C).

4.1 Introduction

It is been argued that humans cannot survive sustained exposure to a wet-bulb temperature T_w higher than a unique value of 35°C because such exposure would lead to a fatal core temperature [93]. Subsequently, this T_w threshold has been used in many studies looking at survivability in global-warming scenarios [e.g., 17, 41, 42, 57, 70, 76, 78, 80, 85, 88, 94]. On the other hand, Vecellio et al. [106] recently showed experimentally that the core temperature starts to rise (by accumulation of metabolic heat) not at a unique T_w but at a range spanning 26 to 30°C. Companion studies [18, 111] found an even wider range of critical wet-bulb temperatures for subjects with different metabolic rates. These results motivate a search for more reliable predictors of heat stress and heat death.

Before building such predictors, it is important to distinguish between 1. the threshold for the core temperature to rise, as measured by Cottle et al. [18], Vecellio et al. [106], and Wolf et al. [111], and 2. the survivability threshold as defined by Sherwood and Huber [93]. The core temperature starts to rise when the accumulated metabolic heat brings the core temperature T_c above its healthy value of 37°C. An elevated core temperature is tolerable for fit and young adults as long as T_c remains at or below 38-39°C [65]. On the other hand, a sustained core temperature of 41-42°C is a state of severe hyperthermia that is not generally survivable[1] [9], and is therefore identified as the survivability threshold.

[1]Note that a heat-related fatality can occur for a variety of reasons. For example, the elevated skin blood flow that precedes an elevated core temperature stresses the cardiovascular system, and heart failure can occur in advance of the fatal core temperature [37]. Therefore, a core temperature of 41-42°C is a conservative threshold for survivability, applicable to young, healthy adults.

For obvious reasons, laboratory experiments do not intentionally induce core temperatures up to the threshold for survivability. Instead, human subjects are stressed only up to the point where their core temperature begins to rise above a standard temperature of 37°C [e.g., 18, 106, 111]. To calculate what combinations of heat and humidity are fatal, we must extrapolate from the experimental data. Although Sherwood and Huber [93] suggest that a core temperature of 41-42°C is induced at a wet-bulb temperature of 35°C, the fact that core temperatures begin to rise at a wide range of wet-bulb temperatures suggests that there is no unique fatal T_w.

In fact, we can understand from first principles why there is no unique T_w corresponding to heat stress or heat death. In a state of nakedness, profuse sweating, and a high rate of skin blood flow (pegging the skin temperature nearly equal to the core temperature T_c), the body has exhausted all of its thermoregulatory mechanisms. Ignoring respiratory ventilation for simplicity, a steady core temperature implies a balance between metabolism, radiation, and turbulent fluxes of sensible and latent heat,

$$Q - \sigma T_c^4 + \sigma T^4 - f(u)\left\{c_p(T_c - T_w) + L\left[q_v^*(T_c) - q_v^*(T_w)\right]\right\} = 0\,, \tag{4.1}$$

where Q is the metabolic heat generation per skin area, $\sigma = 5.67 \times 10^{-8}$ W m^{-2} K^{-4} is the Stefan-Boltzmann constant, u is the wind speed and $f(u)$ is an effective mass flux of turbulent exchange between the skin and air, c_p is the heat capacity of air at constant pressure, L is water's specific latent heat of evaporation, $q_v^*(T)$ is the saturation mass fraction of water vapor, T is the temperature of the air and surroundings, and T_w is the wet-bulb temperature of the air. Consistent with the heat index model, which assumes a person is in the shade, there is no shortwave absorption here and the radiating surfaces are assumed to have the same temperature as the air. In equation (4.1), all the temperatures are understood to be the absolute temperatures, i.e., with units of kelvin.

We can now consider various limits for f. In a hypothetical scenario with no wind (i.e., not even natural convection, which is eliminated in zero gravity), f would be zero and the metabolic heat would need to be matched by net radiation. Therefore, in zero wind, there is a unique maximum temperature $T = (T_c^4 - Q/\sigma)^{1/4}$ that is compatible with a given steady-state core temperature T_c and metabolic rate Q. In the limit of infinite wind speed, f is infinite and there is a unique maximum wet-bulb temperature $T_w = T_c$ compatible with a given T_c. For a finite non-zero wind speed, there is no unique maximum T_w compatible with a given core temperature; instead, the maximum T_w is a function of Q and relative humidity (equivalently, a function of Q and T because the relative humidity can be calculated from T_w and T). These facts are illustrated in Figure 4.1, which plots the most thermally stressful combinations of T and T_w (for three different wind speeds u and two different metabolic rates Q) that are compatible with $T_c = 37^\circ$ C. For $u = 0$ and a given Q, the solution to (4.1) is a locus of points at a single T. For $u = \infty$, the solution to (4.1) is a locus of points at a single T_w. For a given Q, it is only in the limit of infinite wind speed that there is a unique maximum T_w (equal to T_c) that is compatible with a core temperature of T_c, regardless of Q and relative humidity; for all finite wind speeds, the maximum T_w is a function of both Q

and relative humidity. Therefore, there should be no single T_w that predicts when the core temperature will rise above a standard value of 37°C, and no single T_w that corresponds to fatal conditions of T_c = 41-42°C.

Indeed, as shown in the recent empirical studies, the wet-bulb temperature at which humans begin to have elevated core temperatures varies from person to person and with different levels of exertion. To capture this variability, we must use a model of a human's core temperature that incorporates the metabolic rate, ambient temperature and humidity, and the wind speed. For this purpose, we use the model of thermoregulation that underlies the heat index [49, 97]. In the next section, we describe the how this thermoregulation model is built and illustrate how this model can be used to define an index for heat stress.

4.2 The heat index model

Humans use several behavioral and physiological strategies to maintain their core temperature T_c at or close to its standard value of 37°C. The model underlying the heat index makes the simplifying assumption that those strategies form a one-dimensional space [49, 97], i.e., that the different strategies are deployed one after another as opposed to in parallel. For example, in extremely cold conditions, the clothing is infinitely thick and the human chooses only what fraction of the skin to leave exposed. In cold and mild conditions, the area of exposed skin is held constant, but the thickness of clothing is varied. In hot conditions, the clothing thickness is set to zero, but the skin blood flow is modulated. In extremely hot conditions, the skin blood flow is infinite[2], so all thermoregulatory strategies have been exhausted, but the thermoregulatory state can be quantified by the temperature above 37°C at which the core equilibrates.

Because the various strategies are used sequentially, a single real number can be used to encode four pieces of information: the area of exposed skin [which varies only in what 49, called region I], the clothing thickness (varies only in regions II and III), skin blood flow (varies only in regions IV and V), and the equilibrium core temperature (varies only in region VI). There are an infinite number of ways to map this set of strategies, or thermoregulatory states, to a real number. A particularly convenient choice is to map each state to the air temperature that, when combined with a set of commonly experienced reference values for vapor pressure, wind speed, and metabolic rate, would cause a human to adopt that state. This mapping is called the apparent temperature T_a and was defined by Steadman [97] using a reference vapor pressure of p_{v0} = 1.6 kPa, a reference wind speed of u_0 = 1.5 m s^{-1}, and a reference metabolic rate of Q_0 = 180 W m^{-2}. Given this definition of apparent temperature,

[2]The model underlying the heat index is an idealization in several regards, including its assumption that humans can have an infinite skin blood flow. Lu and Romps [49] showed that imposing a realistic upper bound for the skin blood flow introduces, at most, minor corrections to the heat index at the expense of introducing an additional parameter. For the experiments in Wolf et al. [111] that will be discussed in this work, imposing a realistic upper bound would change the predicted equilibrium core temperature by less than 0.5°C.

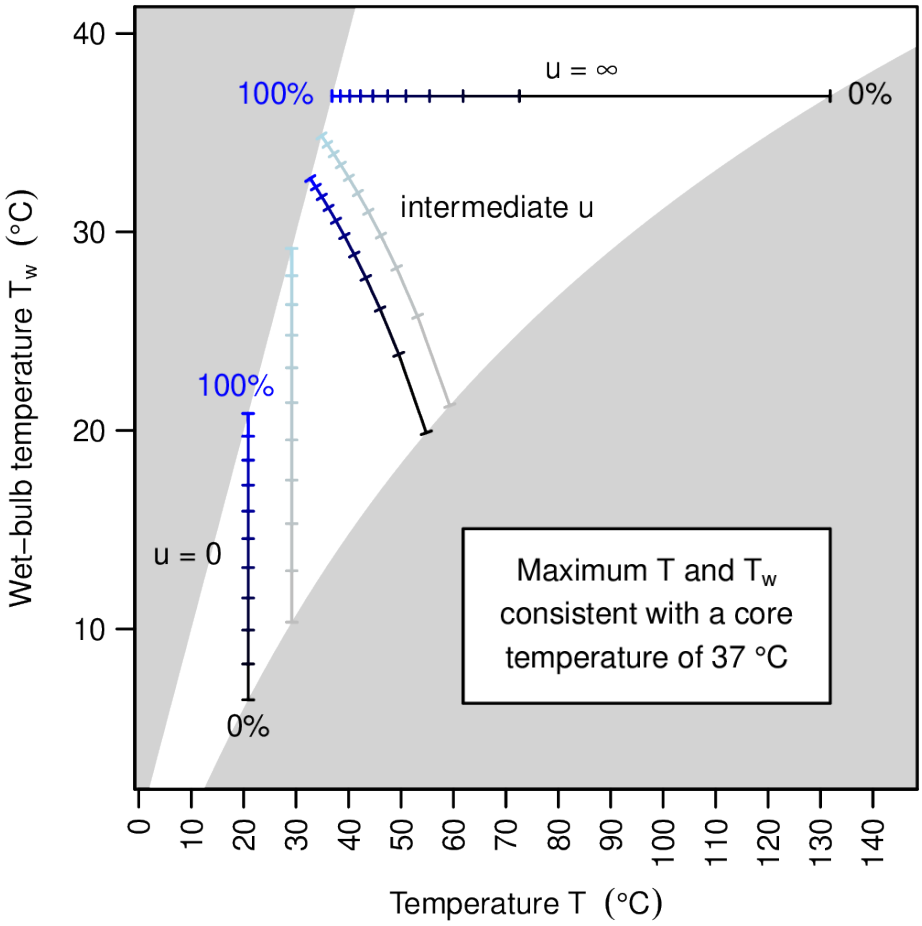

Figure 4.1: Maximum temperature T and wet-bulb temperature T_w that are compatible with a core temperature of $T_c = 37°\mathrm{C}$, plotted for three different wind speeds. For each locus of points, the tick marks indicate 10% increments of relative humidity, ranging from (black) 0% to (blue) 100%. The three black-and-blue curves show the loci of points for a metabolic heat production of $Q = 100$ W m^{-2}. The grey-and-light-blue curves show the same for $Q = 50$ W m^{-2}; the grey-and-light-blue $u = \infty$ curve is hidden underneath the black-and-blue $u = \infty$ curve, which is independent of Q. The two greyed-out regions denote pairs of T and T_w that are unphysical because they would imply a relative humidity greater than one or less than zero.

the thermoregulation model gives us the function $T_a\left(T, p_v, u, Q\right)$. Note that the apparent temperature satisfies the identity $T_a(T, p_{v0}, u_0, Q_0) = T$.

The heat index is a special case of the apparent temperature in which the arguments u and Q are replaced by their reference values of 1.5 m s^{-1} and 180 W m^{-2}, respectively. In other words, the heat index HI is defined as

$$\mathrm{HI}(T, p_v) = T_a\left(T, p_v, u_0, Q_0\right) . \tag{4.2}$$

Therefore, the heat index should be used with care as it is the apparent temperature for the observed temperature and vapor pressure, *but assuming the human has a metabolic rate of 180 W m^{-2} and is in a breeze of 1.5 m s^{-1}*. In this work, we will use the more general apparent temperature to explain the empirical data from Vecellio et al. [106], Cottle et al. [18], and Wolf et al. [111] because their experiments were conducted at various metabolic rates (all below 180 W m^{-2}) in a room with a wind speed much smaller than 1.5 m s^{-1}. Nevertheless, we will use the same model of thermoregulation that underlies the definition of the heat index.

By construction, the equilibrium core temperature is a function of apparent temperature T_a: for apparent temperatures below 71.5 °C, the equilibrium core temperature is 37 °C[3], but it rises monotonically with higher apparent temperatures, as shown in the top panel of Figure 4.2. At an apparent temperature of 93.3 °C, the core temperature equilibrates at 42 °C, which is considered a fatal value if sustained[4]. These two apparent temperature thresholds are labeled in Figure 4.2. This curve, mapping apparent temperature to equilibrium core temperature, is invariant with respect to the metabolic rate: all else equal, a higher metabolic rate will move a person to the right on this curve, but will not change the curve itself.

Since the human body has thermal inertia, a sudden exposure to an apparent temperature at or beyond 93.3 °C does not immediately bring the core to 42 °C. Instead, the time it takes the core to reach 42 °C depends mainly on the apparent temperature and wind speed. The bottom panel of Figure 4.2 plots this "time to death" as a function of apparent temperature for two different cases considered in the next section: "light" exertion (Q = 82.9 W m^{-2})

[3]In the heat-index model, the core temperature stays constant until the body's metabolic heat becomes uncompensable at the apparent temperature of 71.5 °C. This differs from some other thermoregulation models (e.g., Stolwijk and Hardy [100]) that have an "active" system in which the skin blood flow and sweating rate are sensitive functions of the core and/or skin temperatures. In those active models, the core temperature would rise slightly above 37 °C to trigger the necessary vasodilation and sweating even before the apparent temperature exceeds 71.5 °C. The heat-index model is built as a "passive" system, in which these sensitive relationships are approximated by diagnostic relationships, which set the skin blood flow and sweating rate at the values needed to keep the core temperature at 37 °C.

[4]Temperatures of 71.5 and 93.3 °C might sound absurdly high, but these are calculated using the original convention of Steadman [97], who defined the heat index with respect to a reference water-vapor pressure of 1.6 kPa. At that water-vapor pressure, 71.5 °C has a relative humidity of 5% and a wet-bulb temperature of only 30.0 °C. Likewise, 93.3 °C has a relative humidity of 2% and a wet-bulb temperature of only 34.1 °C. With the reference wind speed of 1.5 m s^{-1}, the enormous latent heat of water vapor enables the temperature of a wetted surface, or a sweaty human, to be much lower than the dry-bulb temperature. See the Appendix for a related discussion of practical limits on the sweating rate.

and "moderate" exertion ($Q = 133$ W m^{-2}) under an indoor wind speed ($u = 0.2$ m s^{-1}). These curves are nearly on top of each other: all else equal, a higher metabolic rate will move a person to the right along these curves, but will not substantially alter the curves themselves.

When the apparent temperature T_a is less than 93.3 °C, the time for the core to reach 42 °C is infinite, meaning that the core will equilibrate at a temperature below 42 °C. For T_a above 93.3 °C, the time it takes to reach the fatal core temperature is a function of $\Delta T_a \equiv T_a - 93.3$ °C. Assuming the indoor wind speed, the time it takes to reach a fatal core temperature is nearly independent of the metabolic rate: it takes less than 2 hours if $\Delta T_a \gtrsim 8$ °C and less than 1 hour if $\Delta T_a \gtrsim 20$ °C. The procedure for calculating the time to reach any given core temperature can be found in Lu and Romps [49].

In the following sections, the apparent temperature will be used to explain the empirical data from Vecellio et al. [106], Cottle et al. [18], and Wolf et al. [111]. It will be shown that a unique apparent temperature of 71.5 °C reliably predicts the varying wet-bulb temperatures at which individuals' core temperatures begin to rise under different levels of exertion. Using an apparent temperature of 93.3 °C, we can predict the temperature and humidity at which the individuals' core temperatures would equilibrate at the fatal value of 42 °C given sustained exposure.

4.3 Methods

Here, we briefly describe the experiments of Wolf et al. [111, hereafter, W22] and its companion works [18, 106]. There are two sets of experiments, all conducted indoors. In the first set of experiments, the subjects perform light exertion with an average net metabolic rate of 82.9 W m^{-2}. In the second set, the subjects perform moderate exertion with an average net metabolic rate of 133 W m^{-2}. In each set of experiments, there are six different scenarios. In the first three scenarios, the air temperature T is fixed at about 36°C, 38°C, and 40°C, respectively, while the vapor pressure is gradually increased until the core temperature of the subject starts to rise. In the other three scenarios, the vapor pressure p_v is fixed at around 2.7 kPa, 2.1 kPa and 1.6 kPa, respectively, while the air temperature is gradually increased until the subject's core temperature starts to rise. These 12 empirical combinations of critical (T, p_v) are re-plotted in Figure 4.3 as black round and triangle symbols. Each symbol represents an average of multiple human subjects and the error bar represents the standard deviation.

To predict these critical (T, p_v) using the heat index model, we plug the actual Q and u into the equation

$$T_a\left(T, p_v, Q, u\right) = 71.5\ ^\circ\mathrm{C}\,, \tag{4.3}$$

which then defines the critical curve in temperature-humidity space. For any (T, p_v) on this curve, a positive increment of temperature or humidity will force the core temperature to rise above its standard value of 37°. Since there are two different metabolic rates in the experiment – 82.9 W m^{-2} and 133 W m^{-2} – we obtain two curves from equation (4.3),

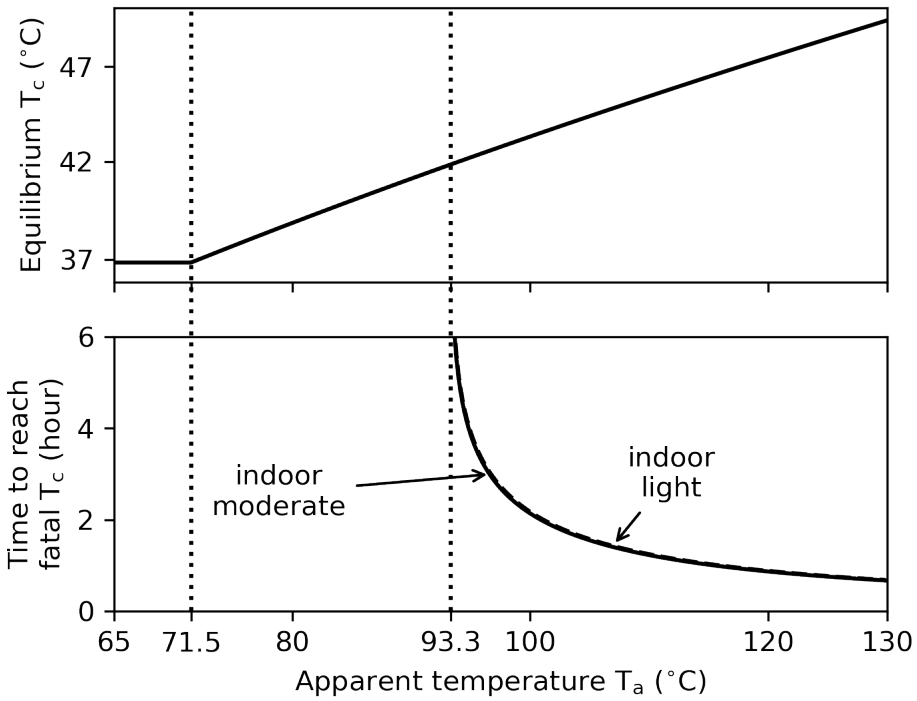

Figure 4.2: (top panel) The equilibrium core temperature as a function of the apparent temperature T_a. The dashed vertical lines mark the thresholds of 71.5 °C (core temperature begins to rises) and 93.3 °C (core temperature would equilibrate at 42 °C). (bottom panel) The time it takes the core to reach the fatal value of 42 °C for the wind speed of 0.2 m s^{-1}. These curves have a very weak, almost imperceptible, dependence on the metabolic rate: the dashed curve is for $Q = 82.9$ W m^{-2} (the mean value for the "light" exertion group defined in the next section) and the solid curve is for $Q = 133$ W m^{-2} (the mean value for the "moderate" exertion group).

one for each level of exertion. Regarding the wind speed, although we have written the apparent temperature T_a as a function of u, T_a is really a function of the body's effective heat transfer coefficient [49]. One approach to dealing with this would be to measure the wind speed experimentally and then convert that to a heat transfer coefficient using a theoretical relationship. W22 quotes a wind speed of 0.45 m s^{-1} from previous work [44] that used the same experimental chamber but with different subjects doing more vigorous exercise. Because there is no forced wind in the chamber, the effective wind speed is induced by the movement of the subjects and natural buoyancy-driven convection, and it will depend on body posture [20, 48, 68, 115]. Due to these sources of uncertainty, we take a different approach: we choose the optimal heat transfer coefficient that minimizes the sum of squared differences in vapor pressure between the two curves and the 12 empirical data points. The heat transfer coefficient obtained using this procedure is 3.0 W m^{-2} K^{-1}; a nearly identical value is obtained by minimizing error in temperature instead of vapor pressure. Using the Churchill and Bernstein [15] relation, this corresponds to a wind speed of 0.2 m s^{-1}, to which we will refer henceforth, with the understanding that it represents a heat transfer coefficient of 3.0 W m^{-2} K^{-1}.

To calculate the survivable limit in the experiments, i.e., the (T, p_v) for which the subjects' core temperatures would have equilibrated at 42 °C, we use the same two metabolic rates (82.9 and 133 W m^{-2}) and the same optimal wind speed (0.2 m s^{-1}). The equation

$$T_a\left(T, p_v, Q, u\right) = 93.3\ ^\circ\mathrm{C} \tag{4.4}$$

then gives curves in temperature-humidity space that define the survivable limit.

4.4 Results

The two black curves in Figure 4.3, labeled by "indoor light" and "indoor moderate", correspond to an apparent temperature of 71.5 °C, with one curve for each exertion level. Despite tuning only a single parameter (the effective wind speed), these curves do a good job of fitting all of the empirical data with two different metabolic rates. The two red curves in Figure 4.3 correspond to the fatal apparent temperature of 93.3 °C. Comparing curves at the same exertion level, we see that the experiments (black curves) were within 13-16 °C (at constant vapor pressure) or 2.5 kPa (at constant temperature) of the survivable limit (red curves). As discussed in section 4.2, exposure to conditions beyond the red curves would not immediately bring the core to 42 °C, but would take a length of time that is a function of the exceedance of T_a beyond 93.3 °C.

In addition to the curves of constant apparent temperature, Figure 4.3 also plots the isopleths of wet-bulb temperature. We see that the indoor light and moderate black curves (apparent temperature = 71.5 °C) occupy a range of wet-bulb temperature from 20 to 32 °C. This explains the wide spread of critical wet-bulb temperatures recorded by Vecellio et al. [106]: the core temperature rises at a single apparent temperature of 71.5 °C, but this apparent temperature translates to a range of wet-bulb temperatures. The isopleths of the

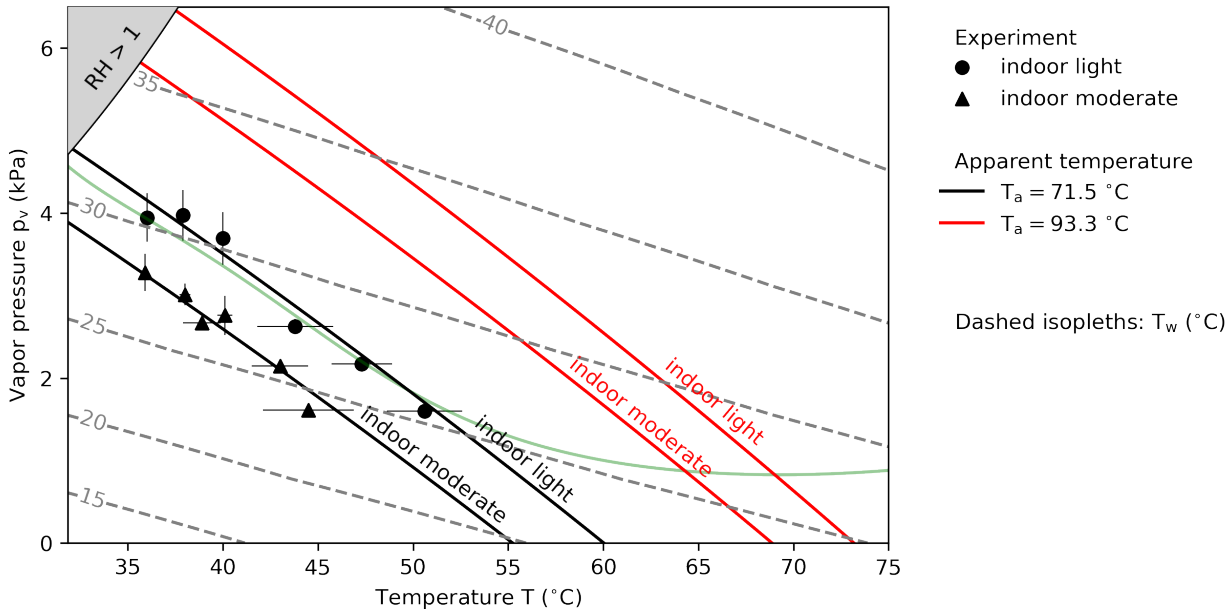

Figure 4.3: (black symbols) Empirical combinations of temperature and vapor-pressure that cause the core temperature to rise above 37 °C with the indoor wind speed. Light exertion is shown with circles and moderate exertion is shown with triangles. Each symbol represents an average of multiple subjects and the error bar represents the standard deviation. (black curves) Constant apparent temperature of 71.5 °C with the indoor wind speed and light or moderate exertion. (red curves) Same as black curves, but with a constant apparent temperature of 93.3 °C, which leads the core temperature to equilibrate at 42 °C. The indoor wind speed of 0.2 m s^{-1} is chosen using an optimization process as described in section 4.3. (dashed contours) Isopleths of wet-bulb temperature. (light green curve) The 125 °F isopleth of the NWS polynomial approximation to the heat index, which exhibits unphysical behavior and matches the "indoor light" points only by coincidence as discussed in section 4.5.

wet-bulb temperature and the apparent temperature have different slopes in temperature-humidity space, and the apparent-temperature isopleths better explain the empirical data measured by W22. As indicated by the indoor light and moderate red curves (apparent temperature = 93.3°C) in Figure 4.3, the subjects' core temperatures should equilibrate at 42 °C at wet-bulb temperatures ranging from 24 to 37 °C, compared to the single threshold of 35 °C proposed by Sherwood and Huber [93].

For a given wind speed, a lower metabolic rate enables a person to endure hotter and more humid conditions. This is consistent with the positions of the "indoor light" and "indoor moderate" curves in temperature-humidity space. As the wind speed is increased, the transfers of sensible and latent heat increasingly dominate the energy balance in equation (4.1), and we expect the curves of constant core temperature would move upwards and more closely align with curves of constant wet-bulb temperature. Indeed, at the limit of infinite wind speed, the curve corresponding to a constant core temperature of T_c is defined by $T_w = T_c$, as discussed in section 4.1. Curves obtained in this way would be appropriate for individuals who are outdoors in strong winds.

4.5 Discussion

We have seen that the apparent temperature is more accurate than the wet-bulb temperature at predicting a human's core temperature. To make this statement quantitative, we can consider the 12 experiments of W22. For each of those experiments, we can use a constant apparent temperature (of 71.5 °C) to predict the wet-bulb temperature at which the core temperature should begin to rise. The errors are then the differences between the predicted and actual wet-bulb temperatures. Likewise, we can use a constant wet-bulb temperature to predict when the core temperature begins to rise. The errors in that method are, again, the differences between the predicted wet-bulb temperature and the actual wet-bulb temperatures.

To ensure a fair comparison, we allow one parameter to be tuned for each prediction method. For the prediction from constant apparent temperature, we tune the wind speed as described in the previous section. Thus, we use 3.0 W m^{-2} K^{-1} (0.2 m s^{-1}). For the prediction from constant wet-bulb temperature, we tune the one free parameter: the constant wet-bulb temperature itself. By minimizing the sum of squared differences between this single wet-bulb temperature and those measured in W22, the optimal value (for predicting a rising core temperature) is found to be 27.6 °C.

Figure 4.4 plots the observed critical T_w versus the predicted critical T_w using a prediction of single T_w threshold of 27.6 °C (grey symbols) and a single T_a threshold of 71.5 °C (black symbols). The prediction from constant apparent temperature explains 95% of the variance (coefficient of determination $R^2 = 0.95$) while the prediction from constant T_w predicts 0% of the variance. The root-mean-square error of the prediction using a constant apparent temperature is 0.4 °C, compared to 2.0 °C for the prediction using a constant wet-bulb

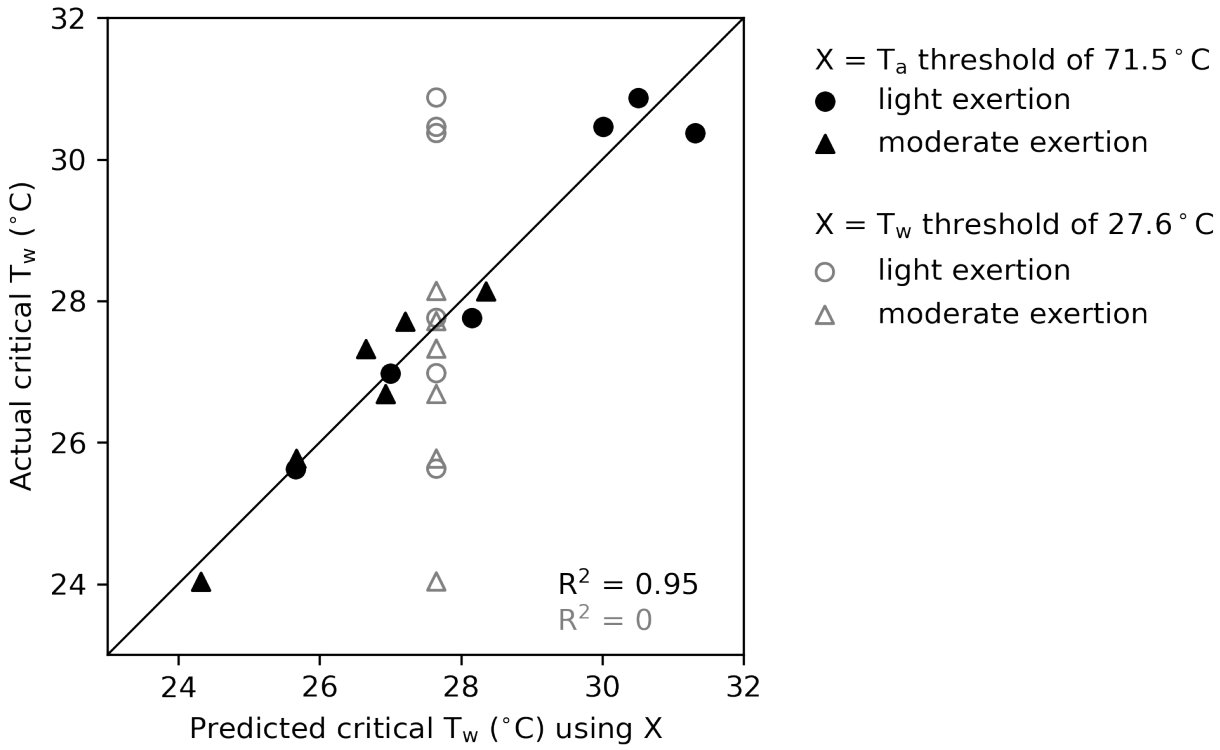

Figure 4.4: Empirical critical wet-bulb temperatures versus the predicted critical wet-bulb temperature, using (black) apparent temperature of 71.5 °C, and (grey) wet-bulb temperature of 27.6 °C, which is the best-fit value for the present experiment.

temperature. Thus, we see that the conditions leading to an elevated core temperature are much more accurately predicted using the apparent temperature.

The success of the heat index model in explaining the empirical results of W22 may be compared with previous such efforts. For example, W22 drew two solid curves in their Figure 2 to fit the light-exertion and moderate-exertion data, but those were polynomial fits to the empirical data, and not constructed from a theoretical model (personal communication). In another attempt, Vecellio et al. [107] plotted the empirical data alongside the National Weather Service's (NWS) polynomial approximation to the heat index [83]. In their Figures 2a and 2d, they plotted isopleths of that polynomial approximation that were intended to correspond to the NWS's definitions of "danger" (an isopleth of 103 °F) and "extreme danger" (an isopleth of 125°F). But there are several problems with that approach. The first problem is that the curves systematically underestimate the danger of moderate exertion (their Figure 2d). The second problem is that a mistake was made in plotting the "danger" curve in their Figures 2a and 2d: if plotted correctly, that "danger" curve would lie far below the empirical data. The third problem is that the "extreme danger" isopleth of that

polynomial is outside the region where the polynomial is valid (i.e., outside the region for which the original heat index was defined), and so it is not grounded in any model of physiology and exhibits unrealistic behavior. When we plot that "extreme danger" isopleth of the NWS approximation in Figure 4.3 (light green), we see that it happens to coincide with the light-exertion data, but the isopleth bends upward at higher temperatures. In particular, the light green curve is at a minimum vapor pressure at ∼70°C, implying that, at constant vapor pressure, 75 °C is *less* dangerous than 70 °C. In addition, since the NWS's polynomial extrapolation is not based on a physiological model, it is not possible to adapt it to different metabolic rates or wind speeds. In fact, it is just a coincidence that the "extreme danger" curve overlaps the light-exertion data: the physiological model underlying the standard heat index assumes a metabolic rate and wind speed (180 W m^{-2} and 1.5 m s^{-1}) that are far from the conditions in the experiments.

4.6 Perspective and Significance

The heat index [97] has been widely used for communicating the danger of high heat and humidity, but little progress has been made in validating its physiological predictions. Quayle and Doehring [74] divided the heat index into ranges labeled "caution", "extreme caution", "danger", and "extreme danger", and those ranges were adopted by the National Weather Service, but those labels were not based on any peer-reviewed physiological model or laboratory data. In addition, some of the heat index values reported by the National Weather Service have been based on polynomial extrapolation rather than a scientific model, leading those values to be in error by as much as 10 °C [82]. In 2020, a United States administrative judge held that there was no scientific basis to the labels (caution, extreme caution, etc.) applied to the heat index by the National Weather Service [11]. That decision, which vacated fines imposed against the United States Postal Service (USPS) by the Occupational Safety and Health Administration (OSHA), calls into question OSHA's ability to enforce protections against excessive heat exposure in the workplace in the absence of experimental validation of the heat index [87]. This is the context for the work presented here, which shows that the heat index, appropriately modified to account for the actual wind speed and metabolic rate, can accurately predict the onset of thermoregulatory failure in a laboratory setting.

Acknowledgments

This work was supported by the U.S. Department of Energy's Atmospheric System Research program through the Office of Science's Biological and Environmental Research program under Contract DE-AC02-05CH11231. We are grateful to Gregory Barber for a helpful conversation.

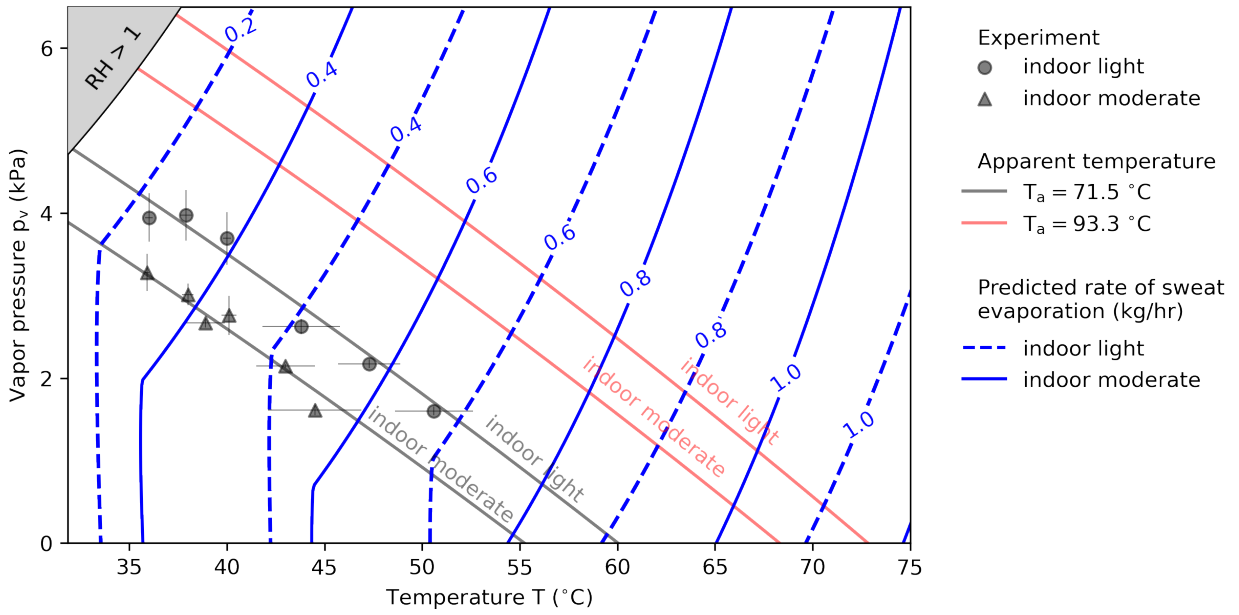

Figure 4.5: (blue contour) The rate of sweat evaporation predicted by the heat-index model for light (dashed) and moderate (solid) exertions with the indoor wind at the corresponding equilibrium core temperature. The other symbols and curves are explained in the caption of Figure 4.3.

Appendix: Sweating rate

The maximum sweating rate for a typical young, healthy, hydrated, and acclimatized adult male is in the range of 1-2 kg hr^{-1} [2, 103]. In Figure 4.5, we add to Figure 4.3 the rate of sweat evaporation predicted by the heat-index model at the predicted equilibrium core temperature (which, for light exertion, is 37 °C below and to the left of the "indoor light" black curve, increasing above and to the right of that curve, and hitting 42 °C on the "indoor light" red curve). The sweating rate increases as one moves from the cold and humid region to the hot and dry region. For the experimental data in W22, the predicted sweating rate ranges from 0.2 to 0.6 kg hr^{-1}, which is well below the sweating-rate limit of 1-2 kg hr^{-1}. For all points on the theoretical black curves, the heat-index model predicts a sweating rate at or below 0.8 kg hr^{-1}. For all points on the two red fatal curves, the predicted evaporation rate is equal to about 1 kg hr^{-1} or less. Therefore, the sweating rates predicted by the heat-index model for indoor conditions, even at fatal air temperatures of around 70 °C at zero humidity, are consistent with the maximum sweating rates measured in human subjects.

In this thesis, we have referred to the combinations of air temperature, relative humidity, wind speed, and metabolic heat that yield hyperthermia (core temperature starts to rise) and fatality (core equilibrates at 42 °C) by their apparent temperatures of 71.5 and 93.3

°C, respectively. These apparent temperatures are the air temperatures in Steadman's reference conditions (water-vapor pressure of 1.6 kPa, an outdoor wind speed of 1.5 m s^{-1}, and metabolic heat of 180 W m^{-2}) that would yield hyperthermia and fatality. At that relatively high reference wind speed of 1.5 m s^{-1}, the predicted rate of sweat evaporation at the equilibrium core temperatures of 37 and 42 °C, respectively, would be 2.4 and 3.4 kg hr^{-1}, respectively. These sweating rates exceed the typical maximum rate reported in the literature of 1-2 kg hr^{-1}. For a real human to perform the same as in the idealized heat-index model in those extreme outdoor conditions, a misting fan would likely be needed to keep the skin surface wet. Without a misting fan, a person under Steadman's reference (outdoor) conditions would suffer from hyperthermia and fatality at air temperatures lower than 71.5 and 93.3 °C, respectively. Since, for an indoor wind speed, the sweating rate predicted by the heat-index model is below the empirical maximum, the heat-index model is accurate for indoor conditions without a misting fan.

Chapter 5

Is a Wet-bulb Temperature of 35 Degree C the Correct Threshold for Human Survivability?

5.1 Introduction

A wet-bulb temperature of 308 K (35 °C, 95 °F) is widely used as the threshold for human survivability in the field of climate science [17, 41, 42, 57, 70, 76, 78, 80, 85, 88, 93, 94]. Despite its use as a predictor of human heat stress, the wet-bulb temperature is defined as the equilibrium temperature of a wetted thermometer in high winds. Since the Lewis number of air is near one, the energy balance of a wetted thermometer can be approximated mathematically as

$$\sigma\left(T^4 - T_{\text{rad}}^4\right) + f\left(u\right)\left\{c_p\left(T - T_a\right) + \rho L\left[q_v^*\left(T\right) - q_a\right]\right\} = 0\,, \tag{5.1}$$

where T is the temperature of the wetted thermometer, T_a is the air temperature, q_a is the specific humidity, ρ is the air density, c_p is the heat capacity of air at constant pressure, T_{rad} is the effective radiating temperature of the surrounding surfaces, L is the latent heat of vaporization of water, q_v^* is the saturated specific humidity, u is the wind speed, and $f(u)$ is an effective mass flux of turbulent exchange between air and the thermometer. When u is large, $f(u)$ is large and the turbulent enthalpy fluxes (sensible plus latent) dominate the energy balance. In that special case, we refer to the temperature T of the wetted thermometer as the wet-bulb temperature T_w, which is defined by

$$c_p\left(T_w - T_a\right) + \rho L\left[q_v^*\left(T_w\right) - q_a\right] = 0\,. \tag{5.2}$$

The reason T_w is potentially relevant to human heat stress is because we can write the enthalpy fluxes off of a human's sweat-covered skin in terms of T_w. For any u, if the sweaty

skin has a temperature T_s, the turbulent enthalpy flux from skin to the air is

$$F = f(u)\left\{c_p(T_s - T_a) + \rho L\left[q_v^*(T_s) - q_a\right]\right\} \tag{5.3}$$

$$= f(u)\left\{c_p(T_s - T_w) + \rho L\left[q_v^*(T_s) - q_v^*(T_w)\right]\right\}, \tag{5.4}$$

where equation (5.2) has been used in the second line to eliminate T_a and q_a in favor of T_w. In other words, the air feels the same as saturated air at temperature T_w. Equation (5.4) implies that whenever the wet-bulb temperature T_w is greater than the skin temperature T_s, the net flow of sensible and latent heat is into the skin.

For this reason, Sherwood and Huber [93, SH10 hereafter] argued that exposure to $T_w \gtrsim$ 308 K (35 °C, 95 °F) for more than a few hours would be fatal. As the argument goes, with a standard core temperature $T_c = 310$ K (37 °C, 98.6 °F) and a basal metabolic rate of 50 W per square meter of skin area (hereafter written as 50 W m^{-2}), the body will move heat from the core to the skin at that rate by keeping the skin temperature T_s at 308 K or below. If $T_w \gtrsim 308$ K, the skin temperature must be greater than 308 K to release heat to the air, but then the body cannot move metabolic heat from the core to the skin at the needed rate. As the metabolic heat accumulates, it heats up the body. If that heating were to continue unabated, it would lead to death by hyperthermia at a core temperature of ∼315 K. As we will now discuss, however, this argument relies on assumptions that can be described as either overly pessimistic (tending to lower the predicted fatal T_w) or overly optimistic (tending to raise the predicted fatal T_w), raising the question of how accurate 308 K is as a threshold for survivability.

The *pessimistic* assumption is that a skin temperature higher than 308 K would be fatal. In reality, the human body is capable of moving basal metabolic heat from the core to the skin with a range of core-skin temperature differences. The body accomplishes this by changing the effective thermal conductivity between the core and skin by modulating the rate of core-to-skin blood flow. Only at a skin temperature close to 310 K is the core temperature guaranteed to rise. And even if the skin temperature is held at a temperature above 310 K, this does not necessarily imply heat death: it simply means the core temperature will equilibrate at some temperature above 310 K. Fit individuals can survive a core temperature that is elevated by a few degrees. It is when the core temperature reaches about 315 K that the hyperthermia becomes fatal [e.g., 9, 31, SH10]. Thus, only a skin temperature near or above 315 K is necessarily fatal.

On the other hand, SH10 made some assumptions that could be described as overly *optimistic*. The first was the omission of radiative exchange between the skin and the surroundings. SH10 justified this by assuming what they called "gale-force winds," guaranteeing that the exchange of energy between the skin and its surroundings is dominated by turbulent fluxes. But, using ERA5 reanalysis [40] and a map of world population [16], we find that an average of 98% of people are in locations where the windspeed is less than 4 m s^{-1} at any moment in time. This suggests that the exchange of infrared radiation is an important consideration. Since the radiating temperature only needs to exceed the skin temperature of

$\sim$308 K to be a net source of radiative power to the body, the assumption of gale-force winds is overly optimistic in very hot conditions. Indeed, a recent experiment [106] demonstrates that when exercising in a chamber with a low wind speed, even young, healthy adults start to have elevated core temperatures at a wet-bulb temperature well below 308 K. Furthermore, SH10 assumed that the humans who are outdoors have a resting metabolic rate around 50 W m^{-2}. This is an overly optimistic assumption for most outdoor workers.

Given this mix of overly pessimistic and optimistic assumptions, it is not clear *a priori* whether a wet-bulb threshold of 308 K is an overestimate or underestimate of what is truly survivable. To properly account for a finite wind speed, metabolic heat production, and radiative exchange, we must use a physiological model of thermoregulation, as provided by the model underlying the heat index [49, 97].

5.2 The heat index

For a given temperature and humidity, the heat index is defined as the air temperature that would be experienced in the same way by a healthy adult at a reference water-vapor pressure of 1.6 kPa. The equivalence of experience is defined via the heat index's model of human thermoregulation, which uses a combination of physiological and behavioral strategies to regulate the core temperature at the standard value of 310 K (37 °C, 98.6 °F). In particular, two pairs of temperature and humidity are equivalent from the human perspective if the human naturally adopts the same behavior (e.g., same choice of clothing) and physiological state (e.g., same skin blood flow) in both.

Like the wet-bulb temperature, the heat index has been widely used to assess the risk of humid heat [4, 19, 21, 25, 26, 45, 51, 56, 67, 69, 72, 75, 77, 79, 96, 104, 112, 114, 117]. Compared to the wet-bulb temperature, the heat index represents the next level of sophistication and realism when it comes to representing heat stress: it incorporates a realistic metabolic rate, infrared radiation, and the body's ability to alter its core-to-skin conductance. As the heat index increases, a person eventually runs out of options for regulating their core temperature, resulting in hyperthermia. In such conditions, the heat index model predicts the new, higher temperature at which the core will equilibrate, enabling an assessment of survivability.

SH10 treated hyperthermia and heat death as closely related, but these two health outcomes occur at distinctly different values of the heat index: 345 K for hyperthermia and 366 K for heat death [49][1]. When the heat index is less 345 K, the human is able to regulate the core temperature at 310 K, possibly with an elevated skin temperature. When the heat heat index exceeds 345 K, the skin temperature comes very close to the core temperature, and the core temperature is forced to rise. While undesirable, a fit and healthy adult can still survive with an elevated core temperature so long as it remains below the fatal value of 315 K. Only with sustained exposure to a heat index exceeding 366 K will the core temperature rise to 315 K [see 49, for the timescales involved].

[1] More precise values are 344.65 and 366.44 K, respectively.

Regarding Earth's future habitability, there are several uncertainties. For example, it is unknown what time series of greenhouse-gas emissions humankind will generate, with any given emissions scenario depending on multiple assumptions about socioeconomic and technological developments [e.g., 102]. Even if the future emissions scenario were known, survivability can differ significantly across populations. For instance, elderly individuals [12, 24] and those suffering from obesity [23] or cardiovascular disease [37, 73] are particularly susceptible to heat-related illnesses. Since people with different underlying health conditions and adaptive capacities will respond differently to the same climate [105], future habitability will depend, in part, on future demographics. In addition, the unknown amount of future acclimatization [6, 7, 32, 39, 89] and behavioral adaptation, such as the prevalence of air conditioning [66], adds to the uncertainty.

To make progress in spite of these complexities, we take the following approach. First, to sidestep the uncertainty in future emissions, we study potential health outcomes not as a function of time, but as a function of global mean temperature. For example, in the RCP8.5 scenario, many climate models predict an increase in global mean temperature of about +4 K in 2100 relative to the pre-industrial period. Of course, some other models and scenarios reach +4 K earlier, some reach +4 K later, and some reach +4 K never. Rather than focusing on *when*, we focus on *how hot* and study, e.g., the potential health outcomes of a +4 K world, assuming that regional warming (and extreme heat in particular) is, to good approximation, a function of the global mean temperature [e.g., 92, 109].

Second, regarding demographics, we use the heat-index model, which is specifically designed to model the thermoregulation of fully acclimatized, young, healthy adults. The heat-index model assumes that these young, healthy adults can sweat profusely, can maintain large core-to-skin blood flow, and have an optimal (i.e., unabashed) approach to clothing. Therefore, by construction, this approach gives an upper limit on anyone's ability to avoid hyperthermia and heat death. The heat-index model has recently been validated against empirical data gathered from young and healthy adults in a laboratory [50]: in the experiment, young and healthy adults were put in a climate chamber, and the temperature or humidity was slowly increased until the subjects started to experience hyperthermia [111]. Lu and Romps [50] showed that the heat index of 345 K (71.5 °C) accurately predicts the onset of hyperthermia in those experiments. Given this validated model for the young and healthy, we do not attempt to model future demographics or the impacts of high heat and humidity on the elderly, those with underlying medical conditions, or those who are poorly acclimatized. It must be borne in mind that those groups will tend to suffer serious health impacts at lower heat-index thresholds than are used in this study.

Third, we avoid the issue of air conditioning and its uncertain availability in future decades by focusing on the habitability of the outdoors. The pre-industrial Earth was supremely habitable in the sense that a person with appropriate clothing, water, and shade could survive the combination of temperature and humidity found anywhere on the planet. This made the outdoors almost universally accessible for work, pleasure, and exploration. In the future, this cannot be taken for granted. Here, we apply the heat-index model to outdoor temperature and humidity, which provides a physiological assessment of an accli-

matized, young, healthy person outdoors in the shade.

5.3 Climate model results

As mentioned in the previous sections, a single value of the wet-bulb temperature ($T_w = 308$ K) is often used as a threshold of survivability, while the heat index has two thresholds: one for hyperthermia (HI = 345 K) and the other for heat death (HI = 366 K). We can quantify the frequencies of these thresholds by looking at a reanalysis and a global climate model. The left panel of Figure 5.1 shows the historical (from 1996 to 2005, inclusive) global population-weighted distributions of instantaneous temperature T (black), annual maximum temperature $T_{\max}$ (blue), annual maximum wet-bulb temperature $T_{w(\max)}$ (red), and annual maximum heat index (orange) from ERA5 hourly reanalysis [40] and a map of world population in 2005 [16]. Although using ERA5 1996-2005 instead of ERA-Interim 1999-2008 as in SH10, the curves shown here qualitatively match the curves shown in Figure 1A of SH10, which also used a 60S-to-60N land area weighting instead of the population weighting used here. The middle panel shows the same curves calculated from the historical (1996-2005)[2] simulations of the CNRM-CM5 climate model [108] from the CMIP5 archive [102][3]. Its curves closely match the curves calculated from the reanalysis, bolstering confidence in the climate-model output. The right panel shows the curves calculated from the CNRM-CM5 simulation of the RCP8.5 scenario in the decade 2291-2300, during which the global mean temperature was 9.2 K higher than in the 1996-2005 historical period and 10 K higher than the 1850-1900 preindustrial period (henceforth referred to as the "+10-K world"). Following SH10, we use this worst-case scenario to illustrate what would happen in extreme warming. As in Figure 1C of SH10, the distribution of $T_{w(\max)}$ in this period of extreme warmth straddles 308 K (35 °C), marked by a dashed line.

As in SH10, the ERA5 reanalysis shows that the historical climate has no wet-bulb temperatures higher than 308 K and no heat index higher than 345 K. On the other hand, 26% of the world's current population lives in locations that would, in a typical year, expose them to $T_w > 308$ K in a +10-K world. We find, however, that only a small fraction of those locations would be fatal for a young and healthy person. Using the heat index, we find that only 1.7% of the current population lives in places in which sustained walking in outdoors shade would be lethal (HI > 366 K) on some day of the year in a +10-K world. But we find that a majority (62%) of people currently live in places that will be intolerable in the sense that, at some point during the year, a young, healthy adult walking in the shade would not be able to maintain a normal core temperature (HI > 345 K).

[2]The period of 1996-2005 is chosen as the baseline because it covers the last ten years in the CMIP5 historical simulations.

[3]CNRM-CM5, bcc-csm1-1, and IPSL-CM5A-LR are the only three CMIP5 climate models for which we could obtain 3-hourly data in the extended RCP8.5 scenarios. We use CNRM-CM5 to make Figures 5.1 and 5.2 because it has the highest spatial resolution. Later, in Figure 5.3 and in the sensitivity-test section, we will use all of the three models and compare their results.

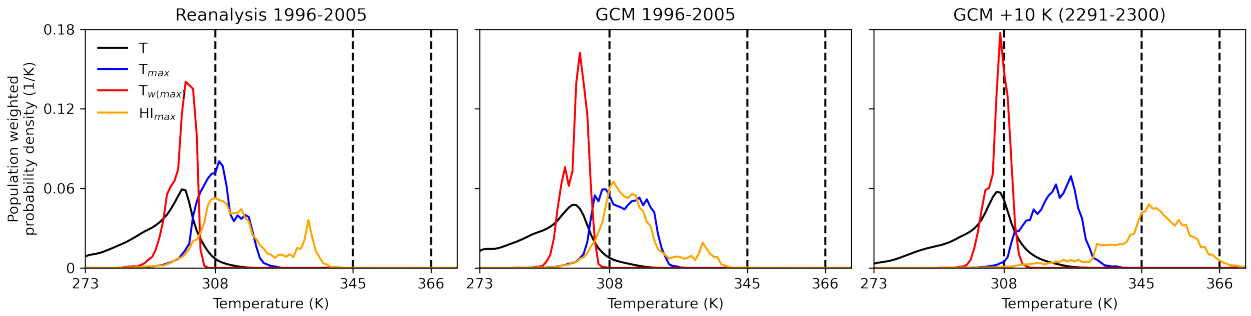

Figure 5.1: (left panel) The global population-weighted distribution of hourly temperature (black), yearly maximum temperature (blue), yearly maximum wet-bulb temperature (red) and the yearly maximum heat index (orange) calculated using ERA5 reanalysis data over the entire globe during 1996-2005, inclusive. (middle panel) Same, but calculated using CNRM-CM5 3-hourly historical data during 1996-2005. (right panel) Same, but calculated using CNRM-CM5 simulation of the RCP8.5 scenario 3-hourly data during 2291-2300, which has a global mean temperature anomaly of +10 K relative to preindustrial. The dashed vertical lines mark $T_w = 308$ K (SH10 proposal), HI = 345 K (hyperthermia), and HI = 366 K (heat death given sustained exposure).

To reveal the spatial and temporal distributions of these exceedances ($T_w > 308$ K, HI $>$ 345 K, HI $>$ 366 K), we plot the map of the return period of each exceedance in Figure 5.2 for the +10-K world. The shortest return period for each exceedance is shown at the bottom right of the map. SH10 used a climate simulation with a slightly higher global-mean temperature than shown here, but the locations of finite return time in the left panel of Figure 5.2 are approximately the same locations with $T_{w(\max)} > 308$ K in Figure 1F of SH10: large swath of Africa, Australia, Arabia, India, South America, Eastern China, and the Midwestern and Eastern United States. But the maps of recurrence time of HI $>$ 345 K and HI $>$ 366 K, shown in the middle and right panels of Figure 5.2, respectively, are qualitatively different. The places predicted to be consistently (once or more per year) fatal (HI $>$ 366 K) to a young, healthy person taking a sustained walk in the shade are the Amazon rainforest, the Sahara desert, the Congo Basin, and the Arabian Peninsula. Other locations that become marginally lethal include parts of eastern China from Shanghai to Beijing and parts of the Midwest United States. The hyperthermic locations (HI $>$ 345 K), however, are much more widespread than predicted by the wet-bulb threshold. Those regions of hyperthermia cover the entire middle and lower latitudes, with a shortest return period of 2 days. In the United States, for example, the Midwest and East Coast see a heat index of 345 K with recurrence times ranging from a few years to a few months. Notably, some of the *shortest* return periods for hyperthermia occur among the *most densely* populated regions of the world, e.g., Bangladesh and northern India. That results in a significant proportion of the world's population experiencing hyperthermia.

To illustrate how much of the current (2005) world population would be exposed to critical

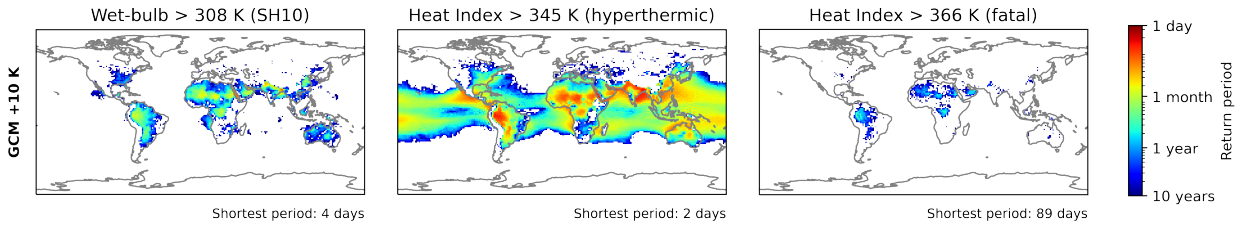

Figure 5.2: The return period for (left) wet-bulb temperature exceeding the widely used threshold value of 308 K, (middle) the heat index exceeding the hyperthermic value of 345 K, and (right) the heat index exceeding the fatal value of 366 K, as calculated from CNRM-CM5 RCP8.5 data during 2291-2300, which has a global mean temperature anomaly of +9.2 K relative to its 1996-2005 mean. The subscript at the right bottom of each map shows the shortest return period in that particular map during 2291-2300.

thresholds at different global-mean temperature anomalies, we use the RCP8.5 scenario in the IPSL-CM5A-LR climate model [29], which has a coarser resolution than CNRM-CM5 but has a 3-hourly output for the entire period of 2006 to 2300. The IPSL-CM5A-LR model also has a higher global mean temperature anomaly of +12.3 K (relative to preindustrial) during 2291-2300, compared to +10 K for CNRM-CM5, allowing a wider temperature range to be probed. The blue curve in Figure 5.3 shows the fraction of world population exposed to $T_w > 308$ K at least once a year in IPSL-CM5A-LR. Similarly, the orange and purple curves are the fractions of world population exposed to a heat index higher than 345 K and 366 K, respectively, at least once per year. These sandwich the blue curve, delivering the same message that the 308-K wet-bulb temperature threshold underestimates the frequency of hyperthermia, but overestimates the frequency of heat death. To smooth the curves, a ten-year averaging window has been applied.

On top of each curve, we plot the results from two other global climate models, CNRM-CM5 and bcc-csm1-1 [113], as round and triangle symbols, respectively. Each symbol represents a ten-year average of the annual fraction of world population exposed to the given threshold during the last ten years of the 21st, 22nd and 23rd centuries. Due to their finer resolution, CNRM-CM5 and bcc-csm1-1 do not output 3-hourly data over the entire extended RCP8.5 period of 2006-2300, and, therefore, we show the time intervals during which data are available. Each symbol is horizontally located at its ten-year mean temperature anomaly. Notice that the three global climate models have different temperature anomalies at the end of each century in the extended RCP8.5 scenarios: for example, in 2291-2300, the temperature anomalies are +12.3 K in IPSL-CM5A-LR, +10 K in CNRM-CM5, and +8.7 K in bcc-csm1-1. Although these models forecast different temperatures for a given time interval, they predict very similar population exposures at a given amount of warming.

Added to Figure 5.3 is a floating ordinate showing the corresponding world population in 2005. Roughly speaking, in a world warmer than pre-industrial by 10 K, around 30% of the world's population (about 2 billion people) would be exposed once or more per year to

a wet-bulb temperature above 308 K, while less than 2% (about 100 million people) would be exposed to fatal conditions and over 60% (nearly 4 billion people) would be exposed to conditions that would cause hyperthermia.

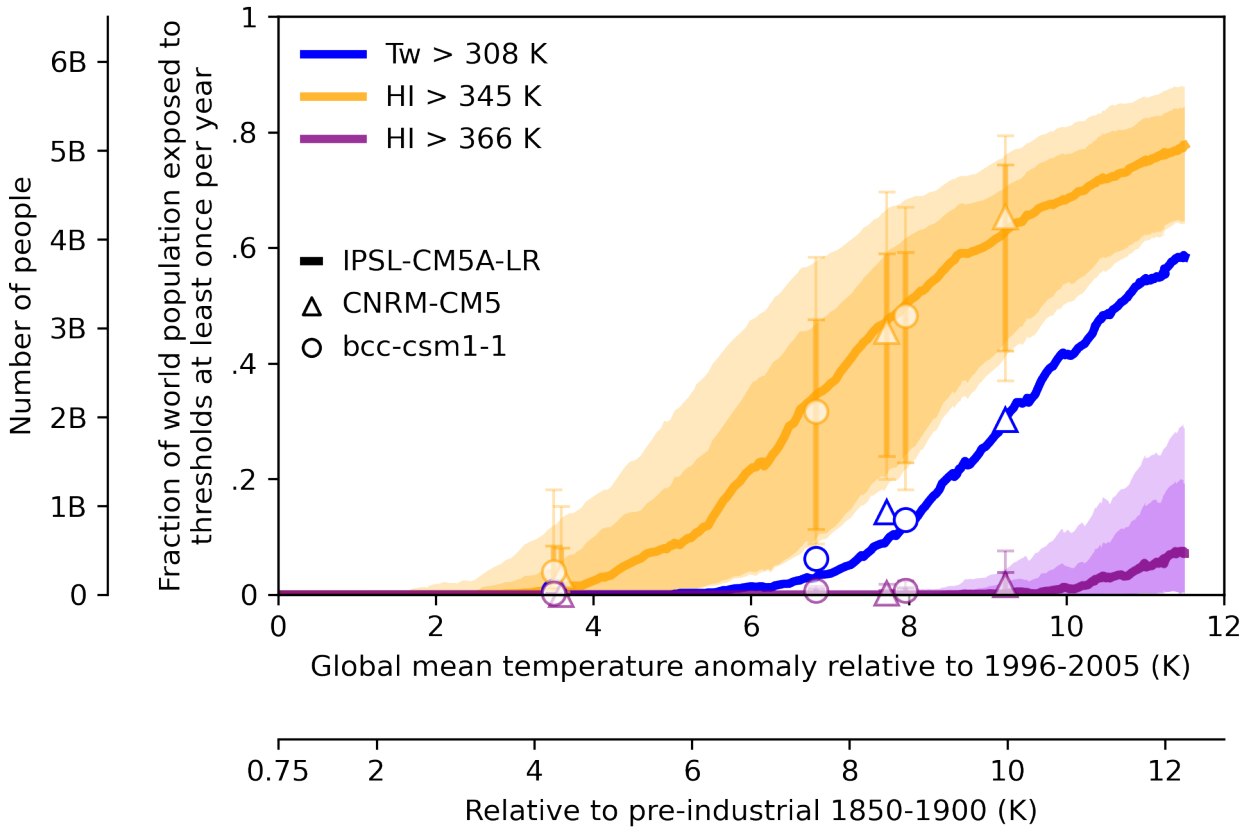

Figure 5.3: The fraction of the 2005 world population experiencing three criteria: wet-bulb temperatures greater than 308 K (blue), heat index greater than 345 K (hyperthermic; orange), and heat index greater than 366 K (fatal; purple) as functions of the global-mean temperature anomaly relative to 1996-2005. The curves plot these fractions for the IPSL-CM5A-LR simulation of RCP8.5 scenario from 2006-2300, inclusive. A ten-year-window averaging is applied to each year smooth the curves. The symbols have the same meaning as the curves, but are calculated using the CNRM-CM5 (round) and the bcc-csm1-1 (triangle) simulations, averaged over the last ten years of the 21st, 22nd and 23rd centuries. The light shadings and the thin error bars are the spreads due to a range of metabolic rates of 50-300 W m^{-2}, and the dark shadings and thick error bars are the spreads due to a range of windspeed of 1-4 m s^{-1}. The floating ordinate shows the corresponding world population in 2005, and the floating abscissa shows the global mean temperature anomaly relative to the pre-industrial period of 1850-1900.

5.4 Sensitivity test

The heat index assumes a metabolic rate at 180 W m^{-2} and an overall wind speed of 1.5 m s^{-1}. This metabolic rate corresponds to a walking pace at 1.4 m s^{-1} [71, 98], and that overall wind speed is converted from the heat transfer coefficient of 12.3 W m^{-2} K^{-1} in Steadman's model [97] using Churchill and Bernstein's relation [15]. Here, we will calculate how sensitive the hyperthermic and fatal thresholds are to these assumptions.

Using the ERA5 wind speed and the roughness length data, and assuming a log-profile wind structure, we find that, at any moment in time, 98% of the population experiences wind speeds less than 4 m s^{-1} at half of the assumed human height of 0.85 m [97]. To explore a range of plausible wind speeds, we will therefore vary the wind speed u in the heat index model from 1 to 4 m s^{-1}, where the lower bound of 1 m s^{-1} is chosen to represent the wind induced by human motion and natural convection. Similarly, to explore different levels of physical exertion, we will use previously defined exertion levels [3], which define a metabolic rate of 50-150 W m^{-2} as light activity and 150-300 W m^{-2} as moderate activity. Any activity requiring a metabolic rate beyond 300 W m^{-2} is considered vigorous. We assume a person would have the freedom and commonsense to avoid vigorous activity during heat stress, and thus we vary the metabolic rate Q over 50-300 W m^{-2}. Note that a resting metabolic rate of 50 W m^{-2} is included in our sensitivity test as the lower bound.

To perform this sensitivity analysis, we must generalize the heat index to an apparent temperature that takes two extra arguments (u and Q) besides the air temperature and humidity. The procedure is a straightforward modification of the heat index. In particular, the apparent temperature for a given T_a, p_v, u, and Q is the air temperature at a $p_{v0} = 1.6$ kPa, $u_0 = 1.5$ m s^{-1}, and $Q_0 = 180$ W m^{-2} that would feel the same in the sense of generating the same behavior (choice of clothing) and same physiology (skin blood flow, equilibrium core temperature). Because the reference state (p_{v0}, u_0, Q_0) is the same as in the original heat index, the apparent temperature generated in this way has the same interpretation, e.g., an apparent temperature of 345 K (366 K) is still the threshold for hyperthermia (lethality).

The results of the sensitivity analysis are shown in Figure 5.3 as the shadings around the curves and the error bars on the points. The dark shading and bars show the spread due to varying u from 1 to 4 m s^{-1} and the light shading and bars show the spread due to varying Q over 50 to 300 W m^{-2}. The wet-bulb temperature depends on neither u nor Q, so adjusting those parameters has no effect on the blue curve. We see that the plausible changes to the metabolic rate or the wind speed effectively shift the orange and purple curves left or right on the abscissa by ∼1-2 K. For example, 10% of the world's population would experience hyperthermic conditions walking in the shade with about 5 K of additional warming (relative to 1996-2005), but 10% of the population would experience hyperthermia performing 300 W m^{-2} of moderate work in the shade with only 3 K of additional warming. Notably, even with these variations in assumed parameters, the commonly used T_w threshold (blue curve) still overestimates lethality and underestimates hyperthermia.

5.5 Discussion

We have shown that the commonly used wet-bulb-temperature threshold of 308 K (35 °C) underestimates the prevalence of hyperthermia and overestimates the prevalence of fatalities. Implicit in the derivation of $T_w = 308$ K as a critical threshold is the assumption that a person is exposed to a wind speed equal to a strong breeze or greater, which would enhance the body's evaporative cooling. In reality, people are usually exposed to much more stagnant winds and, in hot conditions, they absorb infrared radiation from surrounding surfaces that are hotter than their core temperature. This leads to an onset of hyperthermia at wet-bulb temperatures less than 308 K. On the other hand, using $T_w = 308$ K as a fatal threshold is too pessimistic because an elevated core temperature is not necessarily fatal. Only when the core temperature equilibrates at or above 315 K is heat death a common outcome, and this occurs at wet-bulb temperatures greater than 308 K. It is worth noting, however, that this hinges on the assumption of a typical outdoor wind speed in the range of 1-4 m s^{-1}. For a person exerting themselves indoors, where the wind speed is measured in tens of centimeters per second, fatal conditions are typically reached at wet-bulb temperatures lower than 308 K [50].

The three climate models studied here are in broad agreement about the amount of warming that leads to severe health outcomes for people outdoors in the shade. Hyperthermia would start to be a regular occurrence at a global-mean warming of about +3 K relative to preindustrial. For a higher warming of +4 K relative to preindustrial, a large number of people, measured in tens of millions or hundreds of millions, would be exposed to hyperthermic conditions at least once per year. On the other hand, a global-mean temperature anomaly of around +10 K is needed to generate fatal conditions for ∼100 million people every year. As mentioned in section 5.2, it is important to note that these global-mean temperature thresholds for hyperthermia and fatality would be lower if considering people who are in the sun, or people who are exerting themselves to a greater degree, or people with underlying health conditions or age-related declines in sweating capacity or cardiovascular fitness.

Acknowledgments

The authors are grateful to William R. Boos for a helpful conversation and feedback.

Bibliography

[1] Acharya, Payel, Boggess, Bethany, and Zhang, Kai. "Assessing heat stress and health among construction workers in a changing climate: a review". In: *International Journal of Environmental Research and Public Health* 15.2 (2018), p. 247.

[2] Adolph, Edward Frederick and Dill, David B. "Observations on water metabolism in the desert". In: *American Journal of Physiology-Legacy Content* 123.2 (1938), pp. 369–378.

[3] Ainsworth, B E et al. "Compendium of physical activities: classification of energy costs of human physical activities." In: *Medicine and science in sports and exercise* 25.1 (1993). ISSN: 0195-9131.

[4] Amnuaylojaroen, Teerachai et al. "Effect of the Near-Future Climate Change under RCP8.5 on the Heat Stress and Associated Work Performance in Thailand". In: *Atmosphere* 13.2 (2 Feb. 2022), p. 325. ISSN: 20734433. DOI: 10.3390/atmos13020325.

[5] Anderson, G. Brooke, Bell, Michelle L., and Peng, Roger D. "Methods to Calculate the Heat Index as an Exposure Metric in Environmental Health Research". In: *Environmental Health Perspectives* 121.10 (Oct. 2013), pp. 1111–1119. DOI: 10.1289/ehp.1206273.

[6] Arbury, Sheila, Lindsley, Matthew, and Hodgson, Michael. "A Critical Review of OSHA Heat Enforcement Cases". In: *Journal of Occupational and Environmental Medicine* 58.4 (Apr. 2016), pp. 359–363. DOI: 10.1097/jom.0000000000000640.

[7] Arbury, Sheila et al. "Heat illness and death among workers—United States, 2012–2013". In: *Morbidity and mortality weekly report* 63.31 (2014), p. 661.

[8] Berry, Michael et al. "Evaluation of heat-related illness surveillance based on chief complaint data from New Jersey hospital emergency rooms". In: *Online Journal of Public Health Informatics* 5.1 (2013).

[9] Bouchama, Abderrezak and Knochel, James P. "Heat stroke". In: *New England Journal of Medicine* 346.25 (2002), pp. 1978–1988.

[10] Buettner, Konrad J K. "Diffusion of liquid water through human skin". In: *Journal of Applied Physiology* 14.2 (1959), pp. 261–268.

[11] Calhoun, Sharon D. *Secretary of Labor v. United States Postal Service, National Association of Letter Carriers (NALC) and National Rural Letter Carriers' Association (NRLCA)*. Tech. rep. OSHRC Docket No. 16-1713. Occupational Safety and Health Review Commission, July 2020. URL: https://www.oshrc.gov/assets/1/6/16-1713_Decision_and_Order_-_dated.html.

[12] Carleton, Tamma et al. "Valuing the Global Mortality Consequences of Climate Change Accounting for Adaptation Costs and Benefits". In: *The Quarterly Journal of Economics* 137.4 (Apr. 2022), pp. 2037–2105. DOI: 10.1093/qje/qjac020.

[13] Carleton, Tamma A et al. *Valuing the global mortality consequences of climate change accounting for adaptation costs and benefits*. Tech. rep. National Bureau of Economic Research, 2020.

[14] Changnon, Stanley A, Kunkel, Kenneth E, and Reinke, Beth C. "Impacts and responses to the 1995 heat wave: A call to action". In: *Bulletin of the American Meteorological society* 77.7 (1996), pp. 1497–1506.

[15] Churchill, S. W. and Bernstein, M. "A Correlating Equation for Forced Convection From Gases and Liquids to a Circular Cylinder in Crossflow". In: *Journal of Heat Transfer* 99.2 (May 1977), pp. 300–306. ISSN: 0022-1481. DOI: 10.1115/1.3450685.

[16] CIESIN. *Gridded Population of the World, Version 4 (GPWv4): Population Count, Revision 11*. Tech. rep. Palisades, NY: NASA Socioeconomic Data and Applications Center (SEDAC): Center For International Earth Science Information Network, Columbia University, 2018. DOI: 10.7927/H4JW8BX5.

[17] Coffel, Ethan D., Horton, Radley M., and Sherbinin, Alex De. "Temperature and humidity based projections of a rapid rise in global heat stress exposure during the 21st century". In: *Environmental Research Letters* 13.1 (1 Jan. 2018), p. 014001. ISSN: 17489326. DOI: 10.1088/1748-9326/aaa00e.

[18] Cottle, Rachel M. et al. "Validity and reliability of a protocol to establish human critical environmental limits (PSU HEAT Project)". In: *Journal of Applied Physiology* 132 (2 Feb. 2022), pp. 334–339. ISSN: 15221601. DOI: 10.1152/japplphysiol.00736.2021.

[19] Dahl, Kristina et al. "Increased frequency of and population exposure to extreme heat index days in the United States during the 21st century". In: *Environmental Research Communications* 1.7 (July 2019), p. 075002. DOI: 10.1088/2515-7620/ab27cf.

[20] Dear, R. J. de et al. "Convective and radiative heat transfer coefficients for individual human body segments". In: *International Journal of Biometeorology* 40.3 (May 1997), pp. 141–156. DOI: 10.1007/s004840050035.

[21] Delworth, Thomas L., Mahlman, J. D., and Knutson, Thomas R. "Changes in Heat Index Associated with CO_2-Induced Global Warming". In: *Climatic Change* 43.2 (1999), pp. 369–386. DOI: 10.1023/a:1005463917086.

[22] Dematte, Jane E et al. "Near-fatal heat stroke during the 1995 heat wave in Chicago". In: *Annals of Internal Medicine* 129.3 (1998), pp. 173–181.

[23] Dervis, Sheila et al. "A comparison of thermoregulatory responses to exercise between mass-matched groups with large differences in body fat". In: *Journal of Applied Physiology* 120.6 (Mar. 2016), pp. 615–623. DOI: 10.1152/japplphysiol.00906.2015.

[24] Deschênes, Olivier and Moretti, Enrico. "Extreme Weather Events, Mortality, and Migration". In: *Review of Economics and Statistics* 91.4 (Nov. 2009), pp. 659–681. DOI: 10.1162/rest.91.4.659. URL: https://doi.org/10.1162/rest.91.4.659.

[25] Diem, Jeremy E., Stauber, Christine E., and Rothenberg, Richard. "Heat in the southeastern United States: Characteristics, trends, and potential health impact". In: *PLoS ONE* 12 (5 May 2017). ISSN: 19326203. DOI: 10.1371/journal.pone.0177937.

[26] Diffenbaugh, Noah S. et al. "Heat stress intensification in the Mediterranean climate change hotspot". In: *Geophysical Research Letters* 34.11 (June 2007). DOI: 10.1029/2007gl030000.

[27] Disease Control, Centers for and Prevention. "Heat-related mortality – Chicago, July 1995". In: *Morbidity and Mortality Weekly Report* 44.31 (1995), pp. 577–579.

[28] Dosio, Alessandro et al. "Extreme heat waves under 1.5 °C and 2 °C global warming". In: *Environmental Research Letters* 13.5 (2018), p. 054006.

[29] Dufresne, J. -L. et al. "Climate change projections using the IPSL-CM5 Earth System Model: from CMIP3 to CMIP5". In: *Climate Dynamics* 40.9 (2013), pp. 2123–2165. DOI: 10.1007/s00382-012-1636-1.

[30] Fanger, P. O. *Thermal Comfort*. 1970.

[31] Ferris, Eugene B et al. "Heat stroke: clinical and chemical observations on 44 cases". In: *The Journal of Clinical Investigation* 17.3 (1938), pp. 249–262.

[32] Folkerts, Mireille A. et al. "Long Term Adaptation to Heat Stress: Shifts in the Minimum Mortality Temperature in the Netherlands". In: *Frontiers in Physiology* 11 (2020). DOI: 10.3389/fphys.2020.00225.

[33] Frieling, Joost et al. "Extreme warmth and heat-stressed plankton in the tropics during the Paleocene-Eocene Thermal Maximum". In: *Science Advances* 3.3 (2017), e1600891.

[34] Fryar, C D et al. "Mean Body Weight, Height, Waist Circumference, and Body Mass Index Among Adults: United States, 1999-2000 Through 2015-2016". In: *National Health Statistics Reports* 122 (2018).

[35] Fuhrmann, Christopher M et al. "Impact of extreme heat events on emergency department visits in North Carolina (2007–2011)". In: *Journal of Community Health* 41.1 (2016), pp. 146–156.

[36] Gagge, A.P, Stolwijk, Jan A. J., and Nishi, Ysaunobu. "An effective temperature scale based on a simple model of human physiological regulatory response". In: *ASHRAE Transactions* 7.PART I (1972), pp. 247–262.

[37] Gostimirovic, Milos et al. "The influence of climate change on human cardiovascular function". In: *Archives of Environmental & Occupational Health* 75.7 (Mar. 2020), pp. 406–414. DOI: 10.1080/19338244.2020.1742079.

[38] Grady, S C. "Climate Change Vulnerability and Impacts on Human Health". In: *Climate Change in the Midwest: Impacts, Risks, Vulnerability, and Adaptation*. Ed. by Sarah C. Pryor. Bloomington, Indiana: Indiana University Press Bloomington, 2013. Chap. 9, pp. 117–133.

[39] Gubernot, Diane M., Anderson, G. Brooke, and Hunting, Katherine L. "The epidemiology of occupational heat exposure in the United States: a review of the literature and assessment of research needs in a changing climate". In: *International Journal of Biometeorology* 58.8 (Dec. 2013), pp. 1779–1788. DOI: 10.1007/s00484-013-0752-x.

[40] Hersbach, Hans et al. "The ERA5 global reanalysis". In: *Quarterly Journal of the Royal Meteorological Society* 146.730 (July 2020), pp. 1999–2049. ISSN: 0035-9009.

[41] Im, Eun Soon, Kang, Suchul, and Eltahir, Elfatih A.B. "Projections of rising heat stress over the western Maritime Continent from dynamically downscaled climate simulations". In: *Global and Planetary Change* 165 (June 2018), pp. 160–172. ISSN: 09218181. DOI: 10.1016/j.gloplacha.2018.02.014.

[42] Im, Eun-Soon, Pal, Jeremy S., and Eltahir, Elfatih A. B. "Deadly heat waves projected in the densely populated agricultural regions of South Asia". In: *Science Advances* 3.8 (2017), e1603322. DOI: 10.1126/sciadv.1603322.

[43] Kaye, Herb. "Mayor, utility – both fail as heat kills hundreds". In: *People's Weekly World (1990-2013)* (July 1995), p. 9.

[44] Kenney, W Larry and Zeman, Michael J. "Psychrometric limits and critical evaporative coefficients for unacclimated men and women". In: *Journal of Applied Physiology* 92.6 (2002), pp. 2256–2263.

[45] Kim, Ho, Ha, Jong-Sik, and Park, Jeongim. "High temperature, heat index, and mortality in 6 major cities in South Korea". In: *Archives of Environmental & Occupational Health* 61.6 (2006), pp. 265–270.

[46] Kunkel, Kenneth E et al. "The July 1995 heat wave in the Midwest: A climatic perspective and critical weather factors". In: *Bulletin of the American Meteorological Society* 77.7 (1996), pp. 1507–1518.

[47] Lev, Michael and Ryan, Nancy. "City sweats, but survives: Emergency effort, breezes combine to fend off disaster". In: *Chicago Tribune (1963-1996)* (July 1995), p. 2.

[48] Li, Cong and Ito, Kazuhide. "Numerical and experimental estimation of convective heat transfer coefficient of human body under strong forced convective flow". In: *Journal of Wind Engineering and Industrial Aerodynamics* 126 (2014), pp. 107–117. ISSN: 01676105. DOI: 10.1016/j.jweia.2014.01.003.

[49] Lu, Yi-Chuan and Romps, David M. "Extending the Heat Index". In: *Journal of Applied Meteorology and Climatology* 61.10 (2022), pp. 1367–1383.

[50] Lu, Yi-Chuan and Romps, David M. "Predicting fatal heat and humidity using the heat index model". In: *Journal of Applied Physiology* 134.3 (2023), pp. 649–656.

[51] Lyon, Bradfield and Barnston, Anthony G. "Diverse characteristics of US summer heat waves". In: *Journal of Climate* 30.19 (2017), pp. 7827–7845.

[52] Mack, Gary W. and Nadel, Ethan R. "Body Fluid Balance During Heat Stress in Humans". In: *Comprehensive Physiology*. American Cancer Society, 2011, pp. 187–214. ISBN: 9780470650714. DOI: 10.1002/cphy.cp040110.

[53] Mather, James H and Voyles, Jimmy W. "The ARM Climate Research Facility: A review of structure and capabilities". In: *Bulletin of the American Meteorological Society* 94.3 (2013), pp. 377–392.

[54] Meehl, Gerald A and Tebaldi, Claudia. "More intense, more frequent, and longer lasting heat waves in the 21st century". In: *Science* 305.5686 (2004), pp. 994–997.

[55] Mesinger, Fedor et al. "North American regional reanalysis". In: *Bulletin of the American Meteorological Society* 87.3 (2006), pp. 343–360.

[56] Modarres, Reza et al. "Future heat stress arising from climate change on Iran's population health". In: *International Journal of Biometeorology* 62.7 (Apr. 2018), pp. 1275–1281. DOI: 10.1007/s00484-018-1532-4.

[57] Monteiro, Joy Merwin and Caballero, Rodrigo. "Characterization of Extreme Wet-Bulb Temperature Events in Southern Pakistan". In: *Geophysical Research Letters* 46 (17-18 Sept. 2019), pp. 10659–10668. ISSN: 19448007. DOI: 10.1029/2019GL084711.

[58] Moser, Whet. "Chicago Heat Wave: Blame This Spring's Floods". In: *Chicago Magazine* (July 2011).

[59] Nathans, Aaron. "City heat index soars to 119; relief in sight". In: *Indianapolis Star (1923-2004)* (July 1995), p. 1.

[60] National Weather Service. *Heat Index Chart*. Accessed on February 16, 2022. National Oceanic and Atmospheric Administration. 2022. URL: https://www.weather.gov/safety/heat-index.

[61] National Weather Service. *Heat Index Chart*. Accessed on February 16, 2022. National Oceanic and Atmospheric Administration. 2022. URL: https://www.weather.gov/jetstream/hi.

[62] National Weather Service. *Historic July 12-15, 1995 Heat Wave*. Accessed on April 10, 2023. National Oceanic and Atmospheric Administration. 2020. URL: https://www.weather.gov/lot/1995_heatwave_anniversary.

[63] National Weather Service. *The Heat Index Equation*. Accessed on February 16, 2022. National Oceanic and Atmospheric Administration, 2014. URL: https://www.wpc.ncep.noaa.gov/html/heatindex_equation.shtml.

[64] Louis Harry Newburgh, ed. *Physiology of Heat Regulation and the Science of Clothing*. WB Saunders Co., 1949.

[65] Nybo, L. and González-Alonso, J. "Critical core temperature: a hypothesis too simplistic to explain hyperthermia-induced fatigue". In: *Scandinavian Journal of Medicine & Science in Sports* 25.S1 (2015), pp. 4–5. DOI: 10.1111/sms.12444.

[66] O'Neill, Marie S, Zanobetti, Antonella, and Schwartz, Joel. "Disparities by race in heat-related mortality in four US cities: the role of air conditioning prevalence". In: *Journal of Urban Health* 82.2 (2005), pp. 191–197.

[67] Oleson, K. W. et al. "Interactions between urbanization, heat stress, and climate change". In: *Climatic Change* 129.3 (2015), pp. 525–541. DOI: 10.1007/s10584-013-0936-8.

[68] Ono, Takeshi et al. "Numerical and experimental study on convective heat transfer of the human body in the outdoor environment". In: *Journal of Wind Engineering and Industrial Aerodynamics* 96 (10-11 Oct. 2008), pp. 1719–1732. ISSN: 01676105. DOI: 10.1016/j.jweia.2008.02.007.

[69] Opitz-Stapleton, Sarah et al. "Heat index trends and climate change implications for occupational heat exposure in Da Nang, Vietnam". In: *Climate Services* 2-3 (Sept. 2016), pp. 41–51. ISSN: 24058807. DOI: 10.1016/j.cliser.2016.08.001.

[70] Pal, Jeremy S and Eltahir, Elfatih A B. "Future temperature in southwest Asia projected to exceed a threshold for human adaptability". In: *Nature Climate Change* 6.2 (2 Jan. 2016), p. 197. ISSN: 17586798. DOI: 10.1038/nclimate2833.

[71] Parsons, Ken. *Human thermal environments: The effects of hot, moderate, and cold environments on human health, comfort, and performance*. CRC press, 2014.

[72] Perera, T A N T et al. "Identification of thermal hotspots through heat index determination and urban heat island mitigation using ENVImet numerical micro climate model". In: *Modeling Earth Systems and Environment* 8.1 (2022), pp. 209–226.

[73] Peters, Annette and Schneider, Alexandra. "Cardiovascular risks of climate change". In: *Nature Reviews Cardiology* 18.1 (Nov. 2020), pp. 1–2. DOI: 10.1038/s41569-020-00473-5.

[74] Quayle, Robert and Doehring, Fred. "Heat stress: A comparison of indices". In: *Weatherwise* 34.3 (1981), pp. 120–124.

[75] Rahman, Mahzabin Binte et al. "Appraising the historical and projected spatiotemporal changes in the heat index in Bangladesh". In: *Theoretical and Applied Climatology* 146.1 (2021), pp. 125–138. DOI: 10.1007/s00704-021-03705-x.

[76] Ramsay, Emma E. et al. "Chronic heat stress in tropical urban informal settlements". In: *iScience* 24 (11 Nov. 2021). ISSN: 25890042. DOI: 10.1016/j.isci.2021.103248.

[77] Rao, K. Koteswara et al. "Projections of heat stress and associated work performance over India in response to global warming". In: *Scientific Reports* 10 (1 Dec. 2020). ISSN: 20452322. DOI: 10.1038/s41598-020-73245-3.

[78] Raymond, Colin, Matthews, Tom, and Horton, Radley M. "The emergence of heat and humidity too severe for human tolerance". In: *Science Advances* 6.19 (2020), eaaw1838.

[79] Robinson, Peter J. "On the definition of a heat wave". In: *Journal of Applied Meteorology and Climatology* 40.4 (2001), pp. 762–775.

[80] Rogers, Cassandra D.W. et al. "Recent Increases in Exposure to Extreme Humid-Heat Events Disproportionately Affect Populated Regions". In: *Geophysical Research Letters* 48 (19 Oct. 2021). ISSN: 19448007. DOI: 10.1029/2021GL094183.

[81] Romps, David M. "Exact expression for the lifting condensation level". In: *Journal of the Atmospheric Sciences* 74.12 (Dec. 2017), pp. 3891–3900.

[82] Romps, David M. and Lu, Yi-Chuan. "Chronically underestimated: a reassessment of US heat waves using the extended heat index". In: *Environmental Research Letters* 17.9 (Aug. 2022), p. 094017.

[83] Rothfusz, Lans P. *The Heat Index "Equation" (or, More Than You Ever Wanted to Know About Heat Index)*. Technical Attachment SR 90-23. Forth Worth, TX: NWS Southern Region Headquarters, July 1990.

[84] Rowell, L. B. "Human cardiovascular adjustments to exercise and thermal stress". In: *Physiological Reviews* 54.1 (Jan. 1974), pp. 75–159. ISSN: 00319333. DOI: 10.1152/physrev.1974.54.1.75.

[85] Saeed, Fahad, Schleussner, Carl Friedrich, and Ashfaq, Moetasim. "Deadly Heat Stress to Become Commonplace Across South Asia Already at 1.5°C of Global Warming". In: *Geophysical Research Letters* 48 (7 Apr. 2021). ISSN: 19448007. DOI: 10.1029/2020GL091191.

[86] Santee, William R. and Wallace, Robert F. "Comparison of weather service heat indices using a thermal model". In: *Journal of Thermal Biology* 30.1 (Jan. 2005), pp. 65–72. DOI: 10.1016/j.jtherbio.2004.07.003.

[87] Sapper, Arthur G. "An Emperor Without Clothes: No Scientific Basis to Rely on NWS Heat Index Chart". In: *Professional Safety* 65.9 (2020), pp. 22–23.

[88] Schär, Christoph. "Climate extremes: The worst heat waves to come". In: *Nature Climate Change* 6 (2 Jan. 2016), pp. 128–129. ISSN: 17586798. DOI: 10.1038/nclimate2864.

[89] Schickele, Elizabeth. "Environment and Fatal Heat Stroke". In: *Military Medicine* 100.3 (Mar. 1947), pp. 235–256. DOI: 10.1093/milmed/100.3.235.

[90] Semenza, Jan C et al. "Excess hospital admissions during the July 1995 heat wave in Chicago". In: *American Journal of Preventive Medicine* 16.4 (1999), pp. 269–277.

[91] Semenza, Jan C et al. "Heat-related deaths during the July 1995 heat wave in Chicago". In: *New England Journal of Medicine* 335.2 (1996), pp. 84–90.

[92] Seneviratne, Sonia I. et al. "Allowable CO2 emissions based on regional and impact-related climate targets". In: *Nature* 529.7587 (2016), pp. 477–483. DOI: 10.1038/nature16542.

[93] Sherwood, Steven C and Huber, Matthew. "An adaptability limit to climate change due to heat stress". In: *Proceedings of the National Academy of Sciences* 107.21 (2010), pp. 9552–9555.

[94] Sherwood, Steven C. "How Important Is Humidity in Heat Stress?" In: *Journal of Geophysical Research: Atmospheres* 123.21 (2018), pp. 11, 808–11, 810. DOI: 10.1029/2018JD028969.

[95] Simmons, Grant H. et al. "Changes in the control of skin blood flow with exercise training: Where do cutaneous vascular adaptations fit in?" In: *Experimental Physiology* 96.9 (2011), pp. 822–828. ISSN: 09580670. DOI: 10.1113/expphysiol.2010.056176. arXiv: NIHMS150003.

[96] Smith, Tiffany T, Zaitchik, Benjamin F, and Gohlke, Julia M. "Heat waves in the United States: definitions, patterns and trends". In: *Climatic Change* 118.3 (2013), pp. 811–825.

[97] Steadman, R. G. "The assessment of sultriness. Part I: A temperature-humidity index based on human physiology and clothing science". In: *Journal of Applied Meteorology* 18.7 (1979), pp. 861–873. ISSN: 08948763. DOI: 10.1175/1520-0450(1979)018<0861:TAOSPI>2.0.CO;2.

[98] Steadman, R. G. "The Assessment of Sultriness. Part II: Effects of Wind, Extra Radiation and Barometric Pressure on Apparent Temperature". In: *Journal of Applied Meteorology* 18.7 (1979), pp. 874–885. DOI: 10.1175/1520-0450(1979)018<0874:TAOSPI>2.0.CO;2.

[99] Stein, Sharman and Kaplan, Joel. "Scientists probe why heat wave became a killer". In: *Chicago Tribune (1963-1996)* (July 1995), p. 2.

[100] Stolwijk, J. A.J. and Hardy, J. D. "Temperature regulation in man - A theoretical study". In: *Pflügers Archiv für die Gesamte Physiologie des Menschen und der Tiere* 291.2 (1966), pp. 129–162. ISSN: 00316768. DOI: 10.1007/BF00412787.

[101] Storm, Bill and Fowler, Brian. "Evaluating the relationship between heat-related ED visits and weather variables". In: *Emerging Health Threats Journal* 4 (2011), p. 146.

[102] Taylor, Karl E., Stouffer, Ronald J., and Meehl, Gerald A. "An Overview of CMIP5 and the Experiment Design". In: *Bulletin of the American Meteorological Society* 93.4 (Apr. 2012), pp. 485–498. DOI: 10.1175/bams-d-11-00094.1.

[103] Torii, Masafumi. "Maximal sweating rate in humans". In: *Journal of Human Ergology* 24.2 (1995), pp. 137–152.

[104] Tustin, Aaron W et al. "Evaluation of occupational exposure limits for heat stress in outdoor workers – United States, 2011–2016". In: *Morbidity and Mortality Weekly Report* 67.26 (2018), p. 733.

[105] Vanos, Jennifer K. et al. "Simplicity lacks robustness when projecting heat-health outcomes in a changing climate". In: *Nature Communications* 11.1 (2020), p. 6079. DOI: 10.1038/s41467-020-19994-1.

[106] Vecellio, Daniel J. et al. "Evaluating the 35C wet-bulb temperature adaptability threshold for young, healthy subjects (PSU HEAT Project)". In: *Journal of Applied Physiology* 132 (2 Feb. 2022), pp. 340–345. ISSN: 15221601. DOI: 10.1152/japplphysiol.00738.2021.

[107] Vecellio, Daniel J. et al. "Utility of the Heat Index in defining the upper limits of thermal balance during light physical activity (PSU HEAT Project)". In: *International Journal of Biometeorology* (July 2022). DOI: 10.1007/s00484-022-02316-z.

[108] Voldoire, Aurore et al. "The CNRM-CM5.1 global climate model: description and basic evaluation". In: *Climate Dynamics* 40.9-10 (2013), pp. 2091–2121.

[109] Wartenburger, R. et al. "Changes in regional climate extremes as a function of global mean temperature: an interactive plotting framework". In: *Geoscientific Model Development* 10.9 (2017), pp. 3609–3634. DOI: 10.5194/gmd-10-3609-2017.

[110] Whitman, Steven et al. "Mortality in Chicago attributed to the July 1995 heat wave." In: *American Journal of Public Health* 87.9 (1997), pp. 1515–1518.

[111] Wolf, S. Tony et al. "Critical environmental limits for young, healthy adults (PSU HEAT Project)". In: *Journal of Applied Physiology* 132 (2 Feb. 2022), pp. 327–333. ISSN: 15221601. DOI: 10.1152/japplphysiol.00737.2021.

[112] Wu, Jianyong et al. "Estimation and Uncertainty Analysis of Impacts of Future Heat Waves on Mortality in the Eastern United States". In: *Environmental Health Perspectives* 122.1 (2014), pp. 10–16. DOI: 10.1289/ehp.1306670.

[113] Wu, Tongwen et al. "An overview of BCC climate system model development and application for climate change studies". In: *Journal of Meteorological Research* 28.1 (2014), pp. 34–56. DOI: 10.1007/s13351-014-3041-7.

[114] Xie, Jingrui et al. "Relative humidity for load forecasting models". In: *IEEE Transactions on Smart Grid* 9.1 (2018), pp. 191–198.

[115] Xu, Jingxian et al. “Evaluation of the convective heat transfer coefficient of human body and its effect on the human thermoregulation predictions”. In: *Building and Environment* 196 (June 2021). ISSN: 03601323. DOI: 10.1016/j.buildenv.2021.107778.

[116] Xu, Zhiwei et al. “Impact of heatwave on mortality under different heatwave definitions: a systematic review and meta-analysis”. In: *Environment International* 89 (2016), pp. 193–203.

[117] Yip, Fuyuen Y et al. “The impact of excess heat events in Maricopa County, Arizona: 2000–2005”. In: *International Journal of Biometeorology* 52.8 (2008), pp. 765–772.